Final Report

REHABILITATION OF A REINFORCED CONCRETE BRIDGE USING FRP LAMINATES

by

Joseph W. Tedesco
J. Michael Stallings
Mahmoud EL-Mihilmy

sponsored by

The Alabama Department of Transportation
Montgomery, Alabama

March 1998

ACKNOWLEDGMENT

The material contained herein was obtained or developed in connection with a research project, "Rehabilitation of a Reinforced Concrete Bridge Using FRP Laminates," RP 930-341, conducted by the Highway Research Center at Auburn University. The research project was sponsored by the Alabama Department of Transportation (ALDOT) and the Federal Highway Administration (FHWA). Traffic control, test load vehicles and operators for the field testing were provided by the Alabama Department of Transportation Maintenance Bureau. The support, interest, cooperation, and assistance of many personnel from ALDOT and FHWA is gratefully acknowledged. Much work by graduate students Mahmoud EL-Mihilmy, Michael McCauley, Nathan Porter and Robert Williams is gratefully acknowledged. The authors also wish to acknowledge Mr Jackie White for his valuable assistance during the course of this project, and also Mr. John Brooks of FiberCote, Inc. for supplying the composite materials.

DISCLAIMER

The contents of this report reflect the views of the authors who are responsible for the facts and accuracy of the data presented herein. The contents do not necessarily reflect the official views or policies of the Alabama Department of Transportation or Auburn University. The report does not constitute a standard, specification, or regulation.

SUMMARY

Over fifty percent of all bridges in the United States were built before 1940, and approximately 42% o these bridges are structurally deficient. This alarming statistic underscores the importance of developing reliable and cost effective repair and strengthening techniques for existing bridge structures. Rehabilitation needs vary widely, so easily adaptable approaches are desirable. Some bridges need repair because deterioration has resulted in loss of load capacity. Others exhibit only minor deterioration, but were designed for loading significantly less than modern traffic loading.

In the past, various methods have been used to strengthen bridges and many other types of structures. Traditionally structural rehabilitation has been accomplished by methods such as introducing additional beams to the structure, by strengthening existing beams with mechanically attached reinforcing plates, or adding externally post-tensioned cables. In recent years, external bonding of steel plates to the tension face of deficient flexural members has been successfully applied to many structures. However, the use of steel plates has many disadvantages. Some disadvantages are corrosion, difficulty in handling the plates, deterioration of bond at the steel-concrete interface, and the need for massive scaffolding or heavy lifting equipment during installation.

Unidirectional fiber reinforced plastic (FRP) sheets made of carbon (CFRP), glass (GFRP) or aramid (AFRP) fibers bonded together with a polymer matrix (e.g., epoxy, polyester, vinylester) are being used as a substitute for steel. Initial developments in this area took place in Germany and Switzerland. FRP plates are an attractive solution over steel plates because of their ease in handling resistance to corrosion, light weight and high strength. Recent experimental studies have shown that reinforced concrete beams strengthened with externally bonded FRP laminates can exhibit ultimate load capacities as high as three times their original capacity depending on steel ratio, concrete strength, FRP ratio, FRP mechanical properties, properties of the bonding agent, and pre-existing level of

damage of the beams.

While laboratory experiments have illustrated the effectiveness of using FRP in repairs, and some field applications of FRP have been reported, there is a lack of test data illustrating the field performance of FRP repairs. Field test data that quantitatively illustrate the effects of FRP repairs on an existing bridge are the focus of this report. The behavior of a bridge is quantified by measurements of vertical deflections, strains in the primary flexural reinforcement, and strains on the surfaces of the FRP plates, These data are recorded from static and dynamic tests performed both before and after the FRP repairs, with loading by two identical test trucks of known weight and configuration. The data presented in this report are results from a research project conducted for the Alabama Department of Transportation (ALDOT). The overall project included: field application of FRP plates to an existing bridge, field load testing, development of a cross sectional procedure including the FRP, and static and dynamic finite element analyses of the structure. The results from that study are presented and discussed in the report.

The results of the field study conducted to investigate the effectiveness of externally bonding FRP laminates to a deteriorated reinforced concrete bridge have established the procedure as a viable bridge rehabilitation procedure. This conclusive finding is corroborated with results from a comprehensive finite element method analysis of the bridge, as well as with a detailed analytical investigation of the repaired structure. The procedure is recommended as a rehabilitation strategy for similar reinforced concrete bridges exhibiting advanced symptoms of deterioration or distress.

TECHNICAL REPORT STANDARD TITLE PAGE

1. Report No.	2. Government Accession No.	3. Recipient's Catalog No.
4. Title and Subtitle Rehabilitation of a Reinforced Concrete Bridge Using FRP Laminates	5. Report Date March 1998 6. Performing Organization Code	
7. Author(s) Tedesco, J. W., Stallings, J. Michael, EL-Mihilmy, Mahmoud	8. Performing Organization Report No.	
9. Performing Organization Name and Address Auburn University Highway Research Center 238 Harbert Engineering Center Auburn, AL 36849-5337	10. Work Unit No. 11. Contract or Grant No.	
12. Sponsoring Agency Name and Address Alabama Department of Transportation Research and Development Bureau 1409 Coliseum Boulevard Montgomery, AL 36130-3050	13. Type of Report and Period Covered Final 14. Sponsoring Agency Code	
15. Supplementary Notes		

16. Abstract

Many reinforced concrete bridges throughout the Unites States on county and state highway systems are deteriorated and/or distressed to such a degree that structural strengthening of the bridge or reducing the allowable truck loading on the bridge by load posting is necessary to extend the service life of the bridge. The structural performance of many of these bridges can be improved through external bonding of fiber reinforced plastic (FRP) laminates or plates. This report describes the rehabilitation of an existing concrete bridge in Alabama through external bonding of FRP plates to the bridge girders. Field load tests were conducted before and after application of the FRP plates, and the response of the bridge to test vehicle loadings was recorded. Results of the field tests are reported, and the effects of the FRP plates on the bridge response are identified. The repaired bridge structure exhibited a decrease in primary reinforcing bar stresses and vertical midspan deflections. These decreases ranged from 4 to 12% for various static and dynamic loading cases. The report also presents the results of a comprehensive finite element method (FEM) analysis conducted on the bridge, as well as the details of a cross sectional analysis procedure developed for FRP strengthened girders.

17. Key Words: Infrastructure, Bridges, Concrete, Tests, Repair, Fiber Reinforced Plastics, Externally Bonded, Composite Laminates, Finite Element Analysis	18. Distribution Statement No Restriction		
19. Security Classif. (of this report)	20. Security Classif. (of this page)	21. No. of Pages 130	22. Price

Form DOT F 1700.7 (8-69)
TABLE OF CONTENTS

List of Figures vii

List of Tables xi

CHAPTER ONE: INTRODUCTION 1
BACKGROUND 1
FIBER REINFORCED PLASTIC 2
PROJECT OBJECTIVES 2
LITERATURE REVIEW 3

CHAPTER TWO: BRIDGE REHABILITATION 13
DESCRIPTION OF BRIDGE 13
SURFACE PREPARATION OF BRIDGE GIRDERS 18
SURFACE PREPARATION OF COMPOSITES 18
COMPOSITE POSITIONING AND PROPERTIES 18
GENERAL DESCRIPTION OF REHABILITATION PLAN 19
INSTALLATION PROCEDURE 22

CHAPTER THREE: FIELD LOAD TESTS 25
INSTRUMENTATION PLAN 25
DESCRIPTION OF LOAD TESTS 27

CHAPTER FOUR RESULTS OF LOAD TESTS 33
INTRODUCTION 33
DATA ACQUISITION AND REDUCTION 33
EFFECT OF FRP ON REBAR STRESSES 43
EFFECT OF FRP ON GIRDER DEFLECTIONS 50
TRANSFER OF STRESSES THROUGH SPLICE PLATES 54
CONCLUSIONS 54

CHAPTER FIVE: ANALYSIS OF BRIDGE 57
INTRODUCTION 57
FINITE ELEMENT MODEL 57
FEM ANALYSIS 60
Frequency Analysis 60
Damping Characteristics 61
Transient Analysis 68
Results of Transient Analysis 68
Static FEM Analysis Results 73
Parametric Study 92
SECTION ANALYSIS 100
Effect of CFRP Cross Sectional Area on Girder Ultimate Strength 100
Effect of CFRP Tensile Strength on the Ultimate Strength of Girder 101
Design Charts 104
CONCLUSIONS 106

CHAPTER SIX: BRIDGE INSPECTION AND MONITORING 109
INITIAL CONDITION OF CONCRETE BRIDGE MONITORING 109

CONDITION OF GIRDERS IMMEDIATELY FOLLOWING APPLICATION OF FRP ... 109
RESULTS OF PERIODIC INSPECTIONS ... 112

CHAPTER SEVEN: CONCLUSIONS AND RECOMMENDATIONS ... 117
CONCLUSIONS ... 117
RECOMMENDATIONS ... 119

REFERENCES ... 120

APPENDICES ... 122
APPENDIX A: DETAILS OF SECTION ANALYSIS ... 122

List of Figures

Figure 2.1. Reinforcement of the Concrete Slab (All Dimensions are mm) 14

Figure 2.2. Bridge Cross Section (All Dimensions are mm) 14

Figure 2.3. Girder Cross Section (All Dimensions are mm) 15

Figure 2.4. Elevation View of Girder Showing Shear Reinforcement (All Dimension are mm) 16

Figure 2.5. Stirrup Spacing and Shear Capacity Along Span 17

Figure 2.6. Bridge Cross Section Showing Positions of GFRP and CFRP 20

Figure 2.7. Elevation and Bottom Views of Bridge Girder Showing FRP Positions 21

Figure 3.1. Locations of Strain Gages on Girder Cross Section (All Dimension are mm) 26

Figure 3.2. Strain Gages Attached to Splice Plate of Girder 2 26

Figure 3.3. Load Truck Configuration 28

Figure 3.4. Load Truck Positions 1 and 2 (All Dimensions are mm) 29

Figure 3.5. Load Truck Positions 3 and 4 30

Figure 3.6. Load Truck Position 5 32

Figure 4.1. Static Rebar Stresses - Test Truck Positions 1 and 3 47

Figure 4.2. Static Rebar Stresses - Test Truck Positions 2 and 4 47

Figure 4.3. Peak Dynamic Rebar Stresses 49

Figure 4.4. Static Girder Deflections - Test Truck Positions 1 and 3 49

Figure 4.5. Static Girder Deflections - Test Truck Positions 2 and 4 53

Figure 4.6. Peak Girder Deflections from Dynamic Tests - Eastbound Trucks 53

Figure 4.7. Splice Plate Strains at East End of Girder 2 55

Figure 5.1. An Isometric View of the Finite Element Model of the Bridge 59

Figure 5.2. Typical Cross Section of the FEM Model for Repaired Bridge Structure 62

Figure 5.3. Mode Shape Corresponding to Fundamental Vibration Frequency 63

Figure 5.4. Experimental Data Recorded During Dynamic Field Load Test No.3 on Girder B3 Before Rehabilitation 65

Figure 5.5. Modal Damping Variation with the Bridge Natural Frequency 67

Figure 5.6. Dynamic Loading Configuration Simulating Test Trucks 69

Figure 5.7. Time History Used for Truck Loading in the FEM Analysis 70

Figure 5.8. Comparisons of FEM Transient Analysis Results and Recorded Test Data Before Rehabilitation (Test No. 3): (a) Maximum Stresses in Reinforcing Steel Midspan: (b) Maximum Girder Deflections at Midspan 71

Figure 5.9. Comparisons of FEM Transient Analysis Results and Recorded Test Data After Rehabilitation (Test No. 1): (a) Maximum Stresses in Reinforcing Steel at Midspan: (b) Maximum Girder Deflections at Midspan 72

Figure 5.10. Midspan Deflection Time Histories for Girder B1 Before Rehabilitation (Test No.3) . 74

Figure 5.11. Midspan Deflection Time Histories for Girder B2 Before Rehabilitation (Test No.3) . 75

Figure 5.12. Time Histories for Midspan Reinforcing Steel Stresses for Girder B1 Before Rehabilitation (Test No.3) 76

Figure 5.13. Time Histories for Midspan Reinforcing Steel Stresses for Girder B2 Before Rehabilitation (Test No.3) 77

Figure 5.14. Midspan Deflection Time Histories for Girder B1 After Rehabilitation (Test No. 1) 78

Figure 5.15. Midspan Deflection Time History for Girder B2 After Rehabilitation (Test No.1) 79

Figure 5.16. Time Histories for Midspan Reinforcing Steel Stresses for Girder B1 after Rehabilitation (Test No. 1) 80

Figure 5.17. Time Histories for Midspan Reinforcing Steel Stresses for Girder B2 After Rehabilitation (Test No.1) 81

Figure 5.18. Time Histories For Midspan Stresses in CFRP Plate for Girder B2 After Rehabilitation (Test No. 1) 82

Figure 5.19. Maximum Reinforcing Steel Stresses and Girder Deflections at Midspan Before Rehabilitation (Static Load Position 1, Average, East Gage) 83

Figure 5.20. Maximum Reinforcing Steel Stresses and Girder Deflections at Midspan Before Rehabilitation (Static Load Position 2) 84

Figure 5.21. Maximum Reinforcing Steel Stresses and Girder Deflections at Midspan Before Rehabilitation (Static Load Position 3) 85

Figure 5.22. Maximum Reinforcing Steel Stresses and Girder Deflections at Midspan Before Rehabilitation (Static Load Position 4) 86

Figure 5.23. Maximum Reinforcing Steel Stresses and Girder Deflections at Midspan After Rehabilitation (Static Load Position 1) (Avg. East Gage) 87

Figure 5.24. Maximum Reinforcing Steel Stresses and Girder Deflections at Midspan After Rehabilitation (Static Load Position 2) 88

Figure 5.25. Maximum Reinforcing Steel Stresses and Girder Deflections at Midspan After Rehabilitation (Static Load Position 3) 89

Figure 5.26. Maximum Reinforcing Steel Stresses and Girder Deflections at Midspan After Rehabilitation (Static Load Position 4) 90

Figure 5.27. Maximum CFRP Stresses at Midspan for Each Beam (Load Position 2) 91

Figure 5.28. Maximum CFRP Stresses at Midspan for Each Beam (Load Position 3) 91

Figure 5.29. Midspan Deflection Time Histories for Girder B3 for Different CFRP Cross Sectional Areas 94

Figure 5.30. Midspan Deflection Time Histories for Girder B3 with Different CFRP Modulii of Elasticity 95

Figure 5.31. Effect of the CFRP Cross Sectional Area on Reduction of Maximum Girder Deflection and Maximum Stress Reinforcing Steel (Girder B3) 96

Figure 5.32. Effect of the CFRP Modulus of Elasticity on Reduction of Maximum Girder Deflection and Maximum Stress in Reinforcing Steel (Girder B3) 97

Figure 5.33. Effect of Varying CFRP Cross Sectional Area on the Average Change in Static Girder Deflections and Reinforcing Steel Stresses at Midspan 98

Figure 5.34. Effect of Varying the CFRP Modulus of Elasticity on the Average Change in Static Girder Deflections and Reinforcing Steel Stresses at Midspan 99

Figure 5.35. Modified Hognestad Concrete Stress-Strain Curve used in the Sectional Analysis Computer Program 102

Figure 5.36. Effect of CFRP Cross Sectional Area and Elastic Modulus on Enhancement Percentage of Girder Ultimate Capacity 103

Figure 5.37. Typical Design Chart for Girders Strengthened with CFRP 108

Figure 6.1. Sketch of Crack Pattern in Typical Girder Prior to FRP Application 110

Figure 6.2. Typical Crack Patterns in Concrete Girders Prior to FRP Application 111

Figure 6.3. Voids Under GFRP at East End of Girder 2 - North Face 113

Figure 6.4. Voids Under GFRP at East End of Girder 2 - South Face 113

Figure 6.5. Voids Under GFRP at West End of Girder 4 - North Face 114

Figure 6.6. Voids Under GFRP at West End of Girder 4 - South Face 114

Figure 6.7. Voids Under CFRP at West End of Girder 1 115

Figure 6.8. Voids Under CFRP at West End of Girder 2 115

Figure 6.9. Voids Under CFRP at East End of Girder 4 116

Figure 6.10. Largest Void Found Under CFRP 116

Figure A.1. Neutral Axis Position for T-Sections 123

Figure A.2. Design Chart for RC Sections with FRP 130

List of Tables

Table 4.1. Rebar Strains from Static Tests - Before FRP Application 34

Table 4.2. Rebar Strains from Static Tests - After FRP Application 35

Table 4.3. Girder Deflections from Static Tests - Before FRP Application 36

Table 4.4. Girder Deflections from Static Tests - After FRP Application 37

Table 4.5. CFRP Strains from Static Tests 39

Table 4.6. Strains Measured on CFRP Splice Plate (microstrain) ..... 40.

Table 4.7. Peak Rebar Strains from Dynamic Tests - Before FRP Application 41

Table 4.8. Peak Rebar Strains from Dynamic Tests - After FRP Application 41

Table 4.9. Peak Girder Deflections from Dynamic Tests - Before FRP Application 42

Table 4.10. Peak Girder Deflections from Dynamic Tests - After FRP Application 42

Table 4.11. Rebar Stresses from Static Tests - Before FRP Application 44

Table 4.12. Rebar Stresses from Static Tests - After FRP Application 45

Table 4.13. Comparison of Rebar Stresses from Static Tests 46

Table 4.14. Peak Rebar Stresses from Dynamic Tests - Before FRP Application 48

Table 4.15. Peak Rebar Stresses from Dynamic Tests - After FRP Application 48

Table 4.16. Percent Differences in Peak Dynamic Stresses (Mpa) for Test Trucks Traveling Eastbound 48

Table 4.17. Comparison of Strains Measured on CFRP and on Rebar 51

Table 4.18. Comparison of Girder Deflections from Static Tests 52

Table 4.19. Comparison of Peak Girder Deflections from Dynamic Tests 52

Table 5.1. Natural Circular Frequency, Natural Frequency and Natural Period for the First Twenty Modes Extracted from the FEM Frequency Analysis 64

Table 5.2. Comparison Between Maximum Midspan Stresses (Mpa) in CFRP Obtained from Recorded Test Data and the FEM Analysis 92

Table 5.3. Effect pf CFRP Cross Sectional Area on Ultimate Flexural Strength of Girder 105

Table 5.4. Effect of CFRP Tensile Strength on Ultimate Strength Flexural Strength of Girder 105

Table A.1. Values of α, k_2 for Concrete Compressive Strength of 27 Mpa 125

Table A.2. Calculation of $\alpha_c c$ for Example Problem 128

CHAPTER ONE
INTRODUCTION

BACKGROUND

A significant percentage of the bridges in North America were built after the Second World War. Most of them were originally designed for smaller vehicles, lighter loads and a lower traffic volume than commonly experienced today. Over fifty percent of all bridges in the United States were built before 1940, and approximately 42% of these bridges are considered to be structurally deficient (Klaiber et. al., 1987). This alarming statistic underscores the importance of developing reliable and cost effective repair and strengthening techniques for existing bridge structures.

In the past, various methods have been used to strengthen bridges and other types of structures. Traditionally, structural rehabilitation was accomplished by introducing additional beams to the structures or by strengthening existing beams with externally post-tensioned cables. In recent years, external bonding of steel plates to the tension face of the deficient member has been successfully applied in many structures. However, the use of steel plates has many disadvantages, such as corrosion, difficulty in handling the plates, deterioration of bond at the steel-concrete interface and the requirement of massive scaffolding during construction.

Fiber reinforced plastic (FRP) laminates, or plates, provide an attractive alternative to steel plates because of their ease in handling, resistance to corrosion, light weight and high strength. Experimental studies (Saadatmanesh and Ehsani 1991; Meier and Kaiser 1991; Ross et. al. 1994) conducted on both virgin and damaged beams strengthened with externally bonded FRP plates showed this technique to be very effective. The increase in strength exhibited by beams strengthened with FRP plates can be as high as three times their original capacity depending on the steel ratio, concrete strength, FRP ratio, FRP mechanical properties, properties of the bonding agent and the pre-existing level of damage to the beams.

FIBER REINFORCED PLASTIC

Fiber reinforced plastic (FRP) composites are typically made of carbon, aramid or glass fibers bonded together with a polymer matrix (e.g. epoxy, polyester, vinylester). Carbon fiber composites have been widely used for most reinforced concrete repair applications because of their high strength. FRP comes in variety of shapes and fiber orinations such as fabric, prepreg, and laminates.

In brief, FRP consists of two or more different materials combined to produce a new material that possesses mechanical characteristics superior to those of the individual components. FRP is thus a combination of high strength fibers (glass, carbon or aramid) in a polymer matrix. The matrix contains and protects the fibers, and permits stress transfer to the fibers through shear.

PROJECT OBJECTIVES

The overall goal of this project is to develop a procedure to rehabilitate deteriorated reinforced concrete bridge girders by external bonding of FRP laminates. To achieve this goal, an existing deteriorated bridge structure was retrofitted with FRP laminates. The improved structural performance of the rehabilitated structure was evaluated from load tests, field monitoring and inspection and numerical analyses. The bridge rehabilitation procedure is described in Chapter Two; the bridge instrumentation plan and field load tests are discussed in Chapter Three; the results of the field load tests are presented in Chapter Four; and the numerical analyses are discussed in Chapter Five.

The candidate bridge is located on state highway 110 near Union Springs. The structure consists of 13 simple spans of 10.36 m lengths. Each span is comprised of four reinforced concrete T-beams, nearly all of which are exhibiting significant flexural cracking due to routine truck traffic over a 40 year period.

One span from this bridge was repaired with the external bonding of FRP laminates. The laminates were applied to the bottom and sides of the stems of three of four T-beams within the span; the remaining beam was retrofitted with FRP laminates on the bottom of the stem only. All beams

were appropriately instrumented to collect the pertinent data from the load tests. The bridge was inspected frequently throughout the duration of the project to assess the performance of the rehabilitation procedure. The bridge inspection program is described in Chapter Six.

LITERATURE REVIEW

P. A. Ritchie (1988) upgraded fourteen reinforced concrete beams using steel plates as well as, glass and carbon FRP laminates. He reported increases in beam stiffnesses ranged from 18 to 116 percent, and the increases in the ultimate flexural capacity ranged from 47 to 97 percent. The beams with externally bonded plates also exhibited another desirable trait, namely, the cracking patterns changed from several widely spaced cracks with relatively large widths, to many more closely spaced cracks with much narrower widths. Analytically predicted load-deflection responses exhibited fairly good correlation with the experimental data, although the theoretical curves were stiffer. The author indicated that failure did not occur by flexure in the maximum moment region on many beams, but rather by debonding at the plate ends, despite attempts at providing plate end anchorages to postpone interface failure. Based on the experimental evidence, externally bonded FRP plates proved to be a feasible method of upgrading the strength and stiffness characteristics of reinforced concrete beams. Additional studies to investigate stress concentrations near the plate ends to prevent premature failure were also recommended.

H. Saadatmanesh and M. R. Ehsani (1990) tested five reinforced concrete beams, four of them strengthened with epoxy bonded GFRP plates, and the fifth served as a control specimen. The four strengthened beams had the same steel reinforcement ratio and GFRP plate area, however, a different epoxy was used on each beam. The selected epoxies had a wide range of strengths and ductilities. The most ductile epoxy did not enhance the ultimate capacity of the beam because it was too flexible to allow any shear transfer between the concrete and the GFRP plate. On the other hand, the most rigid adhesive experienced a premature failure of the beam with no increase in the peak load compared

to that of the control beam. The remaining two epoxies used in the study did increase the ultimate flexural capacity of the beams by 30 and 110 percent, respectively. It was concluded that an effective adhesive must posses both sufficient stiffness and shear strength to successfully transfer the load from the concrete to the GFRP plates.

U. Meier and H. Kaiser (1991) tested twenty-six rectangular reinforced concrete beams having a 2 meter span, and one beam having a span of 7 meters. The 2 meter span beams were strengthened with 0.3 mm thick CFRP sheets bonded to the beam bottoms. Strengthening with this very thin plate nearly doubled the ultimate flexural capacity of the beams. However, the steel reinforcement in the beams was intentionally under dimensioned. In the case of the seven meter span beam which was reinforced with a 1.0 mm thick CFRP laminate, the reported increase in ultimate flexural capacity was only 22 percent, and a sudden laminate peel-off due to the development of shear cracks in the concrete was also noticed. The influence of bonded CFRP laminates on reducing the number and width of flexural cracks was also studied. Despite the higher ultimate flexural capacity exhibited by the CFRP retrofitted beam, the total width of all cracks was 40 percent less than that experienced by the control beam. Finally, the authors concluded that the ultimate flexural capacity of reinforced concrete beams strengthened with FRP plates could be calculated analytically by a procedure completely analogous to that employed for conventionally reinforced concrete beams.

H. Saadatmanesh and M. R. Ehsani (1991) tested five rectangular concrete beams and one T-beam, strengthened with GFRP plates, under four point loading. The results of the rectangular beam tests indicated that the ultimate flexural strength of reinforced concrete beams can be significantly increased by gluing GFRP plates to the tension face. However, beams having no conventional steel reinforcement failed at a very low load due to premature debonding of the FRP plate. Thus, it was concluded that a minimum amount of steel reinforcement was necessary to limit the width of the flexural cracks to prevent debonding of the composite. Results of the T-beam test indicated that

bonding of the GFRP plate doubled the flexural capacity of the beam. It was also cited that beams strengthened with FRP plates experienced less flexural cracking, reduced crack widths and a delay in the formation of the flexural cracks. However, bonding of the FRP plates reduced the ductility of the beam compared to that exhibited by the conventionally reinforced beam.

W. An, et. al. (1992) developed analytical models based on compatibility of deformations and equilibrium of forces for predicting the load-deflection response for reinforced concrete beams strengthened with FRP plates. Models were derived for both rectangular and T-sections. Using these models, a parametric study was conducted to investigate the effects of several design variables such as FRP plate area, plate modulus, plate tensile strength, concrete compressive strength and steel reinforcement ratio. It was concluded from the results of the study that bonding the FRP plate to the concrete beam increases the stiffness, the yield moment and the ultimate flexural capacity of the beam, particularly for beams having low steel reinforcement ratios. Increasing the concrete compressive strength for beams strengthened with FRP plates resulted in a further increase in the ultimate flexural strength of the section. Although the calculated curvature at the ultimate load decreased as the FRP plate area increased, the area under the moment curvature diagram did not decrease significantly.

B. M. Ghaleb (1992) investigated the use of externally bonded fiber glass plates to increase both the flexural and shear capacity of damaged reinforced concrete beams. His work was divided into four segments. The first segment focused on the selection of the fiber glass material. The second segment addressed the effect of thermal cycling on the bond strength between the FRP and the epoxy glue. The third segment evaluated the performance of damaged beams repaired with FRP plates. The ultimate flexural capacity of the repaired beams were found to have been increased by approximately 60 percent. The fourth segment of the study considered the performance of reinforced concrete beams strengthened for shear. Three repair techniques for shear damaged beams were investigated: FRP side plates, FRP side strips and FRP U-jackets. Shear damaged beams repaired by FRP side strips and FRP

side plates enhanced the shear capacity by 26 and 32 percent, respectively. Beams repaired with FRP U-jackets attained the ultimate flexural capacity without experiencing a shear failure. Thus, it was concluded that the FRP U-jackets was the most effective technique for repairing shear damaged beams.

U. Meier et. al. (1992) extended the concept of strengthening laboratory test beams to girders in existing bridge structures. The Ibach Bridge and the historic wooden bridge in Switzerland were strengthened by external bonding of CFRP plates. The damaged concrete girder in the Ibach Bridge, having a span of 39 meters, was repaired with CFRP laminates. A 6.2 kg CFRP plate was used in the repair in lieu of a 175 kg steel plate. In the second case, the historic wooden bridge was severely deteriorated and a load limit was posted. Two of the most highly loaded cross beams were strengthened using carbon fiber reinforced epoxy resin sheets. Even though the strengthened beams were subjected to extremely high loads, no further signs of deterioration were reported.

S. Raghavachary (1992) conducted a laboratory testing program in which he studied the effect of plate thickness on the ultimate flexural strength of reinforced concrete beams having externally bonded CFRP plates. All beams tested experienced failure by concrete crushing, but exhibited a significant increase in ultimate load capacity. Beams strengthened with three plies of CFRP displayed considerable ductility, exhibiting an almost constant load capacity prior to failure. The ultimate flexural capacity of the beams increased with increasing the number of plies, but not at a proportional rate. The average percentage of increase in stiffness for the FRP plated beams over the control beams was 20%, 47%, and 64% for one, two and three plies respectively. A substantial reduction in the widths of flexural cracks with increasing number of plies was also noticed. Cracks exhibited by the FRP plated beams were more closely spaced and had narrower widths than those experienced by the control beams.

F. Rostasy et. al. (1992) reported the rehabilitation of the Kattenbusch Bridge in Germany with externally bonded GFRP plates. The Kattenbusch Bridge is a continuous eleven span, post-tensioned

concrete bridge. Because the bottom flanges of the box girders were lightly reinforced, wide thermally-induced cracks developed at bottom flange-web junctures of the girders. Field test data recorded for the bridge, both before and after strengthening, indicated a reduction in the reinforcing steel stresses at the service load stage had been achieved.

T. C. Triantafillou and N. Plevris (1992) studied the behavior of reinforced concrete beams strengthened with FRP plates and the associated modes of failure. The authors derived equations describing each failure mechanism using the strain compatibility method, the concept of fracture mechanics and a simple model representing the FRP peel-off debonding mechanism. Seven beams strengthened with FRP plates were tested under four point loading. The experimental results showed that the ultimate flexural capacities of the FRP strengthened beams were superior to that of the control beam. Five of the repaired beams failed due to debonding and subsequent peeling off of the composite. They concluded that the FRP peel-off failure mechanism establishes an upper limit to the composite plate thickness. Beams fitted with FRP plates of greater thickness will exhibit a peel-off failure before achieving the theoretical ultimate flexural capacity.

Y. N. Ziraba (1993) developed a non-linear finite element method (FEM) computer program to analyze reinforced concrete beams strengthened with externally bonded steel and GFRP plates. The author indicated that increasing the plate thickness led to an increase in ultimate flexural capacity, however this strength enhancement was limited by the condition of the beam-plate interface failure. Therefore, it was suggested that a limit should be established for the thickness of the bonded plate in order to prevent premature interface failure. A series of FEM analyses were conducted on a half beam specimen which indicated that the interface failure was a surface phenomenon. Based on the results of the numerical analyses and the available experimental work in the literature, the author suggested that a Moher-Coulomb failure criterion with a tension cut-off should be the material characterization of the steel/glue/concrete interface. Increasing plate curtailment length led to a significant magnification of

the interface stresses. Using a more flexible glue and tapered plates decreased both peeling and shear stresses at the plate ends. Furthermore, for optimal results, the author recommended using thinner plates which are as wide as possible. Roberts' formula (Roberts 1989) for predicting interface stresses was found to be conservative for very thin plates, but underestimates the interface stresses of thicker plates. Newly derived expressions for peak interface shear and peeling stresses were presented for use as design aids. The author also noted that the ACI procedure for shear design for conventionally steel reinforced beams cannot be used for beams with bonded FRP plates because the horizontal cracking which developed near the plate ends did not intersect the stirrups. Based on the experimental evidence of failed beams, the author proposed an alternative expression to evaluate the efficiency of the stirrups in beams strengthened with externally bonded plates.

M. J. Chajes et. al. (1994) performed a series of laboratory tests on reinforced concrete beams with bonded composite fabrics to evaluate the improvement to the ultimate flexural capacity. The fabrics used were made of aramid, E-glass and graphite fibers. Originally, all beams were bonded for flexural considerations without shear strengthening. End tabs were later employed to prevent fabric debonding which occurred in the first series of tests. Beams strengthened with aramid failed due to concrete crushing, while those strengthened with E-glass and graphite fibers failed due to rupture of the composite. These different modes of failure were attributed to the variation in the fabric ultimate strain. The ultimate strain for the aramid fabric was twice that of E-glass and three times that of the graphite. Increases in the ultimate flexural capacity ranged from 36 to 57 percent with corresponding increases in flexural stiffness of 45 to 53 percent. This increase in strength was accompanied by a decrease in ductility. The reported ductility index for beams strengthened with composite was in the vicinity of two or three, while beams without the composite fabric exhibited a ductility index in the range of four to five. The authors developed an analytical model based on the stress-strain relationships of the materials used to predict the load-deflection behavior of the strengthened beams.

A comparison between the experimental results and the analytical model indicated that the behavior of the beams with bonded FRP fabric could be accurately predicted using the developed analytical model.

P. J. Heffernan (1994) conducted a series of laboratory tests to investigate the fatigue behavior of damaged beams post-strengthened with CFRP laminates. The results of seven (3 static plus 4 cyclic) 2.0 m span simple beams and four (2 static plus 2 cyclic) 5.0 m simple span beams were reported. The efficiency of the CFRP reinforcement as compared to an equivalent area of additional conventional steel reinforcing was greater than the modular ratio of the materials, and was dependent upon the relative distance of the additional reinforcements from the neutral axis. For beams subject to static loading, a design procedure based on strain compatibility was found to be reliable. The fatigue life of beams subjected to cyclic loading with a stress range greater than the tensile strength of the reinforcing steel, was governed by the reinforcing steel. Unlike the monotonic loading cases, the 2.0 m beams in the fatigue tests experienced shear cracks after 100,000 cycles. These cracks propagated horizontally, at the reinforcing steel level, toward midspan and eventually precipitated failure of the beam. The author attributed this type of failure to insufficient development length for the CFRP plate. The mode of failure for both monotonic and cyclic loading of the 5.0 m beams was a sudden rupture of the CFRP plate near midspan. The fatigue life of the CFRP strengthened beams appears to be at least equal to that of the conventionally reinforced concrete beam of the same strength. No slippage between the CFRP and the concrete beam as result of cyclic loading was observed. Finally, the effect of beam scale was examined and appeared to be negligible.

N. Plevris and T. Triantafillou (1994) studied the time dependent behavior (due to sustained loading) of reinforced concrete beams strengthened with FRP laminates. An analytical procedure was presented for the deformation of the cross section based on an age-adjusted effective modulus method for the concrete. The analytical model was used to predict the long term deflections of reinforced concrete beams with bonded FRP plates. The authors concluded that bonding the FRP plates to the

concrete beams played a favorable role in mitigating the long term deflection response. Increasing the FRP plate area decreased the creep strains.

R. Qu (1994) performed analytical studies on reinforced concrete beams strengthened with CFRP laminates using the finite element method (FEM). A reasonably accurate load-deflection response was predicted based on the proposed modeling of the material stress-strain relations, failure criterion and concrete properties. The confinement effect of the CFRP plates was implemented by setting the concrete modulus of elasticity after cracking (E_e) to 1/20 E_c. Both theoretical and experimental results confirmed the use of a higher value of E_e for FRP strengthened beams than that for the control beam. The ultimate flexural strength and stiffness of the beams with bonded CFRP laminates was found to be significantly higher than that of the control beam.

C. A. Ross et. al (1994) tested 24 reinforced concrete beams strengthened with CFRP plates externally bonded to the tension face. All beams had the same CFRP cross-sectional area, but had several different reinforcing steel ratios. Considerable enhancement was achieved by bonding of the CFRP laminates to the beams having the lower reinforcing steel ratios. However, the addition of CFRP to the beams having the higher reinforcing steel ratios resulted in significantly less strength enhancement. The peak load for the FRP strengthened beams having the lowest reinforcing steel ratio was as high as three times that of the control beam. It was also observed that retrofitted beams with the lower reinforcing steel ratios failed by delamination of the composite, while the retrofitted beams with the higher reinforcing steel ratios failed by concrete crushing accompanied by horizontal cracking in the vicinity of the tension steel reinforcement. The authors reported that at the load corresponding to yielding of the tensile steel, approximately seventy five percent of the beam stiffness was attributed to the CFRP plates. Thus the authors concluded that a high CFRP modulus was more important than a high tensile strength in increasing flexural stiffness. Based on the experimental observation that the load-deflection curve is multi-linear, an analytical model was developed to predict the load- deflection

response of CFRP strength enhanced beams at several different load stages. Excellent agreement between the analytical model and experimental results was cited. A nonlinear FEM analysis was also conducted to study the behavior of CFRP strengthened beams during various stages of loading. The results of the FEM analysis correlated very well with the test data and the analytical model.

A. Kobayashi, et. al. (1995) used CFRP sheets to upgrade an existing reinforced concrete bridge in Japan. The bridge had been in service since 1977. Many flexural cracks were observed on the undersides of the concrete deck slabs, thus necessitating their repair and strengthening. The deck slabs were originally designed for a maximum vehicle load of 20 tons, however, an evaluation of the reinforcing steel stresses for a 25 ton vehicle (upgraded capacity) indicated that the allowable design stress was exceeded. The bridge was repaired with one ply of CFRP sheets bonded to the bottoms of the deck slabs spanning in the longitudinal direction, and with an additional one ply sheet spanning in the transverse direction of the deck slabs. The total applied cross-sectional area of the composite for the entire bridge was 164 $m^{2,}$, and the entire repair work was completed in two weeks. After all repairs were completed, reinforcing steel strains and deck-slab displacements at midspan were recorded for a 25 ton test truck traveling across the bridge. The comparison of the recorded test data both before and after the bridge repair indicated that the primary reinforcing steel stresses were reduced by 30 to 40 percent and the secondary reinforcing steel stresses were reduced by 20 to 40 percent. The midspan deflections of the deck slabs were decreased by 15 to 20 percent.

M. J. Chajes et. al. (1995) tested twelve reinforced concrete T-beams to study the effect of using externally applied composite fabric as a method of increasing beam shear capacity. Three different types of composite were used in the study so that the effects of the fabric modulus of elasticity and tensile strength could be examined. The selection of the adhesive was based on the results of pull-off tests using 25 mm wide fabric strips bonded to a concrete specimen. Test results for eight beams strengthened for shear were compared with the corresponding results for the four control

beams. Debonding of the fabric from the concrete did not occur in any of the tests. The behavior of the strengthened beams was similar to that exhibited by the control beams both before and after cracking. Before cracking in the beam occurred, recorded strains in the fabric were very low. However, after cracking, the fabric strains increased significantly until failure occurred. The test results indicated that externally bonded composite fabric increased the ultimate shear strength by 60 to 150 percent. An analytical method was presented for predicting the ultimate shear capacity of beams strengthened with bonded composite.

A. Nanni (1995) reported several examples of bridges in Japan strengthened with FRP. The Hata Bridge was strengthened to accommodate additional loads caused by the construction of larger windbreak walls. The strengthening project began in the spring of 1994 with the erection of a suspended light scaffolding to facilitate application of the composite. Approximately 100 m^2 of CFRP was used in the project. The effectiveness of the strengthening method was examined by conducting an on site load test which indicated a considerable reduction in reinforcing steel strains. In another project, the Hiyoshikura Bridge was strengthened to increase the load rating of the structure. The soffit of the deck slab suffered from extensive flexural cracking. The cracks were sealed and approximately 164 m^2 of two ply CFRP was applied to the underside of the deck slab. Upon the completion of the repair work, moving vehicle load tests were conducted. The results of these tests indicated that a 30 to 40 percent reduction in reinforcing steel stresses was achieved.

CHAPTER TWO
BRIDGE REHABILITATION

DESCRIPTION OF BRIDGE

The bridge selected for rehabilitation was built in 1952 and is located on Alabama Highway 110. It has a 7.32 m wide roadway with a 457 mm safety curb, and consists of seven 10.36 m simple spans with an East-West orientation. It was designed in accordance with specifications of the Alabama State Highway Department for an AASHTO H15-44 design load. The primary construction materials are Class "A" bridge concrete and structural carbon steel. All steel reinforcement has deformations in accordance with ASTM-A-305-49 and is intermediate grade new billet or rail steel, as permitted in the specifications.

The bridge deck consists of a 152 mm thick slab with shrinkage and temperature reinforcement of #4 bars spaced at 330 mm on center, as show in Figure 2.1. Transverse reinforcement is provided by #4 bars spaced at 279 mm on center.

Four standard reinforced concrete girders support the deck. Figure 2.2 shows a cross sectional view of the structure. The girders are spaced transversely at 1700 mm clear spacing. Tensile reinforcement for each girder consists of two layers of #11 rebar spaced as shown in Figure 2.3. Shear reinforcement consists of #4 double leg stirrups spaced as shown in Figure 2.4. The bridge girders are subjected to a maximum dead load moment of 172 kN-m, which corresponds to a dead load stress of 58.12 Mpa in the reinforcement at midspan. The factored load moment capacity was calculated to be 380 kN-m. A plot of the girder's factored load shear capacity along the length of the span is given in Figure 2.5

The bridge rehabilitation procedure was implemented in 4 basic steps: surface preparation composite positioning and installation, epoxy preparation, and pressure application. Each of these steps is described in this chapter. The composites were installed in October of 1995.

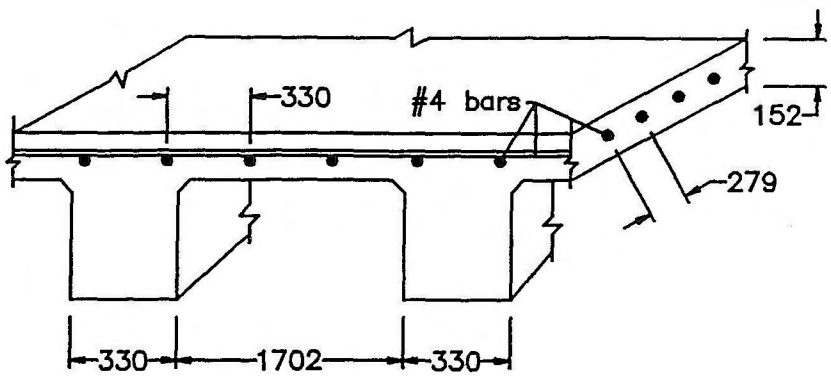

Figure 2.1 Reinforcement of the Concrete Slab (All Dimensions are mm)

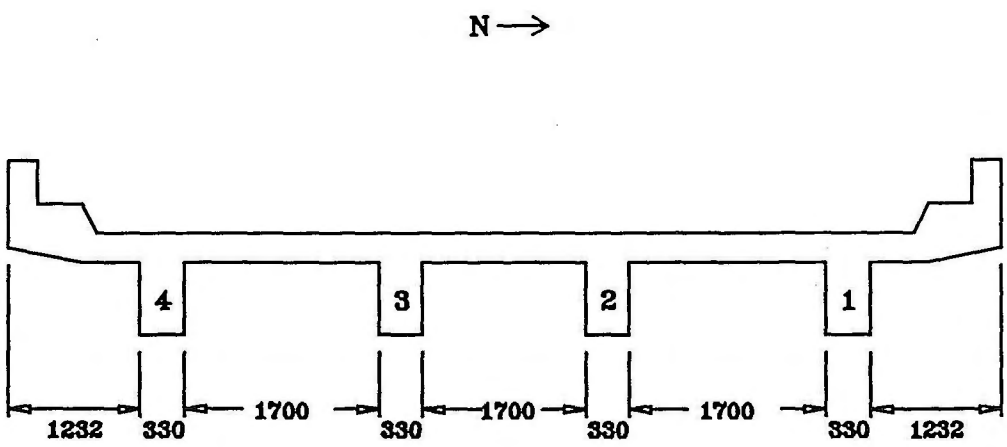

Figure 2.2. Bridge Cross Section (All Dimensions are mm)

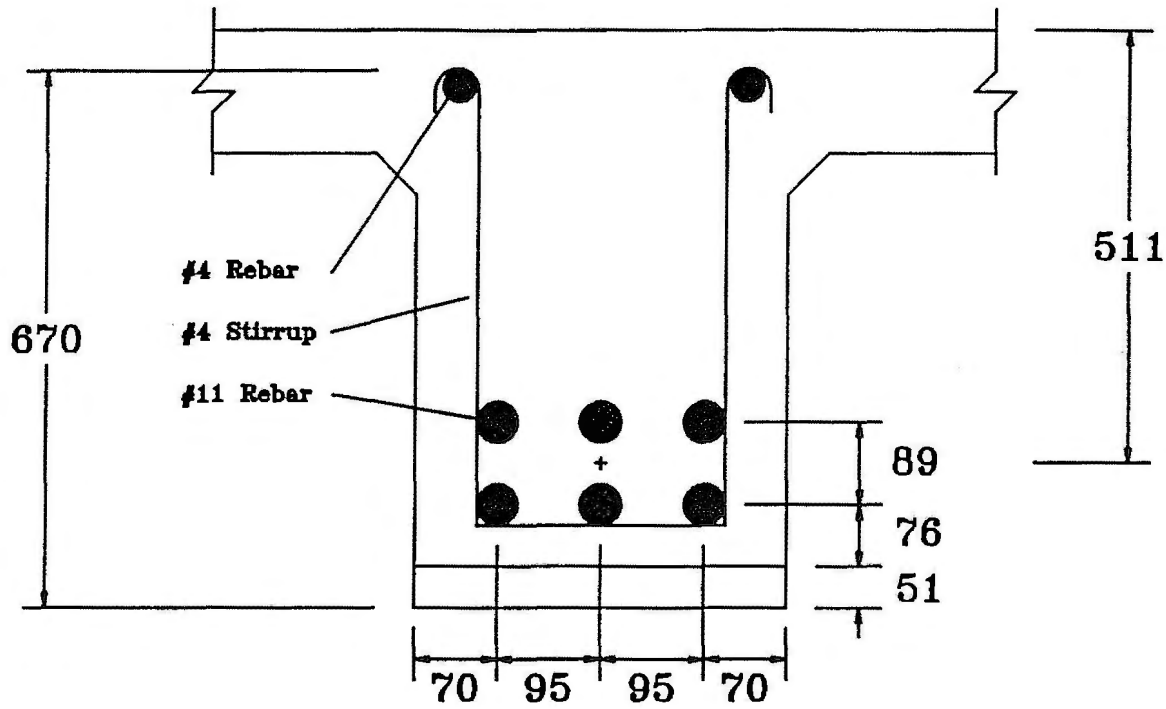

Figure 2.3. Girder Cross Section (All Dimensions are mm)

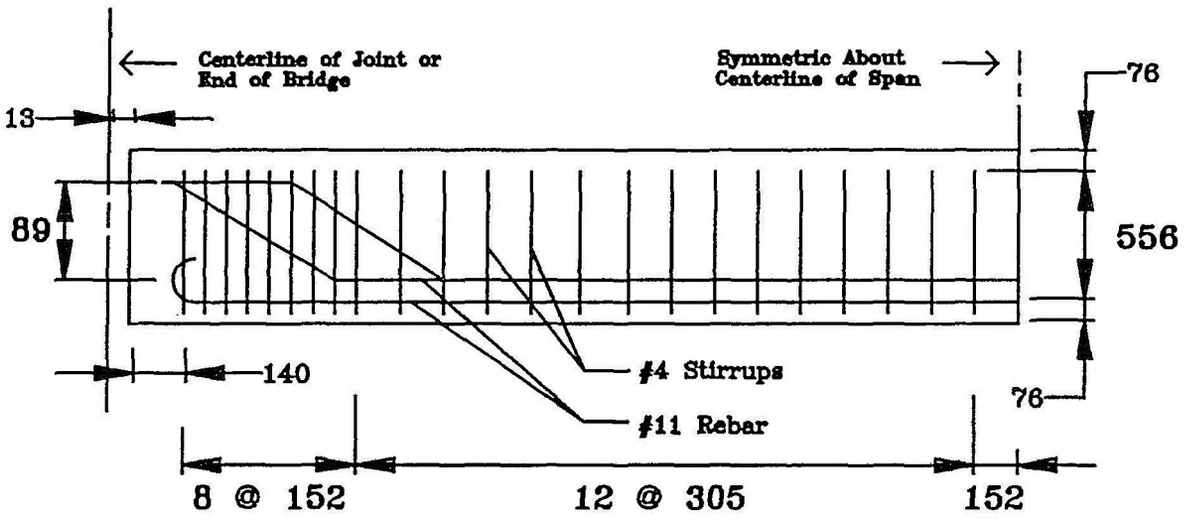

Figure 2.4. Elevation View of Girder Showing Shear Reinforcement
(All Dimensions are mm)

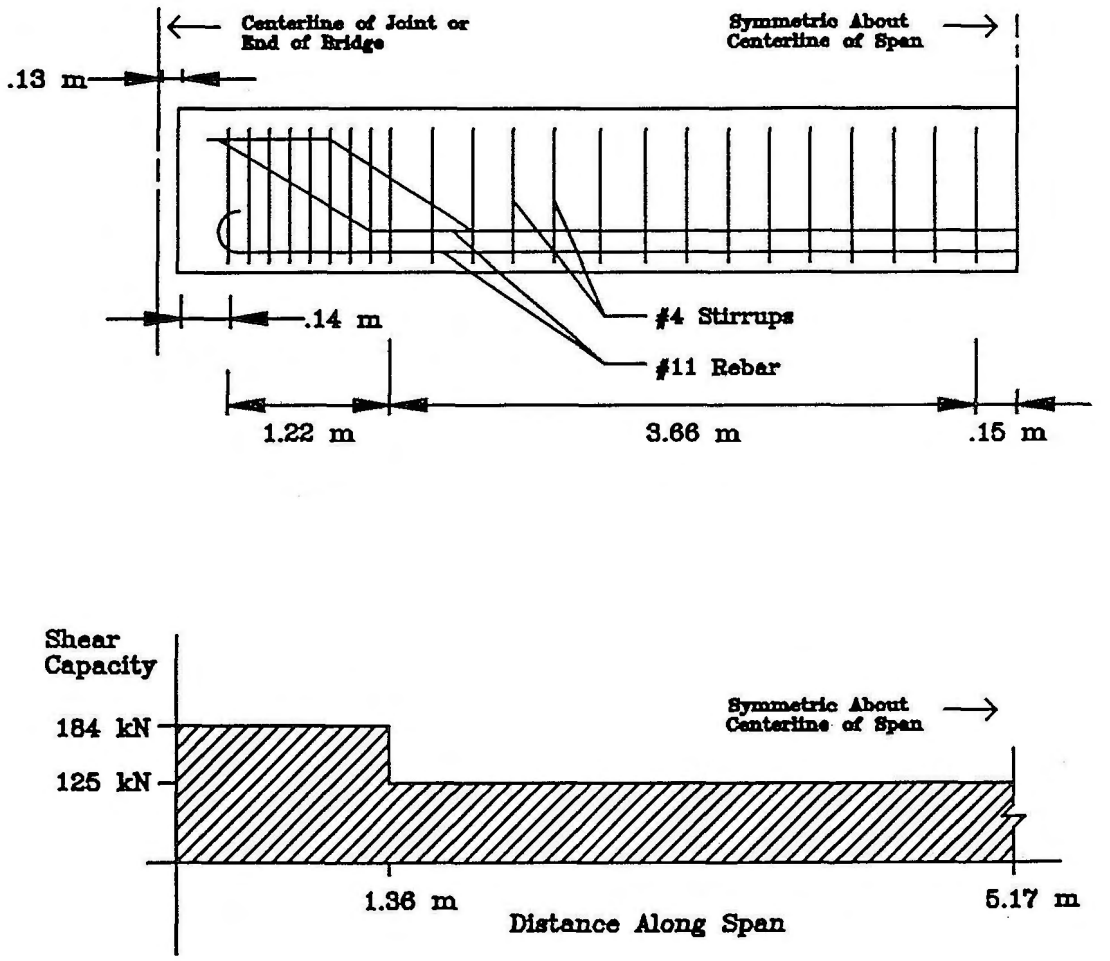

Figure 2.5. Stirrup Spacing and Shear Capacity Along Span

SURFACE PREPARATION OF BRIDGE GIRDERS

To insure the integrity of the bond of the FRP laminates, with the surface of concrete, preparation of the concrete surface was required. First, the bonding surface was smoothed so that the composite would be in full contact with the girder surface. This leveling process was accomplished with a hand held grinder. Areas of extreme roughness on the concrete surface were ground down until relatively flat. Surface flatness was ascertained by placing a yardstick along the girder surface and observing the completeness of contact between the two.

To provide a suitable bonding surface to accommodate the adhesive used to attach the composites, the concrete girders were abraded by sandblasting the girders until the coarse aggregate became visible. The girders were then pressure washed with a solution of mild detergent and hot water to remove the excess dust, grease and other substances that might adversely affect the bond between the girder and the composite.

SURFACE PREPARATION OF COMPOSITES

The smooth surfaces of the composites were scuffed using a 100 grit sanding disc on a hand held rotary sander. The composite plates were laid flat on a table with the girder contact surface facing upward. The surfaces were sanded using a back and forth motion across the width of the composite, along the entire length of the plate. For the plates that were to be spliced together, the outside surface of the last 0.6 m of the ends to which the splice plates were to be attached were also prepared in the same manner. The surfaces were then cleaned with methyl-ethyl-ketone (MEK) to remove excess dust.

COMPOSITE POSITIONING AND PROPERTIES

To facilitate bonding the composites to the girders, each bridge girder was divided into three sections: west, middle and east. Each girder section length matched the length of the composite plate to be attached to that face. A girder section consisted of three surfaces: the north face, south face, and

bottom face. The position of each composite plate was then outlined on the girders. Figures 2.6 and 2.7 illustrate the positions of the FRP plates. Each glass fiber reinforced plastic (GFRP) plate was 356 mm wide, and was positioned so that its bottom edge was 51 mm from the bottom edges of the north and south face of each girder. The carbon fiber reinforced plastic (CFRP) plates were 267 mm wide and were centered on the bottom face of each girder. The splice plates for both the GFRP and CFRP full length plates, were also 356 mm wide and 267 mm wide, respectively, and were 914 mm long. The splice plates were centered lengthwise over the joint between the two full length plates being spliced.

The GFRP plates had overall dimensions of 3.28 m x 356 mm x 1 mm. The unidirectional fibers were oriented parallel to the longitudinal axis of the plate. The GFRP plates had a tensile strength and modulus of elasticity of 448 MPa and 23,720 Mpa, respectively. The CFRP plates had overall dimensions of 3.09 m x 267 mm x 1.3 mm. The unidirectional fibers were oriented parallel to the longitudinal axis of the plate. The CFRP plates had a tensile strength and modulus of elasticity of 1,194 Mpa and 121,420 Mpa, respectively.

GENERAL DESCRIPTION OF REHABILITATION PLAN

The FRP plates were applied to two girders simultaneously, one section at a time, to all three surfaces of each section, with the exception of girder 1 (the northernmost girder). Girder 1 had only the CFRP plates applied to the bottom surface, and served as a standard of comparison to investigate the effects of the GFRP plates bonded to the sides of the other girders. The bridge traffic was restricted during application of the FRP plates, and for a minimum of 6 hours after application until the adhesive bond was set. A uniform pressure of at least 0.034 Mpa was applied over the entire surface of the composite plates for the 6 hours required for curing the adhesive. This pressurization was implemented through a vacuum bag covering all three surfaces of the girder section. The vacuum bag was connected by a hose to a vacuum pump powered by an electric generator. The vacuum pump had

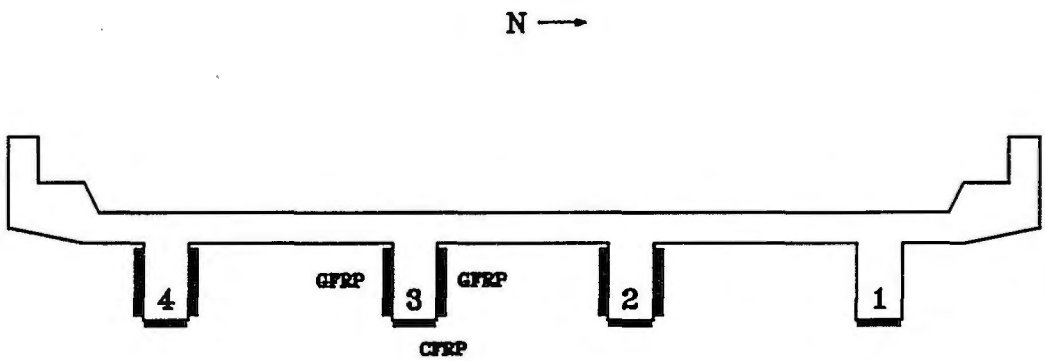

Figure 2.6. Bridge Cross Section Showing Positions of GFRP and CFRP

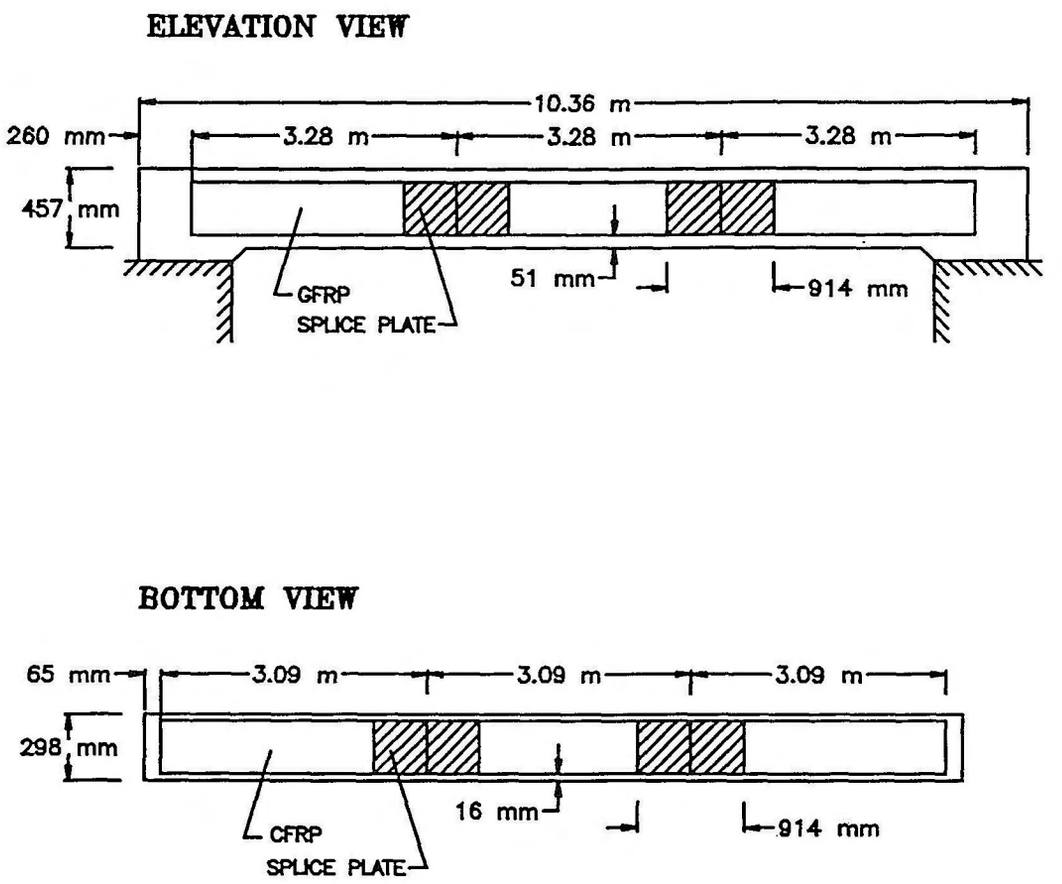

Figure 2.7. Elevation and Bottom Views of Bridge Girder Showing FRP Positions

sufficient capacity to provide the required vacuum for two girder section bags simultaneously. Therefore, the composite plates were applied to one section of two adjacent girders at the same time. A more detailed description of the installation procedure is provided in the next section.

The FRP plates were bonded to the concrete with Dexter-Hysol EA9460 structural adhesive, a two component epoxy that combines high strength with low visctosity, thus enhancing its conduciveness to mixing. The adhesive has a tensile lap shear strength of 24.13 Mpa at 25° C and a peel strength of 5.3 N per linear millimeter. The epoxy has a mix ratio of 1:1 by volume and a pot life of 55 minutes, allowing ample time for application. For this project, two liters of epoxy (one liter of each component) were mixed for each girder section (three full length pieces of FRP per section).

INSTALLATION PROCEDURE

The first step in the FRP installation procedure was to de-grease the surface of both the concrete and the composite plates with MEK. The MEK was applied to the girder surfaces with a spray applicator. Cloth rags soaked with MEK were used to clean surfaces of the composite plates. The composite plates were kept out of direct sunlight in order to maintain them at the ambient temperature underneath the bridge.

The vacuum bag was then prepared. The first step in this preparation was to mark the surface of the concrete girders with the position of the outside edges of the bag. A sheet of 6 mil thick plastic was then cut to the size required to cover the FRP girder section. To facilitate bag handling, the actual size of the bag was cut somewhat larger than the required dimensions. The bag was also marked to match the FRP position lines on the concrete. This marking of both the bag and the concrete girder surface greatly facilitated the process of adhering the vacuum bag to the surface of the girders. The adhesive used to bond the sheet plastic to the concrete girder surfaces was GM Super 77 Spray Adhesive. Prior to the affixing the sheet plastic to the concrete girder surface, the bag was lined and crossed with small ropes. These ropes provided veins through which the vacuum pressure could be

distributed uniformly to all areas of the bag.

The vacuum pressure applied to the bag was generated by an electric powered, 0.37 kw Welch Director 8915 vacuum pump. This pump had an air flow rate of 22.3 liters per minute and was capable of providing the required minimum 0.034 Mpa of uniform pressure for setting of the epoxy. The vacuum line from the pump was attached to a 114 liter tank from which another line ran to the inlet of the bag. The tank acted as a reservoir in which a sufficient amount of pressure could accumulate to insure that the air flow rate through the vacuum line would be large enough to evacuate the bag rapidly. The pump was turned on and allowed to evacuate the tank for at least thirty minutes before the entire FRP application process was completed, at which time the tank valve was opened. The vacuum causes the bag to compress against the composite plates, providing the necessary uniform pressure during the cure time.

Another major step in the installation process was the application of the epoxy to the composite. The two components of the epoxy were first combined in a large can, at a 1:1 volumetric ratio. The epoxy components were mixed with a mixing tool attached to a hand held drill until a uniform, homogenous mixture was obtained. The epoxy was then spread evenly over the entire surface of the composite plate to a thickness of approximately 1.5 mm. The composite plate was then immediately affixed to the girder, taking extreme care to position the plate to match the boundaries previously marked on the concrete. Direct pressure was applied over the surface of the plate with a hand held roller. It required, a splice plate was also installed in this step of the procedure. This procedure was repeated on the next girder section in a similar manner.

Approximately fifteen minutes prior to the time that the vacuum bag was to be installed, each surface of the concrete-vacuum bag interface was sprayed with adhesive. This was done to allow the spray adhesive to reach a level of maximum adherence before the bag was installed. The bag was then installed, making sure that the position of the adhesive on both the plastic and the concrete matched.

Hand pressure was applied along the perimeter of the bag until the concrete-bag interface was in full contact, except for a small area of approximately five inches in length. This small length was left unsealed to accommodate insertion of the vacuum hose. The hose entered the bag as close as possible to one of the air passages provided by the small ropes. The bag was sealed around the vacuum line, using a putty sealant to seal around the line inlet. The bag was further secured against leakage by lining the perimeter with duct tape.

After the bag had been installed on one girder section, the valve controlling the vacuum was opened. The composite was then applied to another girder section in exactly the same manner. The vacuum tank provided separate outlets for each vacuum bag, and the vacuum system was capable of providing a minimum of 0.034 Mpa of pressure to both bags simultaneously. After the installed composite plates were subjected to a uniform pressure for at least six hours, a sufficient set of the epoxy was achieved and the pressure apparatus was removed.

CHAPTER THREE
FIELD LOAD TESTS

Field load tests were performed so that comparisons of the structural behavior of the bridge before and after application of the FRP laminates could be made. The bridge behavior was quantified by measurements of vertical mid-span deflections of the bridge girders, strains in the primary flexural reinforcement, strains in the FRP laminates, and concrete strains on the surface of the bridge beams. Measurements were made for both static and dynamic loading conditions using two identical trucks. The bridge instrumentation plan and details of the load tests are described in this chapter.

INSTRUMENTATION PLAN

Electrical resistance foil strain gages were used to measure the strain response to the load in the rebar, composite plates, and on the surfaces of the concrete girders both before and after the FRP was installed. The gages had preattached lead wires with polyamid encapsulation and were self temperature compensating. All gages had a nominal resistance of 350 ohms. After each gage was mounted, the preattached lead wires were soldered to light gage stranded wire which was connected to a terminal block. Electrical tape was applied to insulate the wires from each other. The whole assembly was then covered with a waterproof neoprene pad with an adhesive backing to protect it from the environment.

Two gages were installed, approximately 100 mm on each side of midspan, on the middle rebar of the bottom row of tensile reinforcement in each girder, as shown in Figure 3.1. Data from only one of the gages was sufficient; the other was provided for redundancy. The gages attached to the rebar had a gage length of 6.35 mm. Strain gages with a gage length of 101.60 mm were installed on the surfaces of the girders, as shown in Figure 3.1. Each girder had a strain gage installed on its inside chamfer at midspan. Prior to FRP application, each girder also had a gage installed on its inside surface 50 mm from the chamfer, as shown in Figure 3.1. This gage was removed before the FRP was installed.

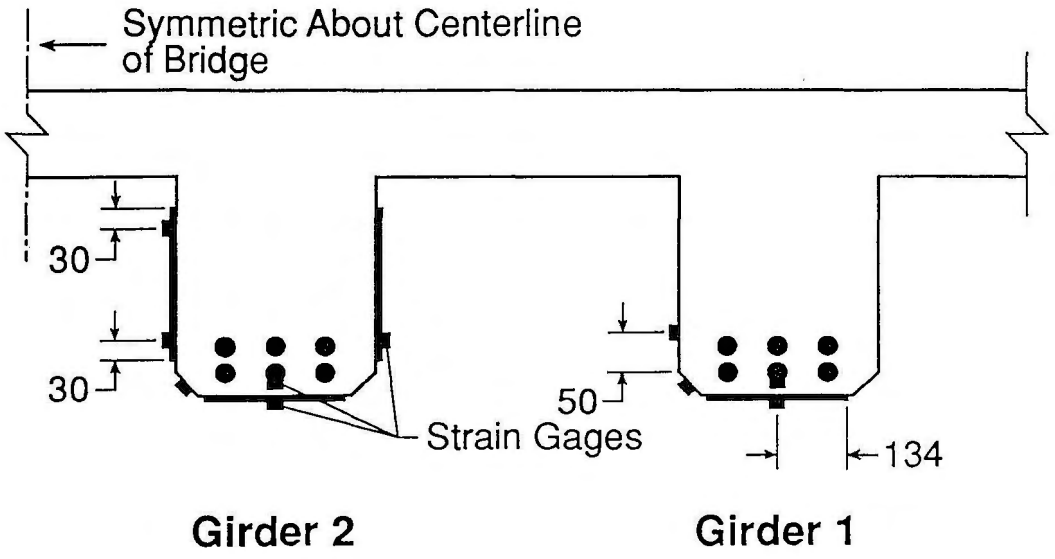

Figure 3.1. Locations of Strain Gages on Girder Cross Section
(All Dimensions are mm)

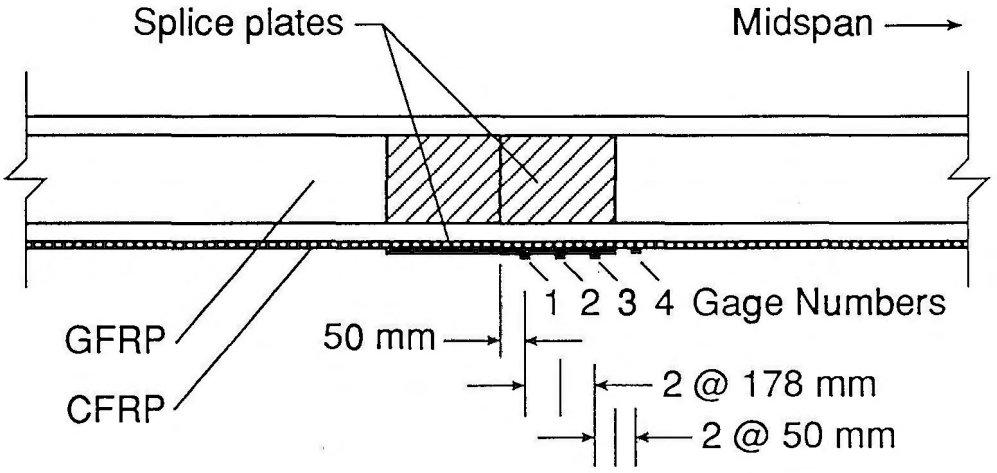

Figure 3.2. Strain Gages Attached to Splice Plate of Girder 2

After application of the FRP, gages were installed on the surfaces of the composite plates. Figure 3.1 shows the position of these gages. These gages had a gage length of 12.70 mm. All gages applied to the FRP were at midspan, except for 4 gages that were installed to the bottom plate splice at the East end of beam 2, as shown in Figure 3.2.

Vertical deflections were measured at midspan of each girder with Linear Variable Differential Transformers (LVDT's). The LVDT's had a range of 2.54 mm, a resolution of .003 mm, and operated with a linearity of less than 0.25% of full scale.

All strain gages were connected to a data acquisition system using a three-wire quarter bridge connection. Shielded cable for the strain gages and LVDT's was used to reduce the electronic noise recorded with the data. The shielded cables were attached to terminal blocks at the gages and were routed to the data acquisition van where they were connected to the data acquisition system through screw terminal blocks.

DESCRIPTION OF LOAD TESTS

Load test were performed both before and after application of the FRP with load test trucks of known axle configuration and weight distribution. The two vehicles used for the load tests are identical load test trucks owned and operated by the Alabama Department of Transportation (ALDOT). These trucks have a 3-axle configuration as shown in Figure 3.3. ALDOT test loading case LC5 was used. This provided a gross vehicle weight of 173 KN distributed as shown in Figure 3.3.

Static and dynamic tests were performed on the bridge. For the static tests, the trucks were positioned with the center axle at midspan in 4 different transverse locations, as shown in Figures 3.4 and 3.5. The positions were chosen to simulate the most extreme load conditions possible. Before the trucks were positioned on the bridge, the data acquisition system was balanced to establish a reference point of zero live load strain. After a zero reference point was established, the trucks were directed to Position 1. Data was then recorded for each sensor. The true value for the live load deflections and

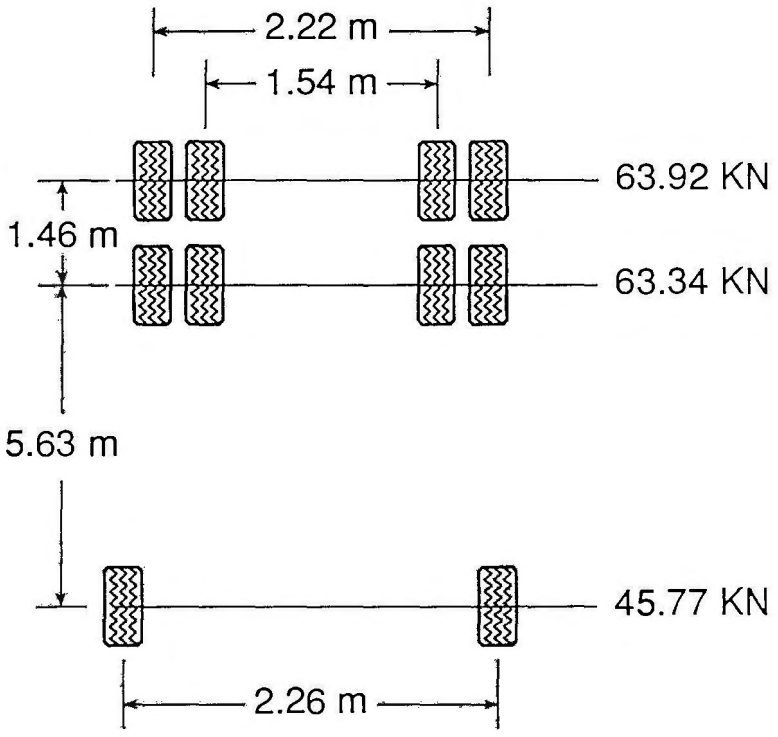

Figure 3.3. Load Truck Configuration

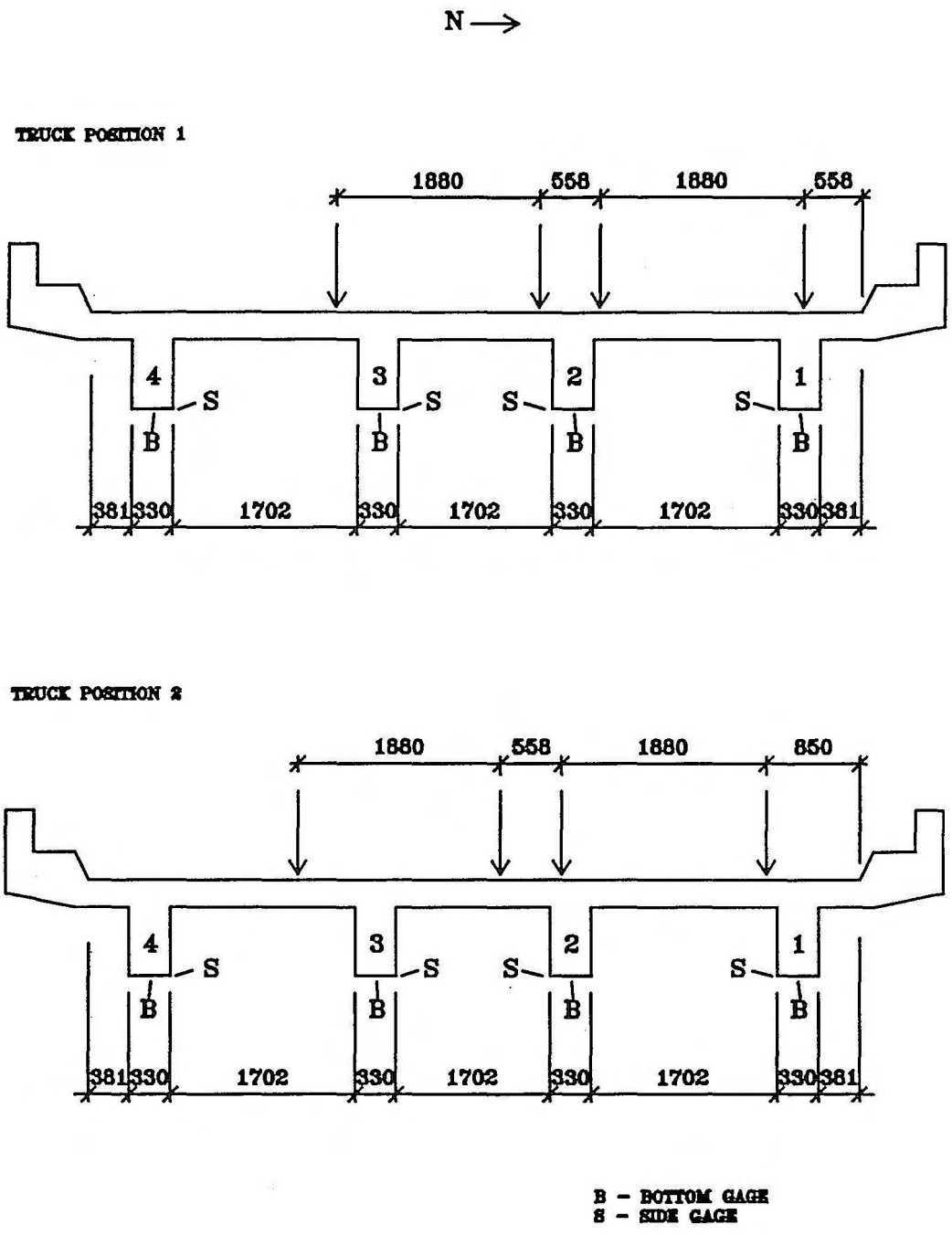

Figure 3.4. Load Truck Positions 1 and 2 (All Dimensions are mm)

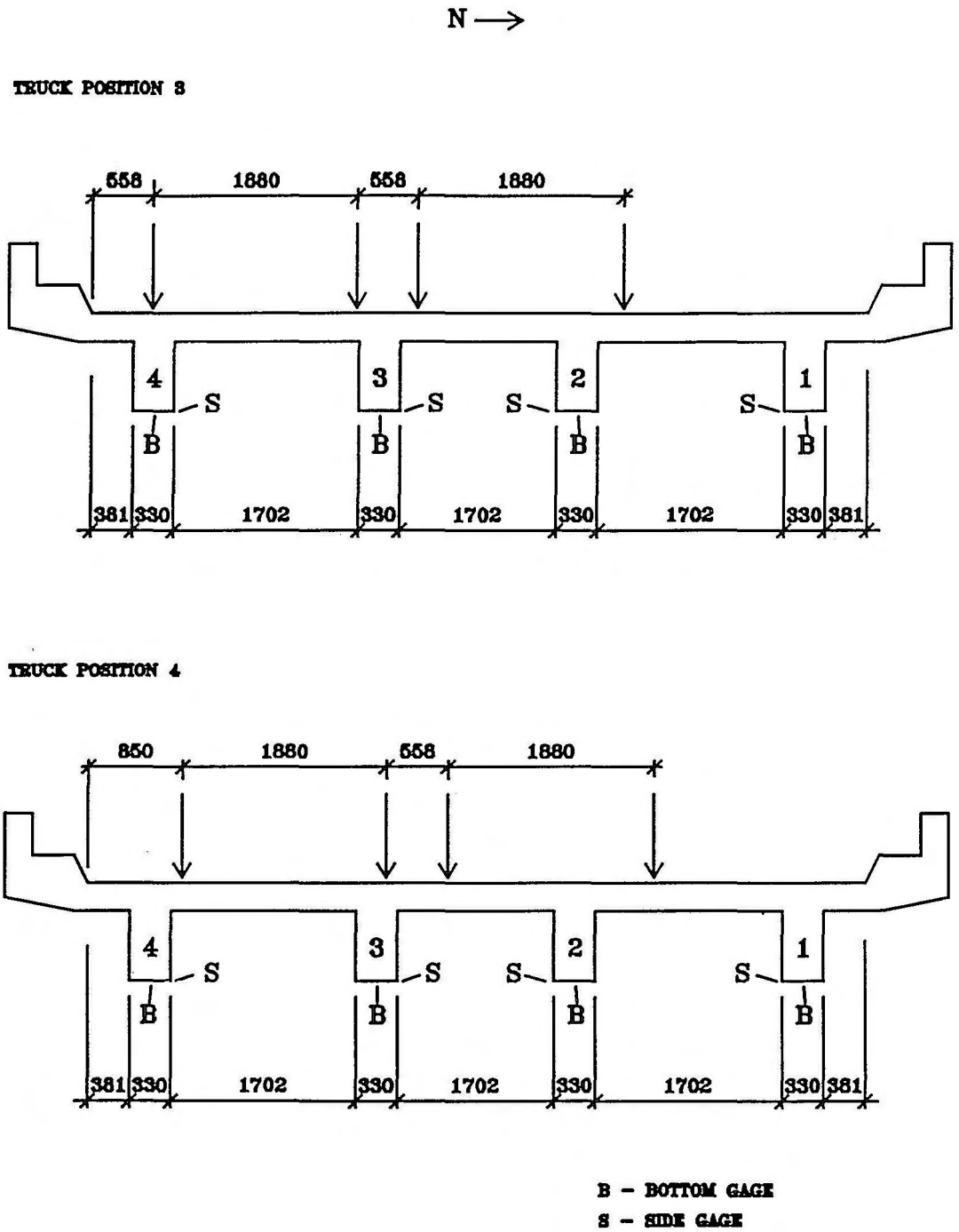

Figure 3.5. Load Truck Positions 3 and 4

strains were determined by subtracting the values taken for each sensor at the zero reference point from the values recorded for each sensor when the test trucks were on the bridge. The trucks were then moved off of the bridge and the whole sequence was repeated for Positions 2 through 4. Static tests were performed twice for each test position. These tests were performed both before and after the FRP was installed.

Dynamic tests were conducted with the same test vehicles traveling side by side at 80 kilometers per hour. Multiple tests were carried out for redundancy. Data was recorded for the trucks traveling in both directions across the bridge. A zero data reference point was established in the same manner described for the static tests. The trucks were then driven across the bridge. A spotter with a clear view of the trucks and the bridge communicated with the data acquisition system operator via a hand held radio. The spotter instructed the system operator when to begin and stop recording data. After the trucks crossed the bridge, the test file number and the speed and direction of the trucks were recorded. This same sequence was then repeated several more times. Prior to FRP installation, 3 load tests were performed with the test trucks traveling westbound and 2 tests were performed with the test trucks traveling eastbound. After FRP application, 4 tests were performed with the test trucks traveling eastbound. An additional static test was performed after FRP application with the tests trucks centered in the traffic lanes, as shown in Figure 3.6. This was done for comparisons of data from the dynamic tests to static data with the trucks in the same transverse position.

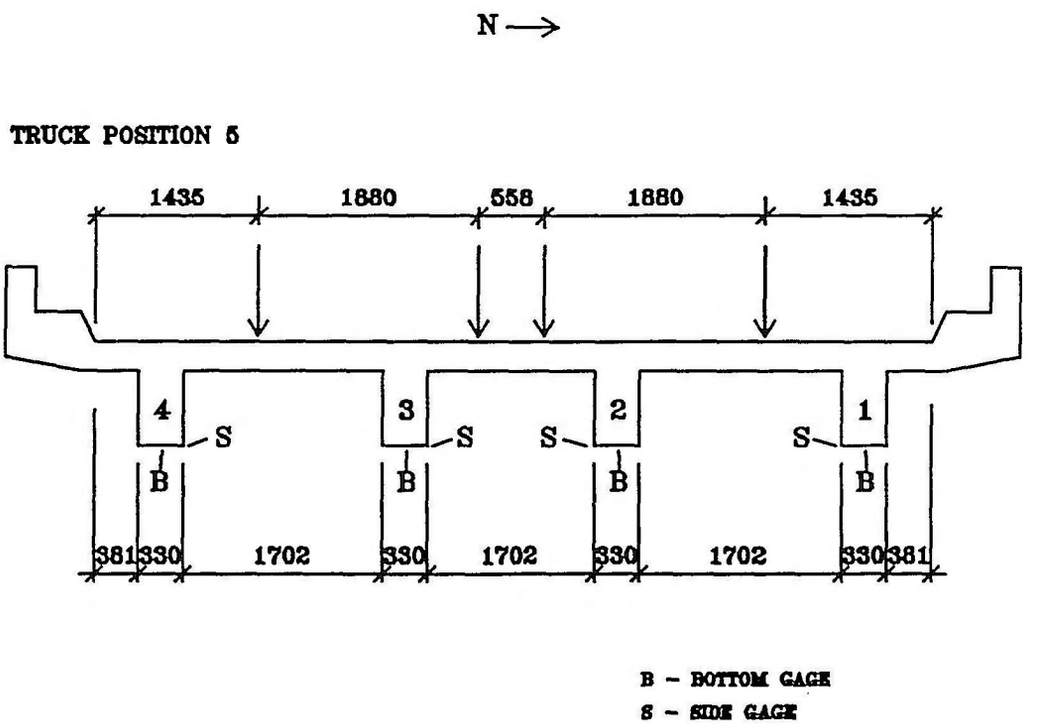

Figure 3.6. Load Truck Position 5

CHAPTER FOUR
RESULTS OF LOAD TESTS

INTRODUCTION

To evaluate the effects of externally bonding FRP plates to the surfaces of the bridge girders, both dynamic and static load tests were performed. These tests, as well as the instrumentation used to gather the test data, are described in Chapter Three. The results of these tests are presented in this chapter. Data is presented to quantify the effect of the FRP reinforcement on rebar strains and girder deflections. Strain compatibility between the rebar and the CFRP is investigated. The effectiveness of the splice plates in transferring the load between the primary FRP reinforcement plates is also discussed. Finally, conclusions are drawn to summarize the overall performance of the FRP strengthening system.

DATA ACQUISITION AND REDUCTION

As described in Chapter Three, load tests were performed in each of the four truck loading positions shown in Figures 3.4 and 3.5. These tests were performed both before and after application of the FRP. For each loading position, strain or deflection values were recorded for each sensor (strain gage or deflection sensor). Measurements for each position were repeated four times. A single value was calculated for each sensor for each position by averaging the values recorded for that sensor in each of the four tests. The rebar strain data from each test and the average values are listed in Tables 4.1 and 4.2. The column headings in those tables indicate the strain gage location. For example, the gage attached to the rebar in girder 1, 100 mm to the west of midspan, is designated R1W. Similarly, the gage R1E is located in girder 1, 100 mm to the East of midspan. When the second round of load tests were performed, after application of the RFP, some of the gages were malfunctioning. In Table 4.1, an entry of "NA" indicates that the gage was not working properly and the data is not available. The girder midspan deflection results from the static tests are shown in Tables 4.3 and 4.4. Strains

Table 4.1. Rebar Strains from Static Tests - Before FRP Application

Loading		Strain Gage Data (microstrain)							
		R1W	R1E	R2W	R2E	R3W	R3E	R4W	R4E
Position 1	Test 1	419	375	518	458	418	388	194	199
	Test 2	420	375	520	459	408	379	179	182
	Test 3	401	359	508	450	406	376	178	184
	Test 4	418	373	520	459	407	377	178	182
	Avg	**415**	**371**	**517**	**457**	**410**	**380**	**182**	**187**
Position 2	Test 1	379	340	498	441	429	398	224	229
	Test 2	374	336	498	439	423	391	220	225
	Test 3	378	339	504	446	415	385	212	218
	Test 4	374	336	497	440	421	391	221	226
	Avg	**376**	**338**	**499**	**442**	**422**	**391**	**219**	**225**
Position 3	Test 1	196	176	411	362	530	493	407	414
	Test 2	199	178	411	362	523	486	407	415
	Test 3	192	172	408	359	531	492	407	414
	Test 4	188	169	401	353	527	489	399	406
	Avg	**194**	**174**	**408**	**359**	**528**	**490**	**405**	**412**
Position 4	Test 1	234	210	429	378	511	475	363	369
	Test 2	241	217	435	383	507	471	357	364
	Test 3	229	207	425	375	508	473	361	367
	Test 4	238	214	431	379	511	473	360	367
	Avg	**236**	**212**	**430**	**379**	**509**	**473**	**360**	**367**

Table 4.2. Rebar Strains from Static Tests - After FRP Application

Loading		Strain Gage Data (microstrain)							
		R1W	R1E	R2W	R2E	R3W	R3E	R4W	R4E
Position 1	Test 1	391	351	NA*	422	372	348	NA	172
	Test 2	381	343	NA	424	373	347	NA	175
	Test 3	NA	354	NA	420	359	334	NA	162
	Test 4	382	344	NA	427	374	348	NA	172
	Avg	**385**	**348**	**NA**	**423**	**370**	**344**	**NA**	**170**
Position 2	Test 1	369	331	NA	410	386	360	NA	207
	Test 2	355	320	NA	408	385	359	NA	209
	Test 3	357	319	NA	419	391	364	NA	202
	Test 4	361	324	NA	409	381	354	NA	203
	Avg	**361**	**324**	**NA**	**412**	**386**	**359**	**NA**	**205**
Position 3	Test 1	189	170	NA	330	463	432	NA	364
	Test 2	194	174	NA	333	467	434	NA	371
	Test 3	181	163	NA	330	476	445	NA	373
	Test 4	184	164	NA	333	480	448	NA	373
	Avg	**187**	**168**	**NA**	**332**	**472**	**440**	**NA**	**370**
Position 4	Test 1	221	199	NA	346	452	423	NA	333
	Test 2	218	204	NA	347	447	418	NA	333
	Test 3	222	196	NA	345	451	421	NA	326
	Test 4	228	199	NA	347	455	424	NA	330
	Avg	**222**	**200**	**NA**	**346**	**451**	**422**	**NA**	**331**

*NA = Not Available

Table 4.3. Girder Deflections from Static Tests - Before FRP Application

Loading		Midspan Deflection (mm)			
		Girder 1	Girder 2	Girder 3	Girder 4
Position 1	Test 1	5.8	7.8	7.1	3.3
	Test 2	6.0	7.9	7.0	3.1
	Test 3	6.0	7.9	6.9	3.1
	Test 4	6.1	7.9	7.0	3.1
	Avg	**6.0**	**7.9**	**7.0**	**3.2**
Position 2	Test 1	5.4	7.7	7.3	3.7
	Test 2	5.4	7.7	7.3	3.7
	Test 3	5.5	7.7	7.2	3.6
	Test 4	5.4	7.7	7.3	3.8
	Avg	**5.4**	**7.7**	**7.3**	**3.7**
Position 3	Test 1	3.0	6.5	8.6	6.4
	Test 2	3.0	6.4	8.5	6.4
	Test 3	3.1	6.5	8.6	6.4
	Test 4	3.1	6.5	8.6	6.2
	Avg	**3.1**	**6.5**	**8.6**	**6.3**
Position 4	Test 1	3.6	6.9	8.3	5.7
	Test 2	3.7	6.9	8.3	5.6
	Test 3	3.6	6.9	8.3	5.7
	Test 4	3.7	7.0	8.3	5.6
	Avg	**3.6**	**6.9**	**8.3**	**5.6**

Table 4.4. Girder Deflections from Static Tests - After FRP Application

Loading		Midspan Deflection (mm)			
		Girder 1	Girder 2	Girder 3	Girder 4
Position 1	Test 1	5.7	7.2	6.2	2.7
	Test 2	5.5	7.3	6.3	2.8
	Test 3	5.6	7.2	6.3	2.8
	Test 4	5.5	7.3	6.4	2.9
	Avg	**5.6**	**7.3**	**6.3**	**2.8**
Position 2	Test 1	5.1	7.2	6.6	3.2
	Test 2	5.2	7.1	6.5	3.2
	Test 3	5.3	7.1	6.6	3.3
	Test 4	5.1	7.1	6.6	3.4
	Avg	**5.2**	**7.1**	**6.6**	**3.3**
Position 3	Test 1	2.9	6.0	7.7	5.6
	Test 2	2.9	6.0	7.8	5.6
	Test 3	3.0	6.0	7.6	5.5
	Test 4	3.1	6.0	7.6	5.5
	Avg	**3.0**	**6.0**	**7.7**	**5.5**
Position 4	Test 1	3.4	6.3	7.4	4.9
	Test 2	3.5	6.3	7.5	5.0
	Test 3	3.5	6.3	7.4	5.0
	Test 4	3.5	6.3	7.4	5.0
	Avg	**3.5**	**6.3**	**7.4**	**5.0**

were also measured at selected locations on the surfaces of the FRP plates. The strains recorded on the bottom of the CFRP plates at midspan and on the CFRP splice plate at the east end of girder 2 are shown in Tables 4.5 and 4.6, respectively.

Prior to application of the FRP, dynamic load tests were performed with test vehicles traveling in both eastbound and westbound directions. The rebar strain data recorded for these tests are show in Table 4.7. After FRP application, the load tests were performed with the trucks traveling eastbound only because a traffic accident a short distance from the bridge restricted traffic flow. The rebar strains recorded for those tests are shown in Table 4.8. Girder midspan deflection results for the dynamic tests are shown in Tables 4.9 and 4.10. The strain and deflection values that appear in Tables 4.7 and 4.10 are the peak values recorded over the time interval beginning just before the truck rolled onto the bridge until just after the truck rolled off of the bridge.

Table 4.5. CFRP Strains from Static Tests

Loading		Strain Data (microstrain)			
		Girder 1	Girder 2	Girder 3	Girder 4
Position 1	Test 1	371	423	NA*	168
	Test 2	366	432	NA	178
	Test 3	371	428	NA	180
	Test 4	363	432	NA	185
	Avg	**368**	**429**	**NA**	**178**
Position 2	Test 1	338	424	NA	211
	Test 2	342	413	NA	210
	Test 3	349	415	NA	217
	Test 4	336	413	NA	220
	Avg	**341**	**416**	**NA**	**215**
Position 3	Test 1	172	334	NA	388
	Test 2	173	337	NA	389
	Test 3	179	335	NA	381
	Test 4	182	337	NA	392
	Avg	**177**	**336**	**NA**	**388**
Position 4	Test 1	208	348	NA	338
	Test 2	210	351	NA	344
	Test 3	210	349	NA	349
	Test 4	215	352	NA	350
	Avg	**211**	**350**	**NA**	**345**

*NA = Not Available

Table 4.6 Strains Measured on CFRP Splice Plate (microstrain)

Gage*	Test	Position 1	Position 2	Position 3	Position 4
Gage 1	Test 1	558	535	443	470
	Test 2	556	533	437	467
	Test 3	551	514	442	460
	Test 4	566	543	442	467
	Avg	**558**	**531**	**441**	**466**
Gage 2	Test 1	552	529	421	446
	Test 2	539	519	417	444
	Test 3	534	508	418	440
	Test 4	535	515	420	440
	Avg	**540**	**518**	**419**	**443**
Gage 3	Test 1	434	428	340	362
	Test 2	430	414	339	360
	Test 3	426	409	338	355
	Test 4	432	411	340	356
	Avg	**431**	**416**	**339**	**358**
Gage 4	Test 1	540	529	414	442
	Test 2	539	518	417	447
	Test 3	539	517	421	444
	Test 4	542	521	429	447
	Avg	**540**	**521**	**420**	**445**

*See Figure 3.2 for gage locations.

Table 4.7. Peak Rebar Strains from Dynamic Tests - Before FRP Application

Test No.	Strain Gage Data (microstrain)							
	R1W	R1E	R2W	R2E	R3W	R3E	R4W	R4E
(a) Test Trucks Traveling Eastbound								
3	436	391	553	485	559	521	406	415
5	404	361	529	465	538	503	418	429
Avg	**420**	**376**	**541**	**475**	**549**	**512**	**412**	**422**
(b) Test Trucks Traveling Westbound								
1	475	424	687	604	763	712	584	592
2	500	449	728	639	772	721	562	572
4	490	439	713	627	770	720	599	611
Avg	**488**	**437**	**709**	**623**	**768**	**718**	**582**	**592**

Table 4.8. Peak Rebar Strains from Dynamic Tests - After FRP Application

Test No.	Strain Gage Data (microstrain)							
	R1W	R1E	R2W	R2E	R3W	R3E	R4W	R4E
(a) Test Trucks Traveling Eastbound								
1	408	367	NA*	434	468	438	NA	360
2	398	359	NA	439	479	448	NA	369
3	390	348	NA	472	536	501	NA	426
4	402	359	NA	469	518	483	NA	394
Avg	**400**	**358**	**NA**	**454**	**500**	**468**	**NA**	**387**

Table 4.9. Peak Girder Deflections from Dynamic Tests - Before FRP Application

Test No.	Midspan Deflection (mm)			
	Girder 1	Girder 2	Girder 3	Girder 4
(a) Test Trucks Traveling Eastbound				
3	6.5	8.9	9.5	6.5
5	6.0	8.5	9.3	6.8
Avg.	**6.3**	**8.7**	**9.4**	**6.7**
(b) Test Trucks Traveling Westbound				
1	7.1	11.0	12.5	8.9
2	7.4	11.5	12.8	8.7
4	7.2	11.3	12.7	9.3
Avg.	**7.2**	**11.3**	**12.7**	**9.0**

Table 4.10 Peak Girder Deflections from Dynamic Tests - After FRP Application

Test No.	Midspan Deflection (mm)			
	Girder 1	Girder 2	Girder 3	Girder 4
(a) Test Trucks Traveling Eastbound				
1	5.8	7.6	7.8	5.4
2	5.7	7.7	8.0	5.5
3	5.7	8.5	9.1	6.5
4	5.9	8.4	8.8	6.1
Avg	**5.8**	**8.1**	**8.4**	**5.8**

EFFECT OF CFRP ON REBAR STRESSES

The stresses that correspond to the rebar strains presented in Tables 4.1 and 4.2 are shown in Tables 4.11 and 4.12. The stresses were obtained by multiplying the strains by the elastic modulus of the steel (200,000 MPa). Table 4.13 compares the stresses from the static load tests prior to FRP application to those from static tests after FRP application. For the comparisons shown in Table 4.13, the calculated stresses in each girder are based on the same strain gage, both before and after the FRP was applied. The gages used were R1W, R2E, R3W, and R4E.

Table 4.13 indicates that the rebar stresses were reduced by application of the FRP. The reductions range from 4% in girder 1 for loading positions 2 and 3 to 12% in girder 3 for position 4. The average stress reduction for all girders is 8%. The results shown in Table 4.13 are presented graphically in Figures 4.1 and 4.2. These figures indicate that the largest rebar stresses are induced in the interior girders. The test trucks were positioned to give the most extreme loading conditions possible, hence the interior girders are loaded more heavily due to the special limitations presented by the bridge deck and curb. It is noted in Table 4.13 that the largest reduction in rebar stress is also found in an interior girder, girder 3.

For each test loading position, Table 4.13 indicates that the smallest strain reductions are always observed in girder 1. GFRP plates were not bonded to the sides of this girder, as shown in Figure 2.6. This indicates that the GFRP plates bonded to the girder sides had a significant effect on the overall stiffening of the bridge.

Tables 4.14 and 4.15 show the rebar stresses measured at midspan of each girder for the dynamic tests performed before and after FRP application, respectively. Comparisons are made in Table 4.16 to show the effect of the FRP on the rebar stresses. The comparisons are made using data for Eastbound test trucks both before and after applications of the FRP. The stress values that appear in Table 4.16 are taken from Tables 4.14 and 4.15. The information presented in Table 4.16 is

Table 4.11. Rebar Stresses from Static Tests - Before FRP Application

Loading		Rebar Stresses (MPa)							
		R1W	R1E	R2W	R2E	R3W	R3E	R4W	R4E
Position 1	Test 1	84	75	104	92	84	78	39	40
	Test 2	84	75	104	92	82	76	36	36
	Test 3	80	72	102	90	81	75	36	37
	Test 4	84	75	104	92	81	75	36	36
	Avg	**83**	**74**	**103**	**91**	**82**	**76**	**36**	**37**
Position 2	Test 1	76	68	100	88	86	80	45	46
	Test 2	75	67	100	88	85	78	44	45
	Test 3	76	68	101	89	83	77	42	44
	Test 4	75	67	99	88	84	78	44	45
	Avg	**75**	**68**	**100**	**88**	**84**	**78**	**44**	**45**
Position 3	Test 1	39	35	82	72	106	99	81	83
	Test 2	40	36	82	72	105	97	81	83
	Test 3	38	34	82	72	106	98	81	83
	Test 4	38	34	80	71	105	98	80	81
	Avg	**39**	**35**	**82**	**72**	**106**	**98**	**81**	**82**
Position 4	Test 1	47	42	86	76	102	95	73	74
	Test 2	48	43	87	77	101	94	71	73
	Test 3	46	41	85	75	102	95	72	73
	Test 4	48	43	86	76	102	95	72	73
	Avg	**47**	**42**	**86**	**76**	**102**	**95**	**72**	**73**

Table 4.12 Rebar Stresses from Static Tests - After FRP Application

Loading		Rebar Stresses (MPa)							
		R1W	R1E	R2W	R2E	R3W	R3E	R4W	R4E
Position 1	Test 1	78	70	NA*	84	74	70	NA	34
	Test 2	76	69	NA	85	75	69	NA	35
	Test 3	NA	71	NA	84	72	67	NA	32
	Test 4	76	69	NA	85	75	70	NA	34
	Avg	**77**	**70**	**NA**	**85**	**74**	**69**	**NA**	**34**
Position 2	Test 1	74	66	NA	82	77	72	NA	41
	Test 2	71	64	NA	82	77	72	NA	42
	Test 3	71	64	NA	84	78	73	NA	40
	Test 4	72	65	NA	82	76	71	NA	41
	Avg	**72**	**65**	**NA**	**82**	**77**	**72**	**NA**	**41**
Position 3	Test 1	38	34	NA	66	93	86	NA	73
	Test 2	39	35	NA	67	93	87	NA	74
	Test 3	36	33	NA	66	95	89	NA	75
	Test 4	37	33	NA	67	96	90	NA	75
	Avg	**37**	**34**	**NA**	**66**	**94**	**88**	**NA**	**74**
Position 4	Test 1	44	40	NA	69	90	85	NA	67
	Test 2	44	41	NA	69	89	84	NA	67
	Test 3	44	39	NA	69	90	84	NA	65
	Test 4	46	40	NA	69	91	85	NA	66
	Avg	**44**	**40**	**NA**	**69**	**90**	**84**	**NA**	**66**

*NA = Not Available

Table 4.13. Comparison of Rebar Stresses from Static Tests

Girder	Before FRP (MPa)	After FRP (MPa)	Percent Difference
(a) Loading Position 1			
Girder 1	83	77	7
Girder 2	91	85	7
Girder 3	82	74	10
Girder 4	37	34	9
(b) Loading Position 2			
Girder 1	75	72	4
Girder 2	88	82	7
Girder 3	84	77	8
Girder 4	45	41	9
(c) Loading Position 3			
Girder 1	39	37	4
Girder 2	72	66	8
Girder 3	106	94	11
Girder 4	82	74	10
(d) Loading Position 4			
Girder 1	47	44	6
Girder 2	76	69	9
Girder 3	102	90	12
Girder 4	73	66	10

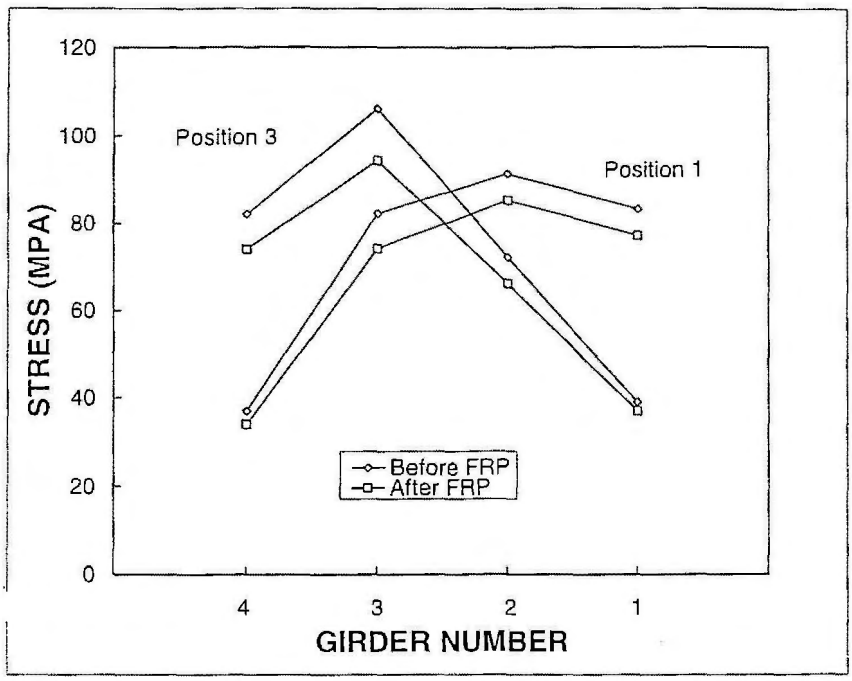

Figure 4.1. Static Rebar Stresses - Test Truck Positions 1 and 3

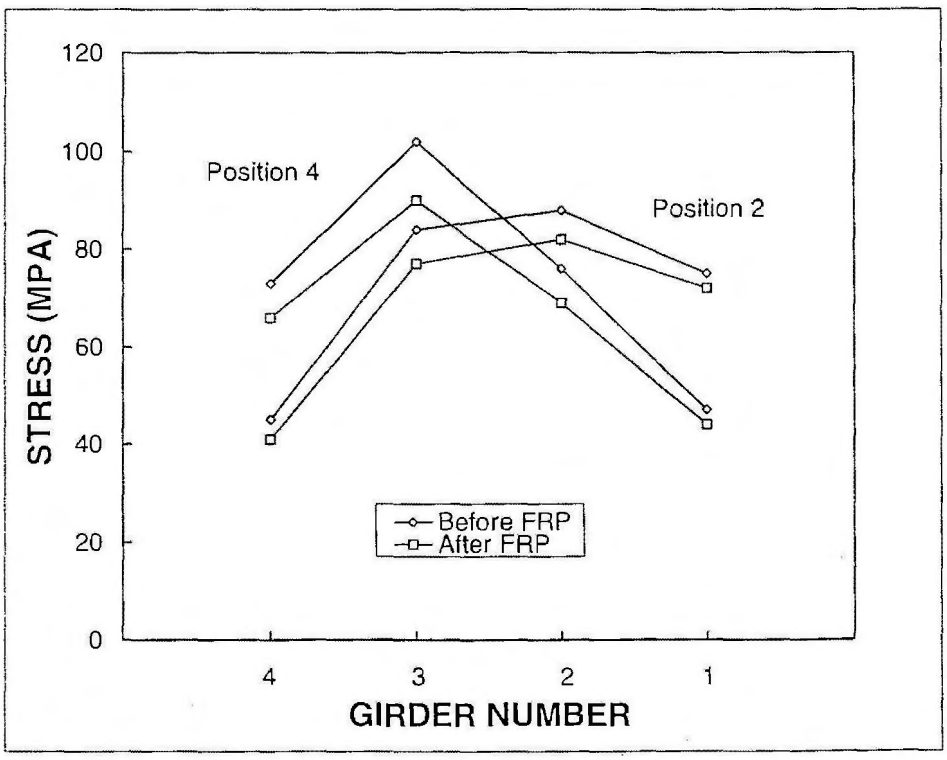

Figure 4.2. Static Rebar Stresses - Test Truck Positions 2 and 4

Table 4.14. Peak Rebar Stresses from Dynamic Tests - Before FRP Application

Test No.	Peak Rebar Stress (MPa)							
	R1W	R1E	R2W	R2E	R3W	R3E	R4W	R4
(a) Test Trucks Traveling Eastbound								
3	87	78	111	97	112	104	81	83
5	81	72	106	93	108	101	84	86
Avg.	**84**	**75**	**109**	**95**	**110**	**103**	**83**	**85**
(b) Test Trucks Traveling Westbound								
1	95	85	137	121	153	142	117	118
2	100	90	146	128	154	144	112	114
4	98	88	143	125	154	144	120	122
Avg	**98**	**88**	**142**	**125**	**154**	**144**	**116**	**118**

Table 4.15. Peak Rebar Stresses from Dynamic Tests - After FRP Application

Test No.	Peak Rebar Stress (MPa)							
	R1W	R1E	R2W	R2E	R3W	R3E	R4W	R4
(a) Test Trucks Traveling Eastbound								
1	82	73	NA*	87	94	88	NA	72
2	80	72	NA	88	96	90	NA	74
3	78	70	NA	94	107	100	NA	85
4	80	72	NA	94	104	97	NA	79
Avg	**81**	**72**	**NA**	**91**	**100**	**94**	**NA**	**77**

*NA = Not Available

Table 4.16. Percent Differences in Peak Dynamic Stresses (Mpa) for Test Trucks Traveling Eastbound

Girder	Before FRP (MPa)	After FRP (MPa)	Percent Difference
Girder 1	84	81	4
Girder 2	95	91	5
Girder 3	110	100	9
Girder 4	84	77	8

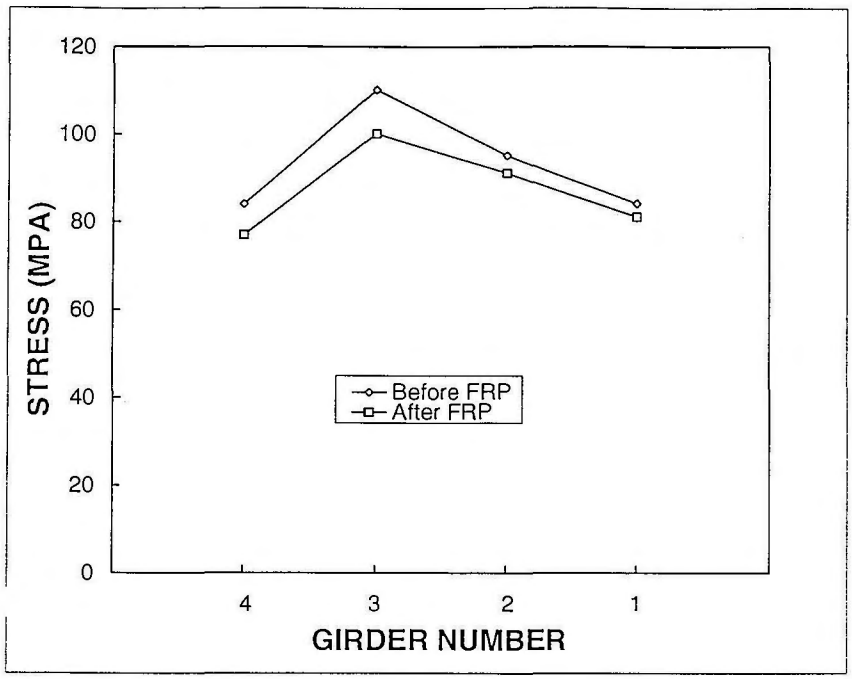

Figure 4.3. Peak Dynamic Rebar Stresses

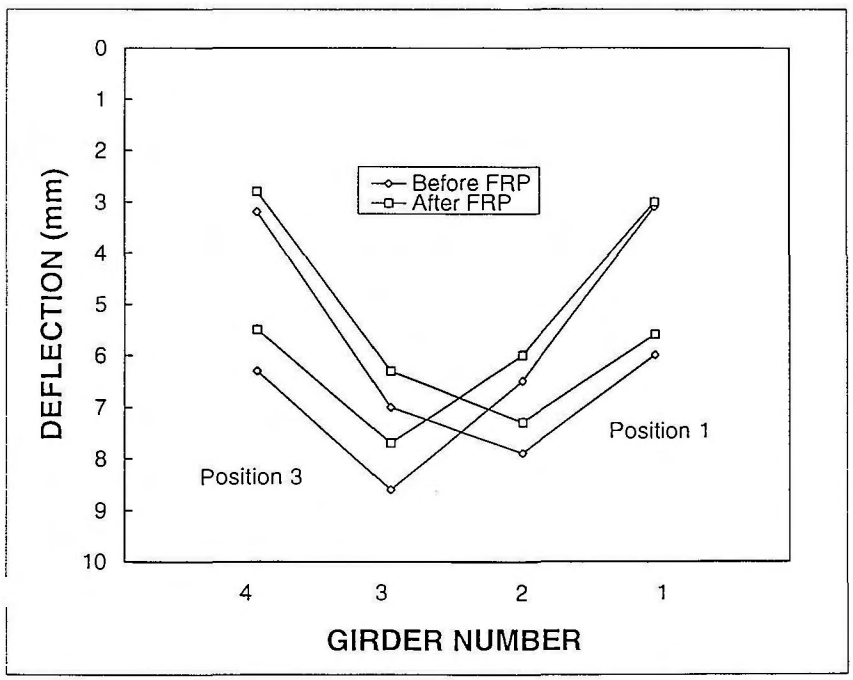

Figure 4.4. Static Girder Deflections - Test Truck Positions 1 and 3

illustrated graphically in Figure 4.3. Table 4.16 and Figure 4.3 indicate that the dynamic rebar stresses were reduced by to application of the FRP. The reductions range from 4% in girder 1 to 9% in girder 3, with an average reduction of 7%. Once again, the largest stress is observed in an interior girder, as is the largest reduction of stress. It is also noted that the smallest stress reduction again occurred in girder 1, which did not have GFRP plates bonded to its sides.

To investigate strain compatibility between the girders and the composite plates, the strains recorded in the rebar are compared to the strains recorded on the surfaces of the CFRP plates at the same location on the beam, and are presented in Table 4.17. The table shows that the difference between the strains are small. This result was expected since the difference between the distances of the rebar gages and the CFRP gages form the neutral axis of the girders is relatively small. This indicates that the bond between the composite and the concrete is rigid and exhibits linear elastic behavior.

EFFECT OF FRP ON GIRDER DEFECTIONS

The static midspan girder deflections shown in Tables 4.3 and 4.4 are compared in Table 4.18 and presented graphically by Figures 4.4 and 4.5. Deflection reductions due to the presence of the FRP range from 2% in girder 1 for loading position 3 to 12% in girder 4 for each of the test positions. For each loading position, the results indicate that the largest deflections were measured in the interior girders, as expected. Again, the smallest reduction in deflection for each loading position occurs at girder which did not have GFRP plates bonded to its sides. It is also noted in Table 4.18 that the largest reduction in deflection is observed at girder 4 for every loading position.

The reductions in peak dynamic deflections shown in Table 4.19 range from 8% in Girder 1 to 12% in Girder 4. This largest reduction of 12% is consistent with the static test results. The smallest reduction in peak dynamic deflection was at Girder 2 and not at the exterior Girder 1, which is the trend of all the other test results. However, as shown in Table 4.19, the reductions of peak dynamic deflection at Girders 1 and 2 are almost equal.

Table 4.17. Comparison of Strains Measured on CFRP and on Rebar

Girder	Rebar Strain (Microstrain)	CFRP Strain (MPa)	Percent Difference
(a) Loading Position 1			
Girder 1	385	368	-4
Girder 2	423	429	1
Girder 3	370	NA*	NA
Girder 4	170	178	5
(b) Loading Position 2			
Girder 1	361	341	-6
Girder 2	412	416	1
Girder 3	386	NA	NA
Girder 4	205	215	5
(c) Loading Position 3			
Girder 1	187	177	-5
Girder 2	332	336	1
Girder 3	472	NA	NA
Girder 4	370	388	5
(d) Loading Position 4			
Girder 1	222	211	-5
Girder 2	346	350	1
Girder 3	451	NA	NA
Girder 4	331	345	4

*NA = Not Available

Table 4.18. Comparison of Girder Deflections from Static Tests

Girder	Before FRP (mm)	After FRP (mm)	Percent Difference
(a) Loading Position 1			
Girder 1	6.0	5.6	7
Girder 2	7.9	7.3	8
Girder 3	7.0	6.3	10
Girder 4	3.2	2.8	12
(b) Loading Position 2			
Girder 1	5.4	5.2	5
Girder 2	7.7	7.1	8
Girder 3	7.3	6.6	10
Girder 4	3.7	3.3	12
(c) Loading Position 3			
Girder 1	3.1	3.0	2
Girder 2	6.5	6.0	8
Girder 3	8.6	7.7	10
Girder 4	6.3	5.5	12
(d) Loading Position 4			
Girder 1	3.6	3.5	4
Girder 2	6.9	6.3	9
Girder 3	8.3	7.4	11
Girder 4	5.6	5.0	12

Table 4.19 Comparison of Peak Girder Deflections from Dynamic Tests

Girder	Before FRP (mm)	After FRP (mm)	Percent Difference
Girder 1	6.3	5.8	8
Girder 2	8.7	8.1	7
Girder 3	9.4	8.4	11
Girder 4	6.6	5.8	12

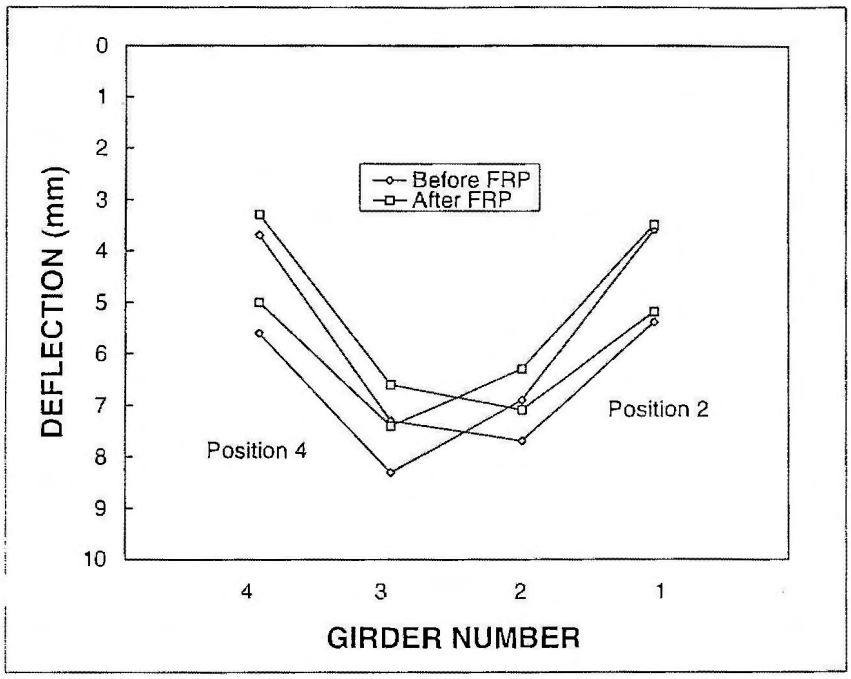

Figure 4.5. Static Girder Deflections - Test Truck Positions 2 and 4

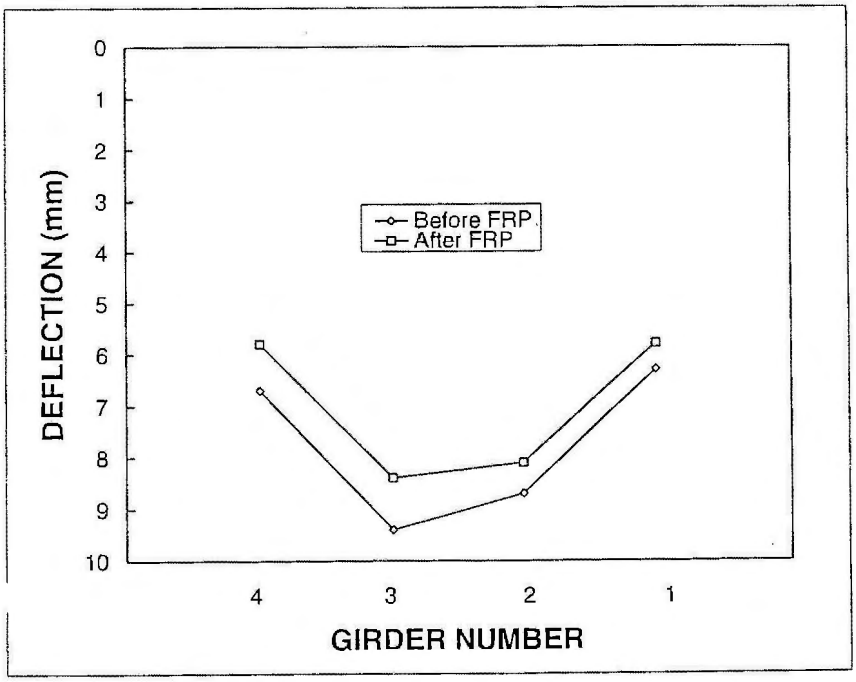

Figure 4.6. Peak Girder Deflections from Dynamic Tests - Eastbound Trucks

TRANSFER OF STRESS THROUGH SPLICE PLATES

To investigate the performance of the splice plates in transferring stress in the primary FRP reinforcement, strain gages were attached to the splice plates of the CFRP on the east end of girder 2, as shown in Figure 3.2. Recorded strain values are presented in Table 4.6 and illustrated graphically in Figure 4.7. The results show that the strains are maximum at the center of the splice plate, and decrease toward the end of the plate. The increase in strain toward the center of the splice indicates that shear stresses in the adhesive layer between the primary CFRP plate and the splice plate transfers force into the splice plate. This force increases from the end of the splice plate toward the center. Figure 4.7 shows that the strain measured on the primary plate and on the splice plate near the joint are approximately the same. This indicates that the bond between the splice plate and the primary plate transfers stress as effectively as the bond between the primary plate and the concrete. This suggests that the use of splice plates is a valid mechanism for providing continuous FRP reinforcement along the entire length of beams.

CONCLUSIONS

The field test results reported in this chapter were used to investigate the effect of externally bonded FRP composite plates on the structural performance of the bridge girders. Dynamic and static tests were performed. Rebar strains and girder deflections were measured at midspan for both the dynamic and static tests. The efficiency of stress transfer through the splice plates of the CFRP was also investigated.

In each case investigated, bonding of the composite plates to the bridge girders had a significant effect on the behavior of the structure. Rebar strain reductions ranged from 4% to 12% for the static tests and from 4% to 9% for the dynamic tests. Girder deflection reductions ranged from 2% to 12% for the static tests and from 7% to 12% for the dynamic tests.

The relative strength enhancement associated with the GFRP plates bonded to the sides of the

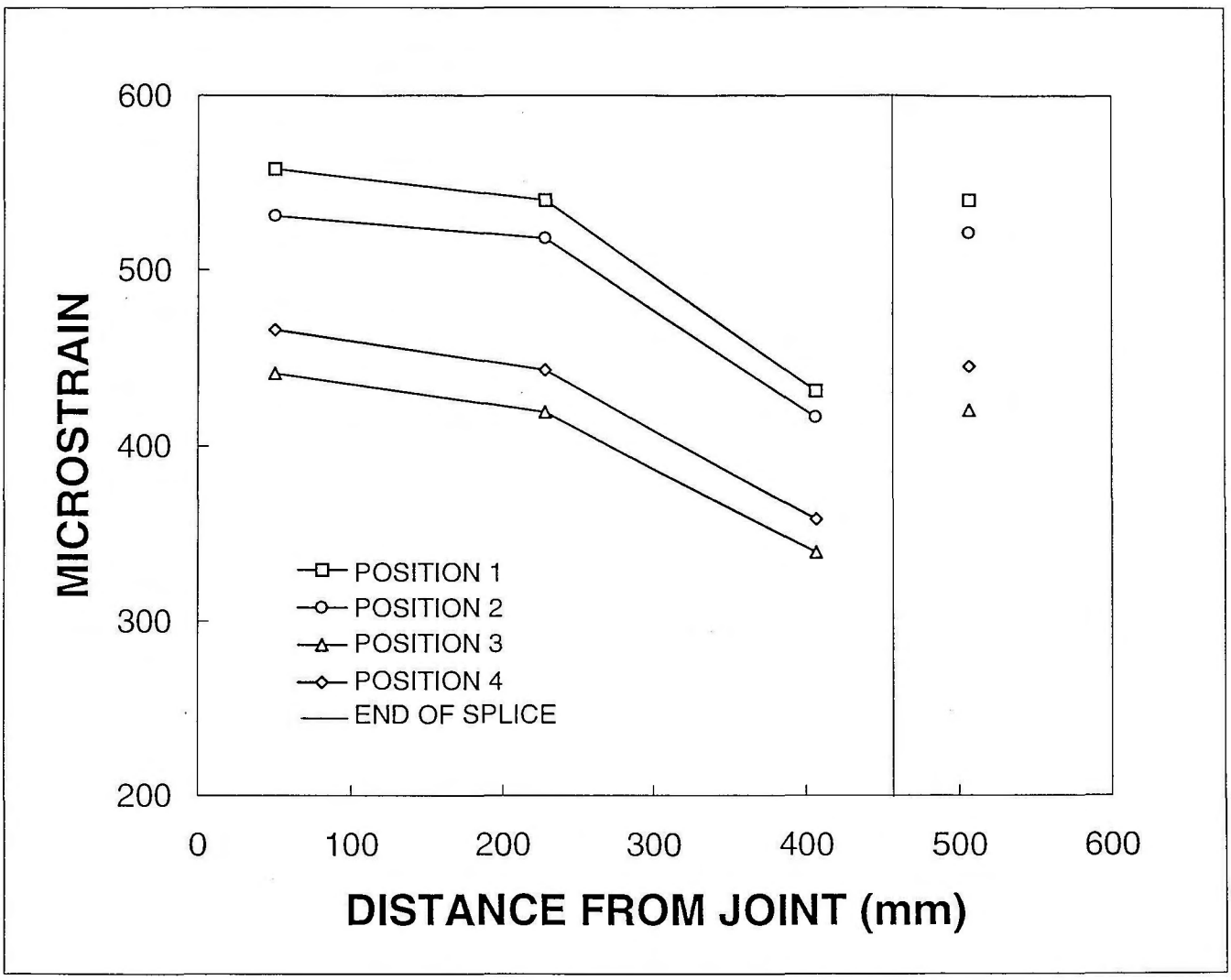

Figure 4.7. Splice Plate Strains at East End of Girder 2

girders was also investigated. Without exception, the test results indicated that the girder which did not have GFRP plates bonded to its side surfaces experienced smaller reductions in both the measured rebar strains and girder deflections. Therefore it is concluded that the laterally bonded GFRP plates also have a significant effect on the structural performance of the bridge. In addition, the compatibility between the strains measured in the rebar and the bottom CFRP plates indicate that an effective bond was achieved between the concrete and the composite. It can also be concluded from the strain data recorded on the surface of the splice plate that the composite splice design is an effective way to transfer stress between plates of primary reinforcement. The data shows that the load was transferred effectively through the splice. The splice plate design allows for the application of multiple pieces of FRP reinforcement to be applied along the entire length of a structural member, thus greatly facilitating the rehabilitation procedure.

CHAPTER FIVE
ANALYSIS OF BRIDGE

INTRODUCTION

The effectiveness of strengthening the bridge with externally bonded FRP laminates was investigated by performing a comprehensive three dimensional finite element method (FEM) analysis. Both static and dynamic analyses were conducted, and the FEM analysis results were compared with the field load test results. The same truck loading positions used in the actual field load tests, as described in Chapter 3, were implemented in both the static and dynamic FEM analyses. A sensitivity study to assess the effects of altering the cross sectional area and the modulus of elasticity of the FRP laminates used in the rehabilitation on girder deflections and reinforcing steel stresses was also conducted.

A section analysis procedure, based on strain compatibility and equilibrium equations, was also developed in an attempt to evaluate the ultimate flexural capacity of the FRP repaired bridge girders. Using this methodology, a parametric study was conducted to assess the strength enhancement provided to the ultimate load capacity of the bridge and to identify the associated modes of failure. The primary parameters in the study were the FRP cross sectional area, modulus of elasticity and tensile strength. Finally, from the results of the section analysis study, design charts were developed which may be employed for future bridge upgrading.

FINITE ELEMENT MODEL

To verify the accuracy of the FEM analysis, the results of the recorded field test data reported in Chapter 3 were compared with the FEM results. The bridge span investigated was a simple span of four girders, each having a length of 10.36m. The width of the span was 7.32m. Each girder was reinforced with 6 No. 11 bars in the tension zone as shown in Figure 2.3.

To accurately model the bridge, a three dimensional FEM model was constructed. The bridge

structure was categorically analyzed using a judiciously selected combination of finite elements. The deck and girders were modeled independently of each other in order to simulate the effect of the existing cracks in the girders. Although the original bridge structure is symmetric, the loading conditions were unsymmetric and the FRP bonded side plates were not installed on all girders. Therefore, a three-dimensional model for the entire bridge was required. An isometric view of the FEM model is shown in Figure 5.1. In the actual bridge, the concrete girders exhibited extensive flexural and shear cracking. These cracks extended through the entire stem of each girder and virtually along their entire length as illustrated in Figures 6.1 and 6.2. Therefore the elastic modulus of the girders was modified to simulate their extensive cracked state. The modulus of elasticity of the deck was calculated using the American Concrete Institute (ACI, 1995) standard of $4730\sqrt{f_c'}$, where f_c' is the concrete compressive strength in Mpa.

The bonding of the FRP laminates to the damaged concrete surfaces prevented the cracks from opening when the bridge was subjected to loading, and tended to stiffen the girders. This improved stiffness of the cracked concrete due to the bonding of the FRP laminates was estimated to be 30-40% above that of the unrepaired cracked concrete girders.

The FEM analyses were conducted on the Alabama Super computer Authority (ASA) Cray C90 Super computer through implementation of the ADINA (ADINA, 1990) finite element computer programs. The FEM model consists of 1440 three dimensional, eight node solid elements for the concrete deck slab, 1280 eight node solid elements (having a reduced modulus of elasticity to simulate the effect of cracks) to model the concrete girders, and 160 truss elements to model the steel reinforcing bars (located at the C.G. of the reinforcement). The total number of degrees of freedom for the FEM model is approximately 15,000. The bonded FRP laminates were represented with 160 truss elements to model the CFRP plates located at the mid bottom nodes of the girders. In addition, another 720 truss elements were employed on the sides of the girders to represent the GFRP plates. A

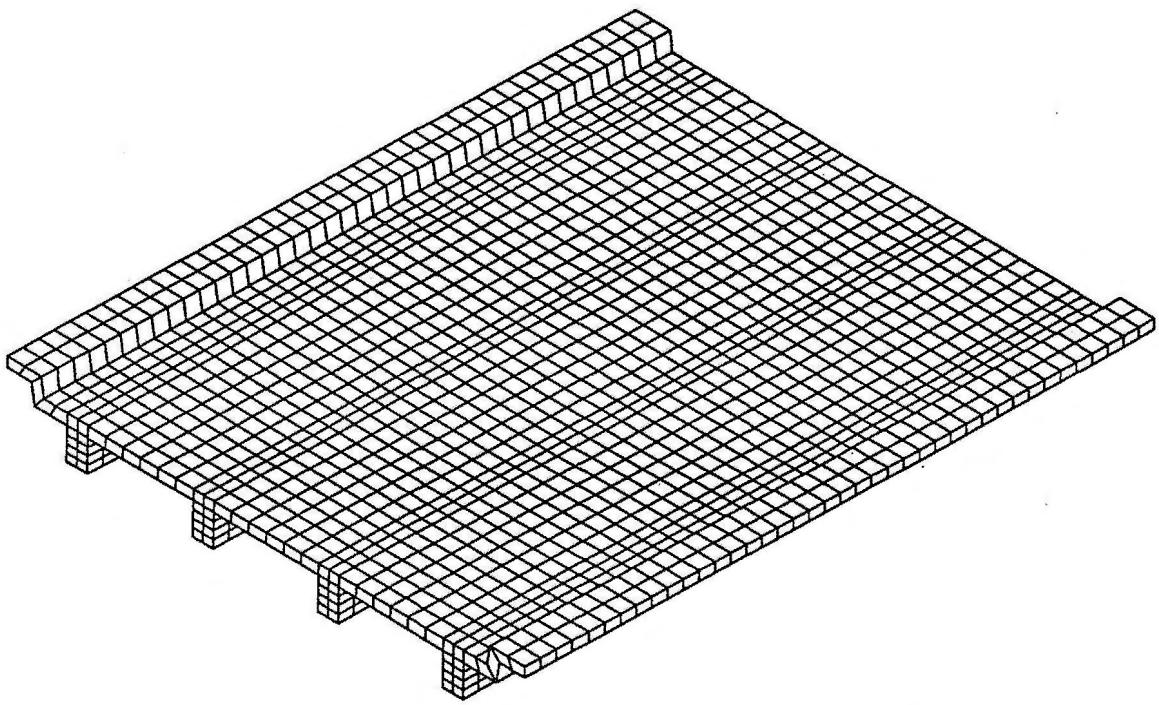

Figure 5.1. An Isometric View of the Finite Element Model of the Bridge

typical cross section of the FEM model of the bridge is presented in Figure 5.2.

FEM ANALYSES

A comprehensive series of three-dimentional FEM analyses were conducted for the bridge structure described in the previous chapters of this report. Both static and dynamic analyses were performed to verify the accuracy of the FEM model and to replicate the field load tests described in Chapters Three and Four. The dynamic analysis studies included frequency analyses to establish the dynamic characteristics of the bridge, and transient analyses to simulate the dynamic field load tests. A parametric study was also conducted to quantify the effects of varying several cross section characteristics and mechanical properties of the FRP laminates upon the bridge girder structural responses.

Frequency Analysis

The previously described FEM model was used to conduct a frequency analysis of the bridge. This analysis was performed to establish the dynamic characteristic of the bridge and to verify the accuracy of the FEM model by comparing the calculated fundamental frequency and the mode shape with those observed in the field tests. Also, the results of the frequency analysis, along with the damping ratio for the fundamental mode determined from the filed tests, were used to determine the constants required to construct the Rayleigh damping matrix required for the transient analysis. Moreover, the integration time step used in the transient dynamic analysis was selected to be approximately 1/10 of the fundamental bridge period obtained from the frequency analysis.

The first twenty natural frequencies and the corresponding mode shapes for the bridge were determined using the subspace iteration method (Bathe, 1996) and are presented in Table 5.1. The first vibration mode shape was identified as the symmetric flexural mode having an axis of symmetry about midspan as illustrated in Figure 5.3. The fundamental natural period obtained from this frequency analysis was 0.097 sec, as indicated in Table 5.1. This result was compared to the fundamental

natural period for the bridge determined from field test results. To this end, the bridge period was measured from the time history recorded by the rebar strain gage located at midspan of girder B3 during dynamic field load test No.3, which was conducted before rehabilitation. This strain time history is presented in Figure 5.4. The natural period measured from this time history was 0.099 sec, which agrees very well with the FEM result of 0.097 sec.

Damping Characteristics

The true damping characters of a structure are very complex and difficult to define. Moreover the physical damping matrix, [c], is difficult to determine analytically or even to estimate. However modal damping ratios (ζ) are more easily calculated or estimated. A Rayleigh damping formulation was employed in the dynamic FEM analyses. Rayleigh damping implies that, the system damping matrix is proportional to the mass and the stiffness matrices by means of two constants, a_0 and a_1. The Rayleigh damping matrix is given by:

$$[C] = a_0 [M] + a_1 [K] \qquad \ldots\ldots\ldots\ldots \quad 5.1$$

where [C], [M] and [K] are the damping, mass and stiffness matrices, respectively. The constants a_0 and a_1 are alternately related to the system damping by the expression:

$$\zeta_n = \frac{a_o}{2\ \omega_n} + \frac{a_1\ \omega_n}{2} \qquad \ldots\ldots\ldots\ldots \quad 5.2$$

where ζ_n is the modal damping ratio for mode n, and ω_n is the corresponding natural frequency (rad/sec).

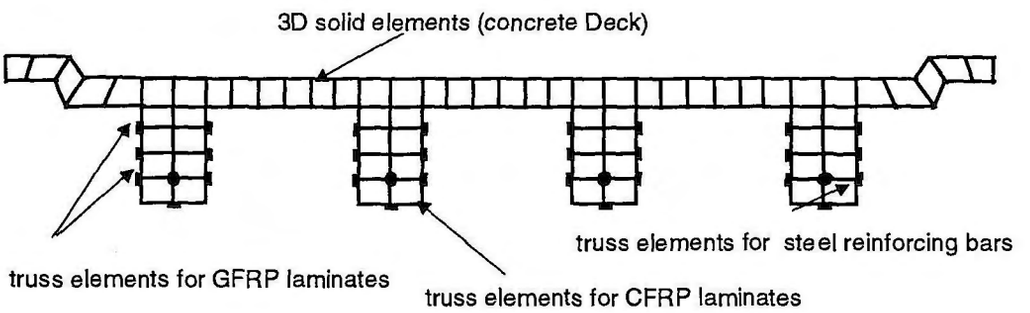

Figure 5.2. Typical Cross Section of the FEM Model for Repaired Bridge Structure.

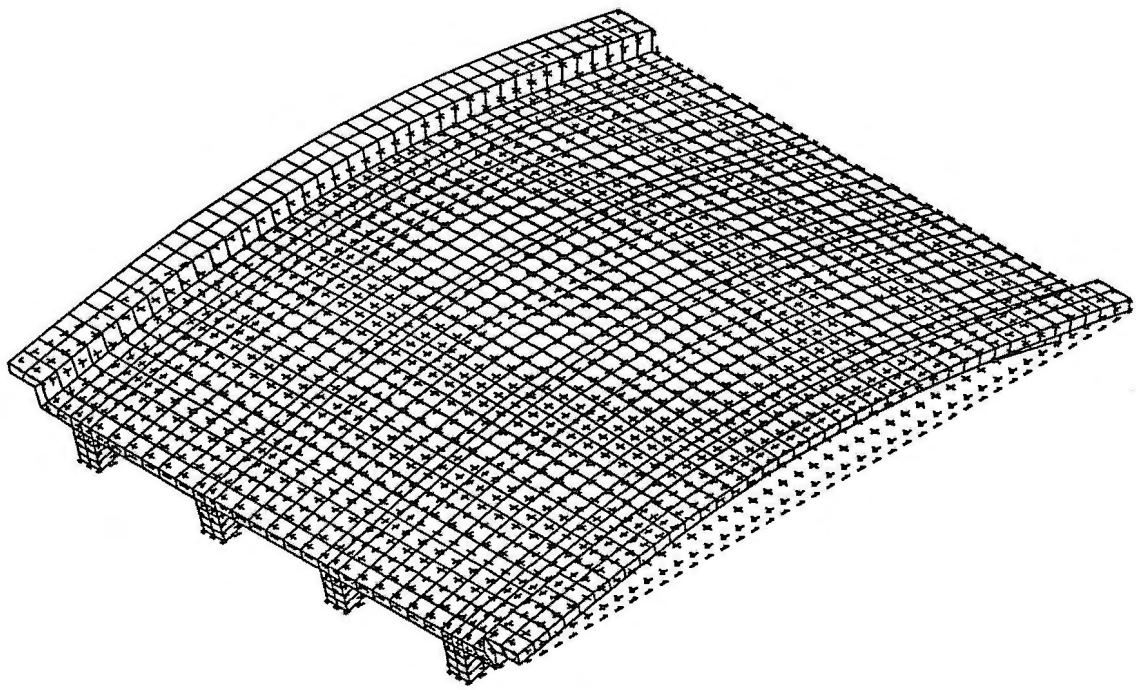

Figure 5.3. Mode Shape Corresponding to Fundamental Vibration Frequency

Table 5.1. Natural Circular Frequency, Natural Frequency and Natural Period for the First Twenty Modes Extracted from the FEM Frequency Analysis.

Mode Number	Frequency (rad/sec)	Natural Frequency, Hz	Natural Period, sec.
1	64.71	10.30	0.0971
2	81.83	13.02	0.0768
3	110.70	17.62	0.0568
4	173.23	27.57	0.0363
5	196.41	31.26	0.0320
6	221.90	35.32	0.0283
7	226.69	36.08	0.0277
8	257.78	41.03	0.0244
9	299.96	47.74	0.0209
10	324.36	51.62	0.0194
11	352.56	56.11	0.0178
12	362.56	57.70	0.0173
13	398.29	63.39	0.0158
14	403.59	64.23	0.0156
15	412.63	65.67	0.0152
16	463.91	73.83	0.0135
17	471.25	75.00	0.0133
18	494.19	78.65	0.0127
19	515.54	82.05	0.0122
20	524.68	83.51	0.0120

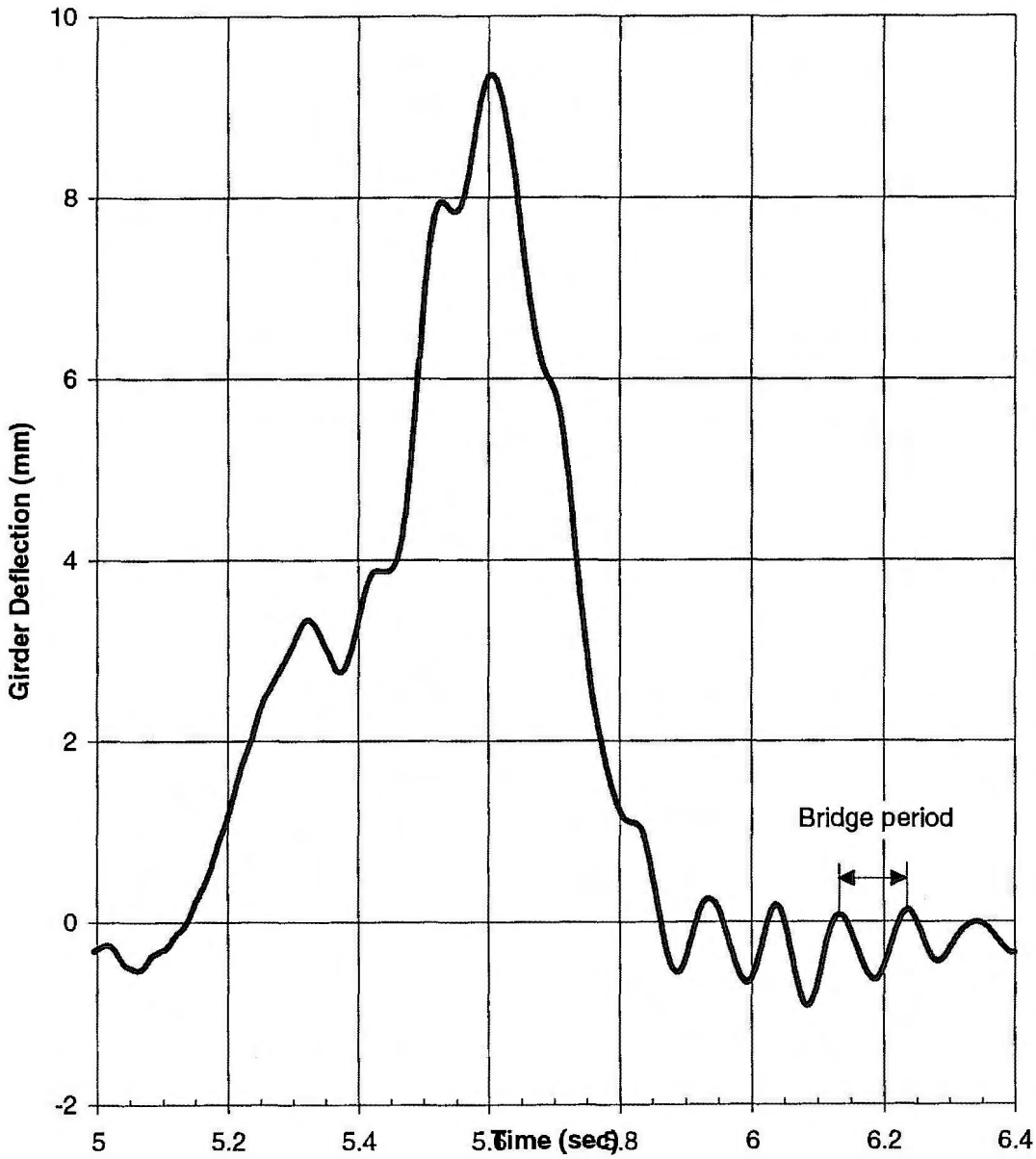

Figure 5.4. Experimental Data Recorded During Dynamic Field Load Test No. 3 on Girder B3 Before Rehabilitation.

The constants a_o and a_1 are determined from the simultaneous equations obtained by applying Equation 5.2 twice for any two modes which results in the following expression:

$$\begin{pmatrix} a_o \\ a_1 \end{pmatrix} = 2 \frac{\omega_r \, \omega_s}{\omega_s^2 - \omega_r^2} \begin{bmatrix} \omega_s & -\omega_r \\ \frac{-1}{\omega_s} & \frac{1}{\omega_r} \end{bmatrix} \begin{pmatrix} \zeta_r \\ \zeta_s \end{pmatrix} \qquad \ldots\ldots\ldots\ldots \quad 5.3$$

Using the information extracted from the frequency analysis, the coefficients a_o and a_1 can be evaluated. The first modal damping ratio (ζ_1)was determined from the logarithmic decrement (δ) of the mid span deflection time history recorded for beam B3 during the dynamic field test No. 3 (refer to Table 4.9), shown in Figure 5.4. The calculated average value of ζ_1, using Equation 5.4 is 0.018 (i.e. 1.8% of critical damping). The expression for the calculation of ζ_1 is given by

$$\zeta_1 = \frac{\ln (y_1 / y_2)}{2 \pi} \qquad \ldots\ldots\ldots\ldots \quad 5.4$$

where y_1 and y_2 represent the amplitudes of two successive peaks of the free vibration segment of the deflection time history shown in Figure 5.4.

The contribution of the higher modes to the dynamic response is usually small, therefore the damping ratio ζ_3 corresponding to the third frequency, ω_3, was set equals to 0.05 and used in the analysis. Substituting these values for ζ_1 and ζ_3 into Equation 5.3 yielded the values a_o=-2.21 and a_1=0.0011. Then, the proportional damping matrix defining the required values for damping ratio for the specified frequencies is determined from the Rayleigh damping expression as given by Equation 5.1. This relation is represented graphically in Figure 5.5.

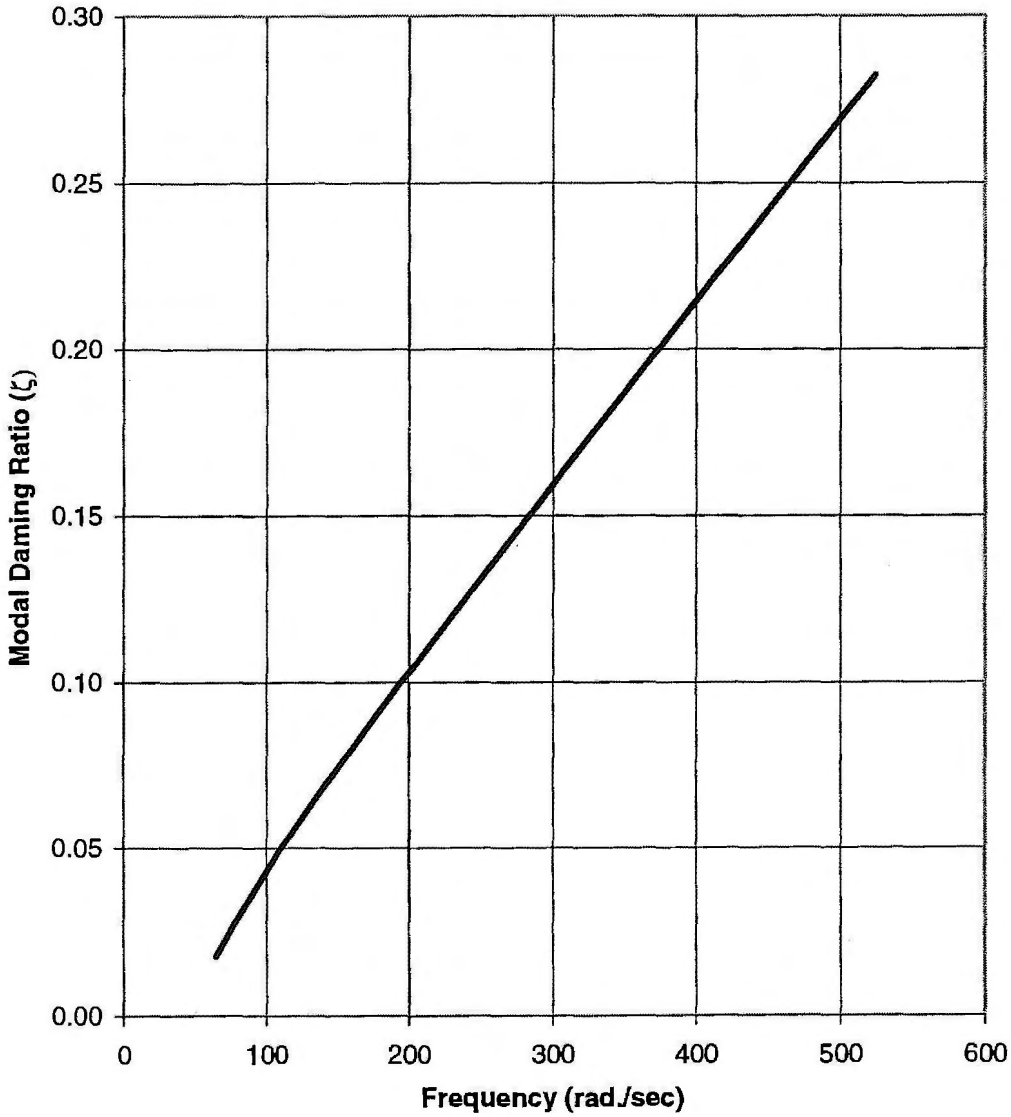

Figure 5.5. Modal Damping Variation with the Bridge Natural Frequency.

Transient Analysis

To assess the effectiveness of the FRP strengthening technique on reducing the reinforcing steel stresses and girder deflections, two dynamic analyses were performed; one for the bridge before rehabilitation, and the other after installing the FRP laminates. In each of these analyses, the actual dynamic field load tests described in Chapter 3 were simulated. The dynamic tests were performed using two trucks traveling side by side in a symmetric pattern along the bridge longitudinal axis as illustrated in Figure 5.6. The truck wheel loads in the FEM model were represented as moving concentrated loads assigned to pre-specified nodes. The specific nodal loads were calculated according to their distance from the wheel path. To accurately model the load conditions, these loads were specified in the time domain with the trapezoidal load-time history shown in Figure 5.7. This load-time history is shifted along the longitudinal axis of the structure, according to the truck speed and the node spacing, as the truck moves across the bridge. A computer program was developed to calculate the appropriate load time histories for either one or two load trucks.

In the transient analyses, an integration time step of 0.002 sec was selected to insure accuracy of the results, and the integration was carried out over 400 time steps. The Newmark method for direct time integration with a consistent mass matrix and a Rayleigh damping formulation, as previously described in this section, were employed in the numerical analysis. Due to the extensive flexural cracking in the bridge girders, a reduced value for the modulus of elasticity of the girder finite elements was employed to simulate the stiffness degradation.

Results of Transient Analyses

Comparisons of the FEM transient analysis results with the recorded field test data, both before (refer to Table 4.7 and 4.9) and after (refer to Table 4.8 and 4.10) installing the FRP laminates, are shown in Figure 5.8 and Figure 5.9, respectively . It is apparent from these comparisons that the FEM model provides a very good prediction for both the maximum girder deflections and the reinforcing bar

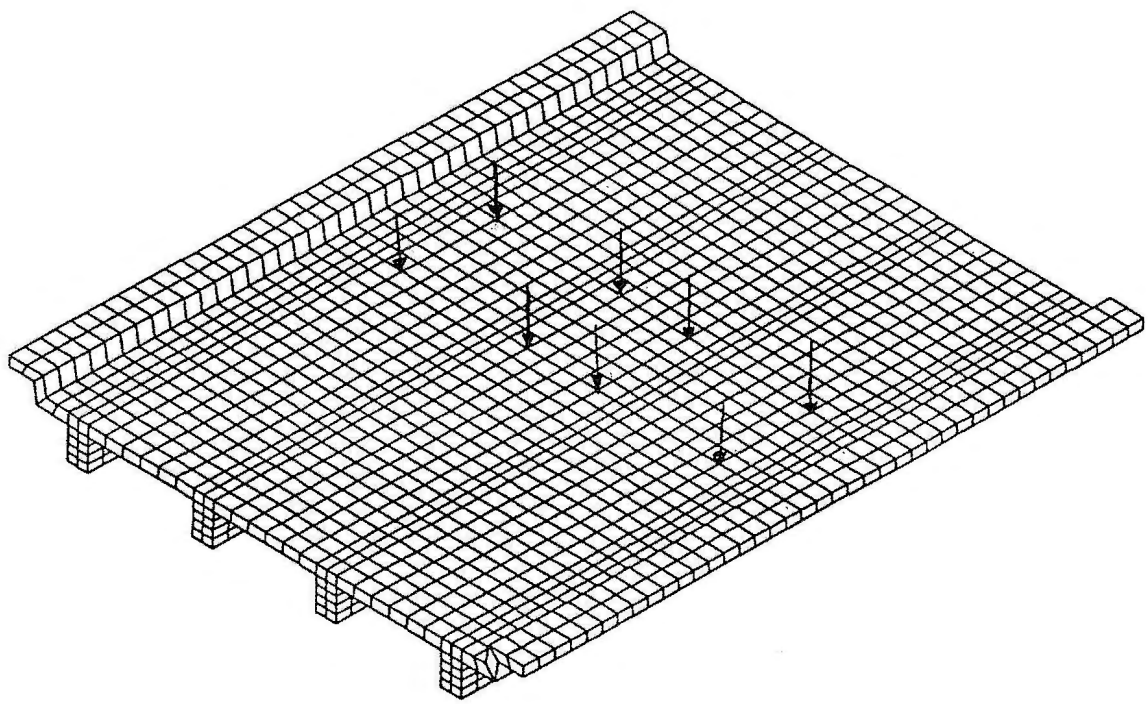

Figure 5.6. Dynamic Loading Configuration Simulating Test Trucks.

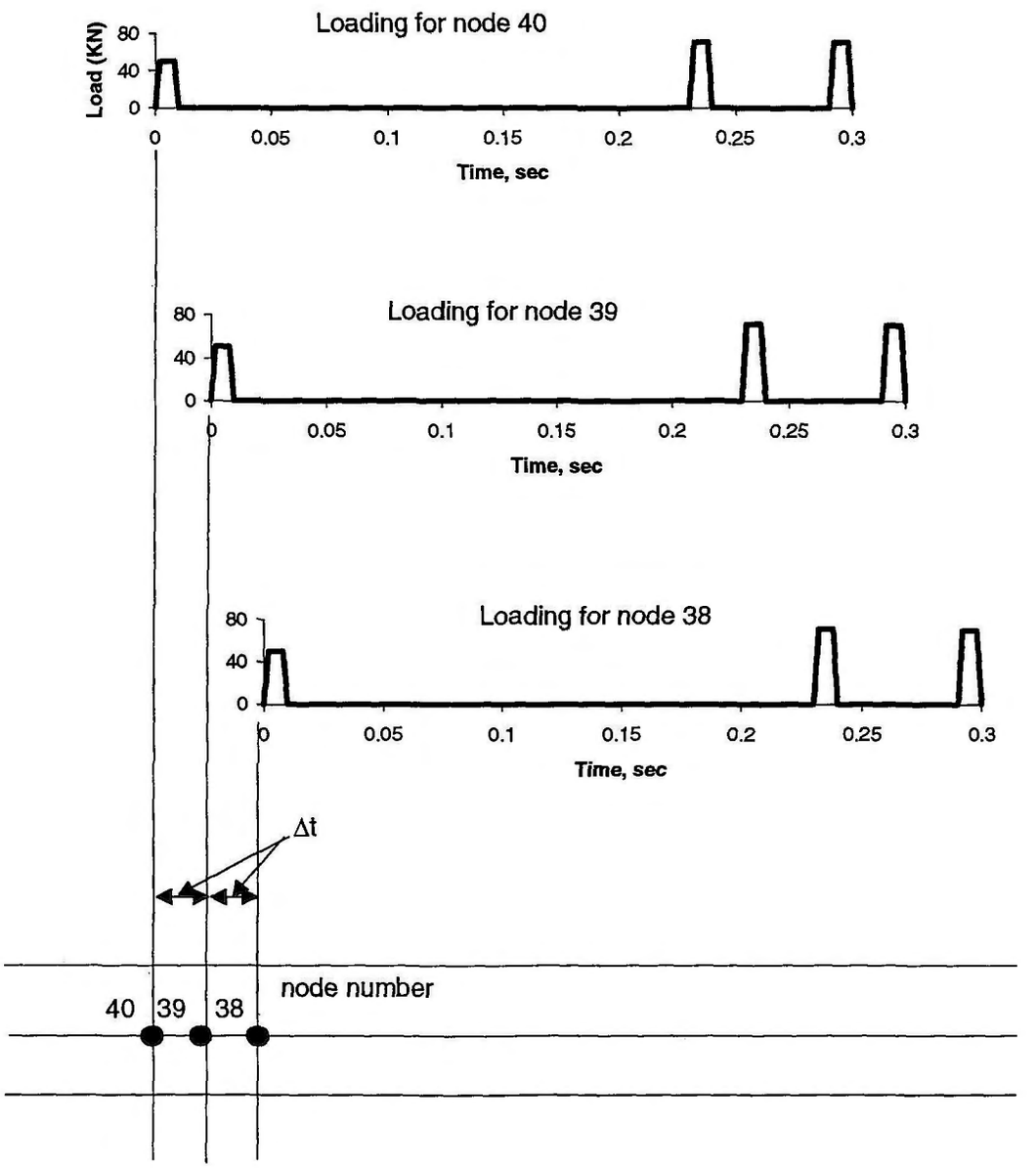

Figure 5.7. Time History Used for Truck Loading in the FEM Analysis.

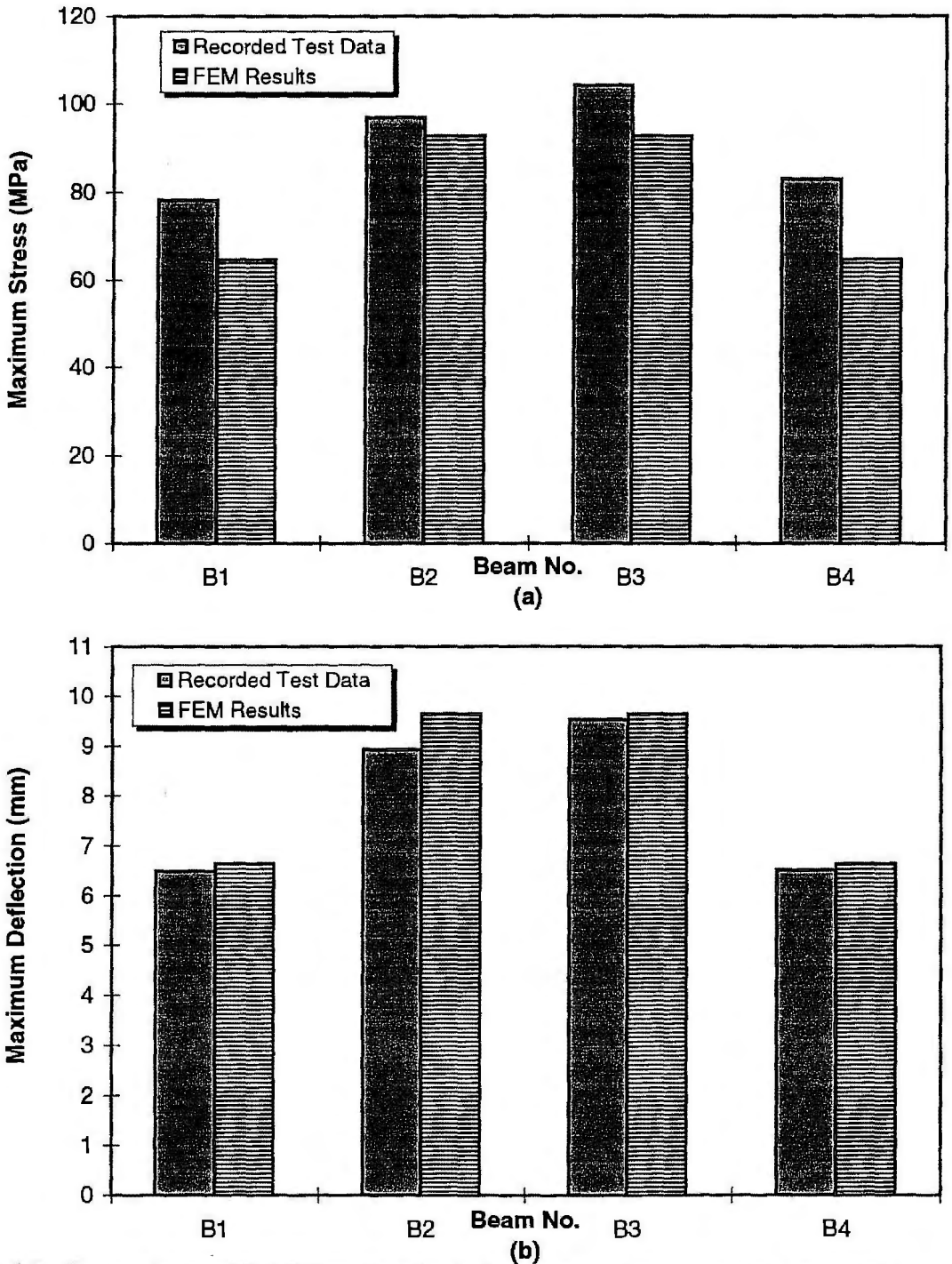

Figure 5.8. Comparisons of FEM Transient Analysis Results and Recorded Test Data Before Rehabilitation (Test No.3): (a) Maximum Stresses in Reinforcing Steel at Midspan; (b) Maximum Girder Deflections at Midspan.

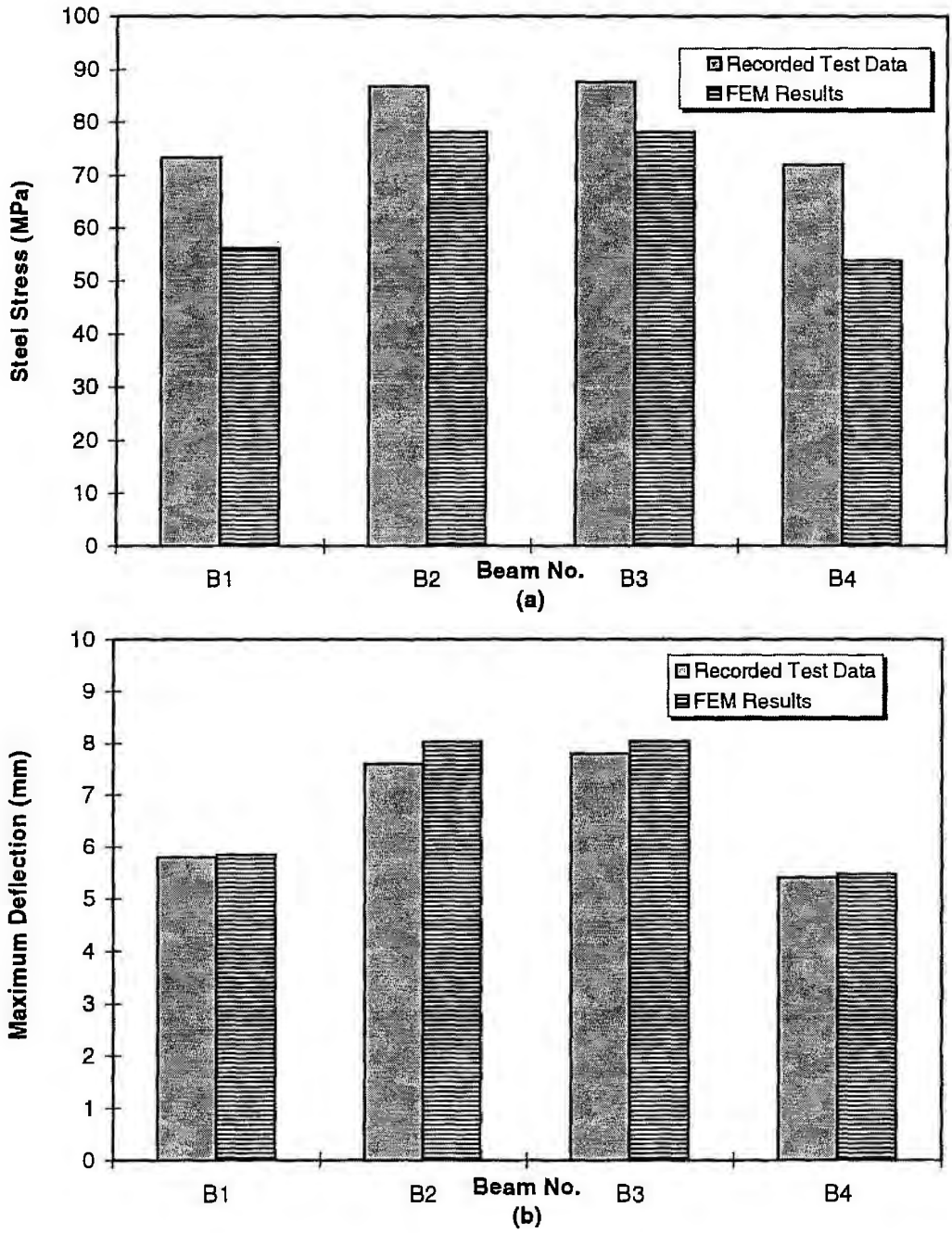

Figure 5.9. Comparisons of FEM Transient Analysis Results and Recorded Test Data After Rehabilitation (Test No. 1): (a) Maximum Stresses in Reinforcing Steel at Midspan: (b) Maximum Girder Deflections at Midspan.

stresses in both instances.

The variation of mid-span girder deflections and steel reinforcing bar stresses with time, recorded during the field tests, both before (test No. 3) and after (test No. 1) bonding the FRP laminates, were compared with the corresponding results obtained from the FEM analysis. These comparisons are presented in Figure 5.10 through Figure 5.17. Finally, a comparison of the field load test and FEM results of the time histories (test no. 1) for stresses in the CFRP plate at midspan of girder B2 is presented in Figure 5.18. Excellent correlation between the measured (field) and predicted (FEM) results are noted in each instance.

Static FEM Analysis Results

The results obtained from the FEM analysis before installing the composite laminates are presented Figures in 5.19 through 5.22 for the four static load configurations described in Chapter Three. Very good correlation of the FEM results, for both girder deflections and reinforcing steel stresses, with the field test data is noted. The reinforcing steel stresses obtained from the FEM analysis are slightly lower than the results obtained from the filed tests. This is attributed to the modeling simplification of lumping together the physical properties of the six reinforcing bars at the center of gravity location of the reinforcing steel area, while in the actual field test, the recording gage was mounted on the underside of the bottom most bar.

The results of the FEM analysis after installing the FRP laminates are presented in Figures 5.23 through 5.26. The FEM analysis results agree very well with the static load test data for both the girder deflections and reinforcing steel stresses. Also, the average decrease in midspan girder deflection and steel reinforcing stresses predicted by the FEM analysis is equal to 10%. This is approximately equal to the actual recorded decrease using the field test data. Finally, Table 5.2, Figure 5.27 and Figure 5.28 present comparisons between CFRP stresses obtained from the FEM analysis and the recorded test data. Excellent correlation of these results is also noted.

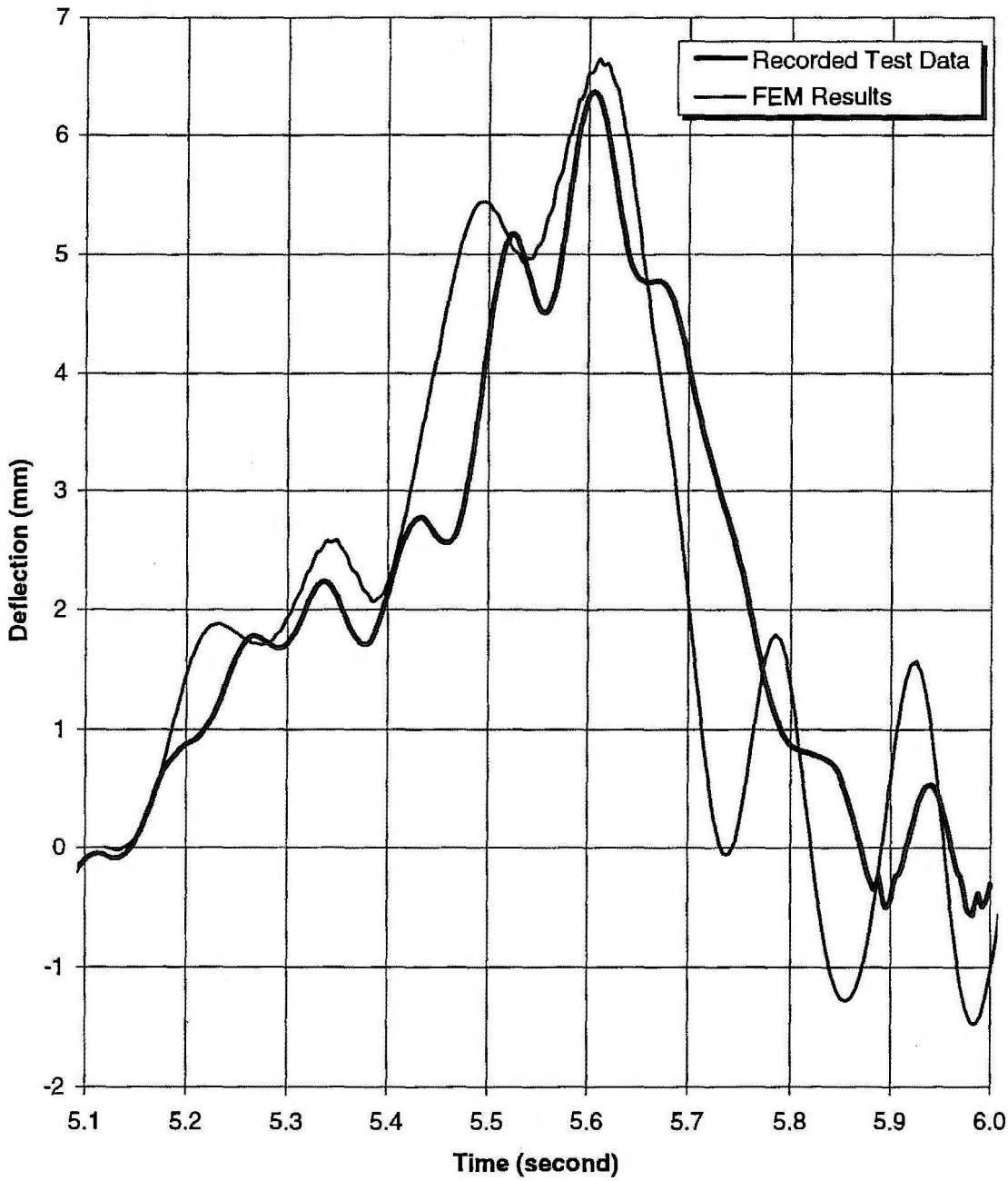

Figure 5.10. Midspan Deflection Time Histories for Girder B1 Before Rehabilitation (Test No. 3).

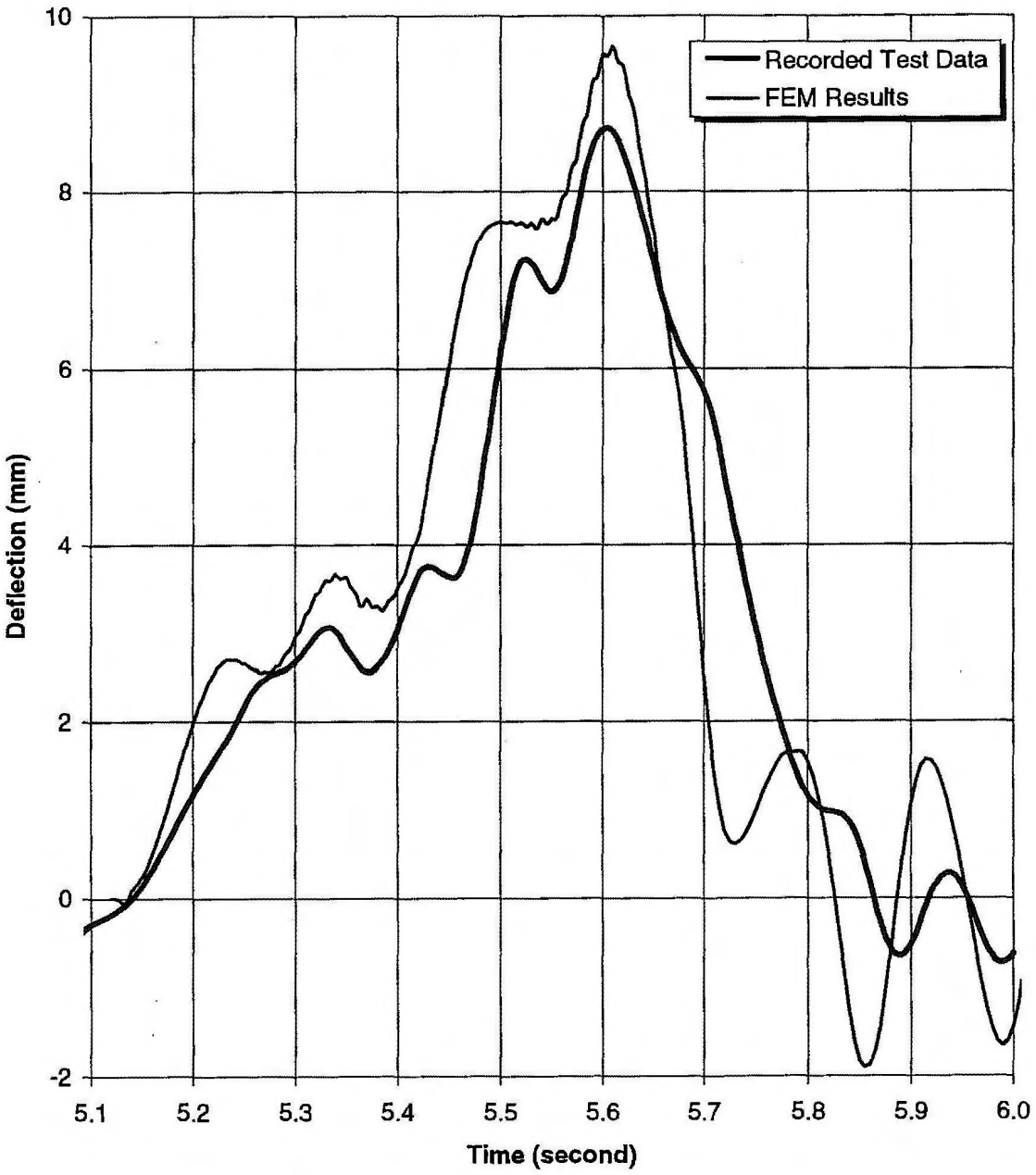

Figure 5.11. Midspan Deflection Time Histories for Girder B2 Before Rehabilitation (Test No. 3).

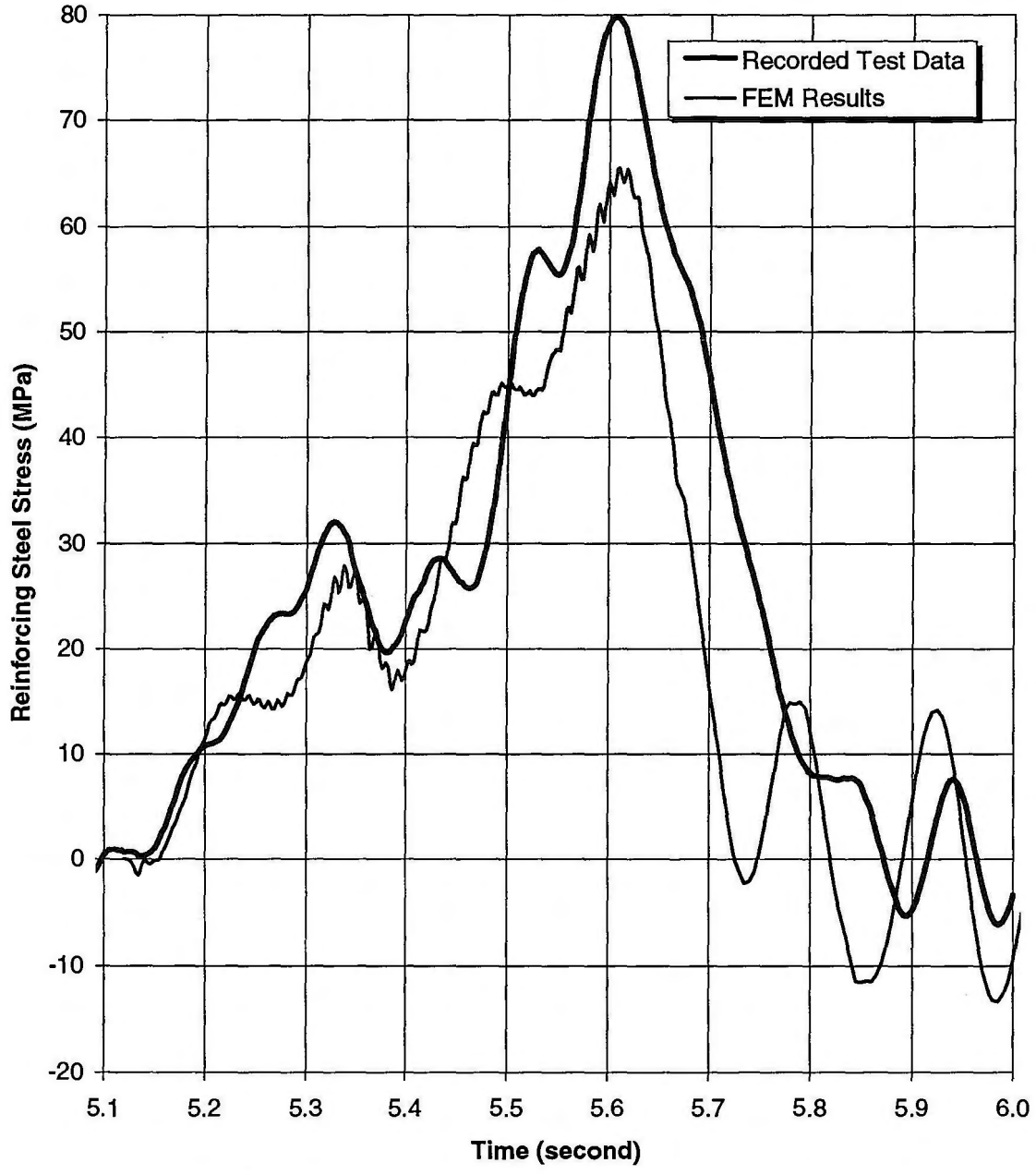

Figure 5.12. Time Histories for Midspan Reinforcing Steel Stresses for Girder B1 Before Rehabilitation (Test No.3).

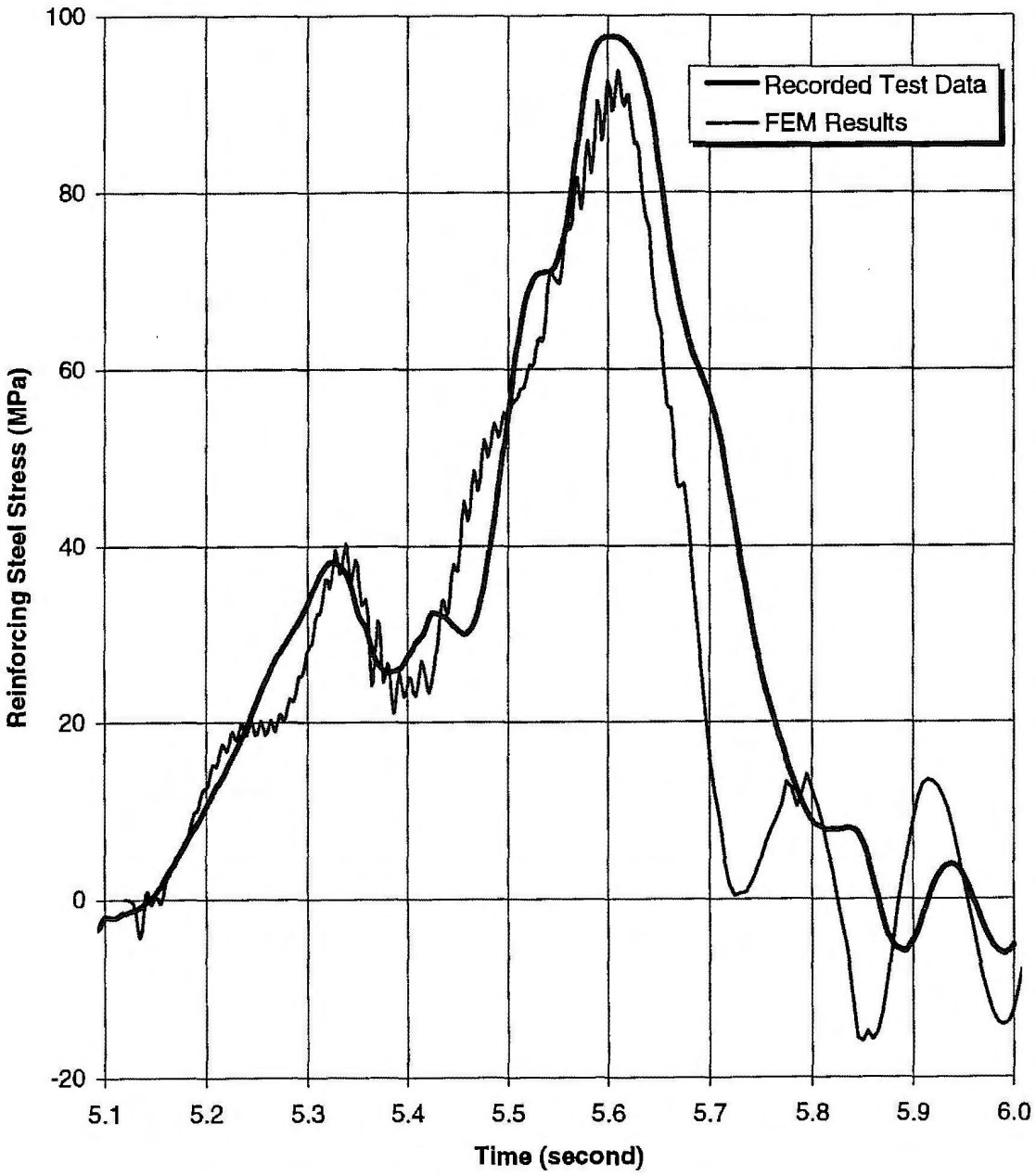

Figure 5.13. Time Histories for Midspan Reinforcing Steel Stresses for Girder B2 Before Rehabilitation (Test No. 3).

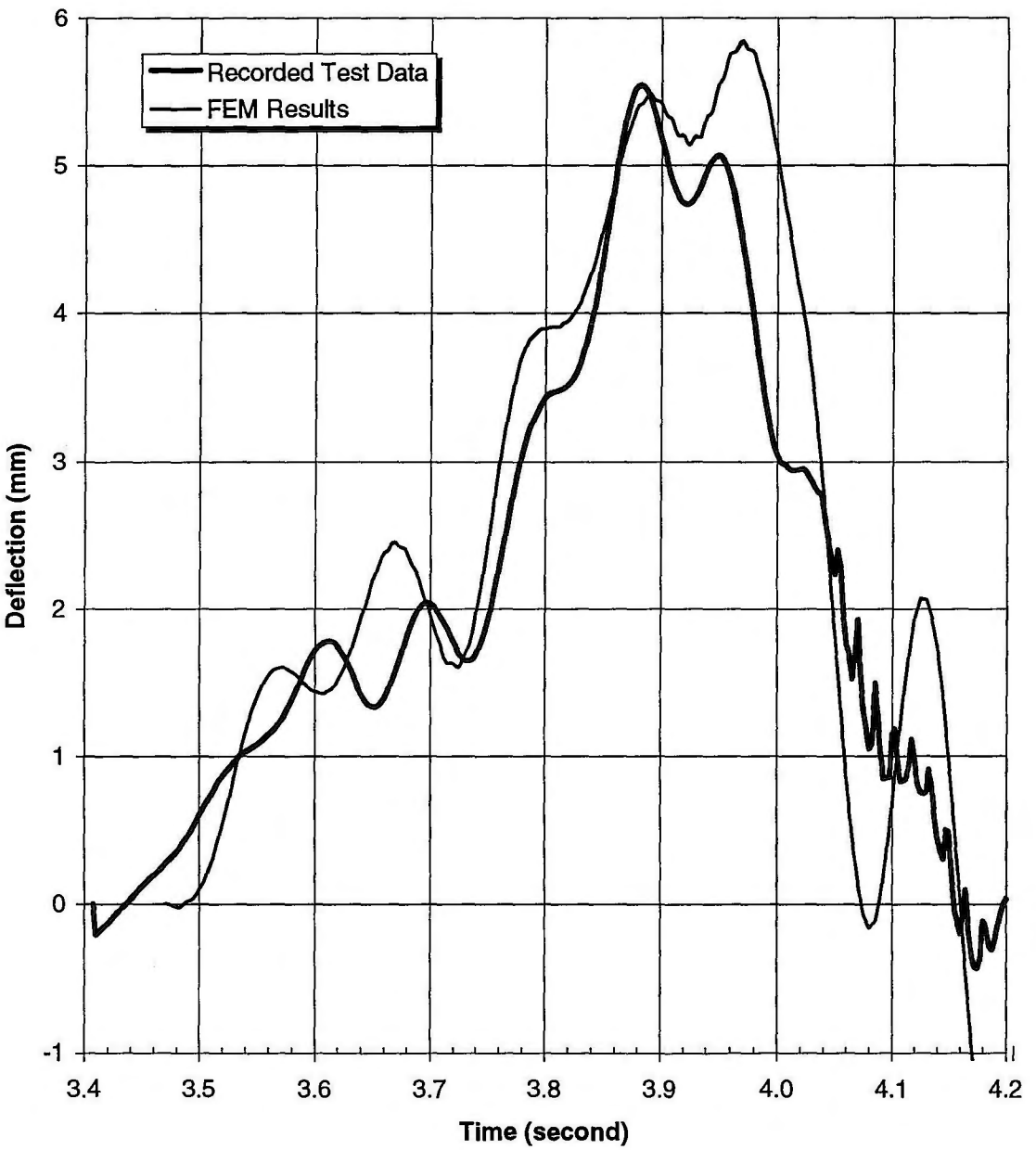

Figure 5.14. Midspan Deflection Time Histories for Girder B1 After Rehabilitation (Test No. 1).

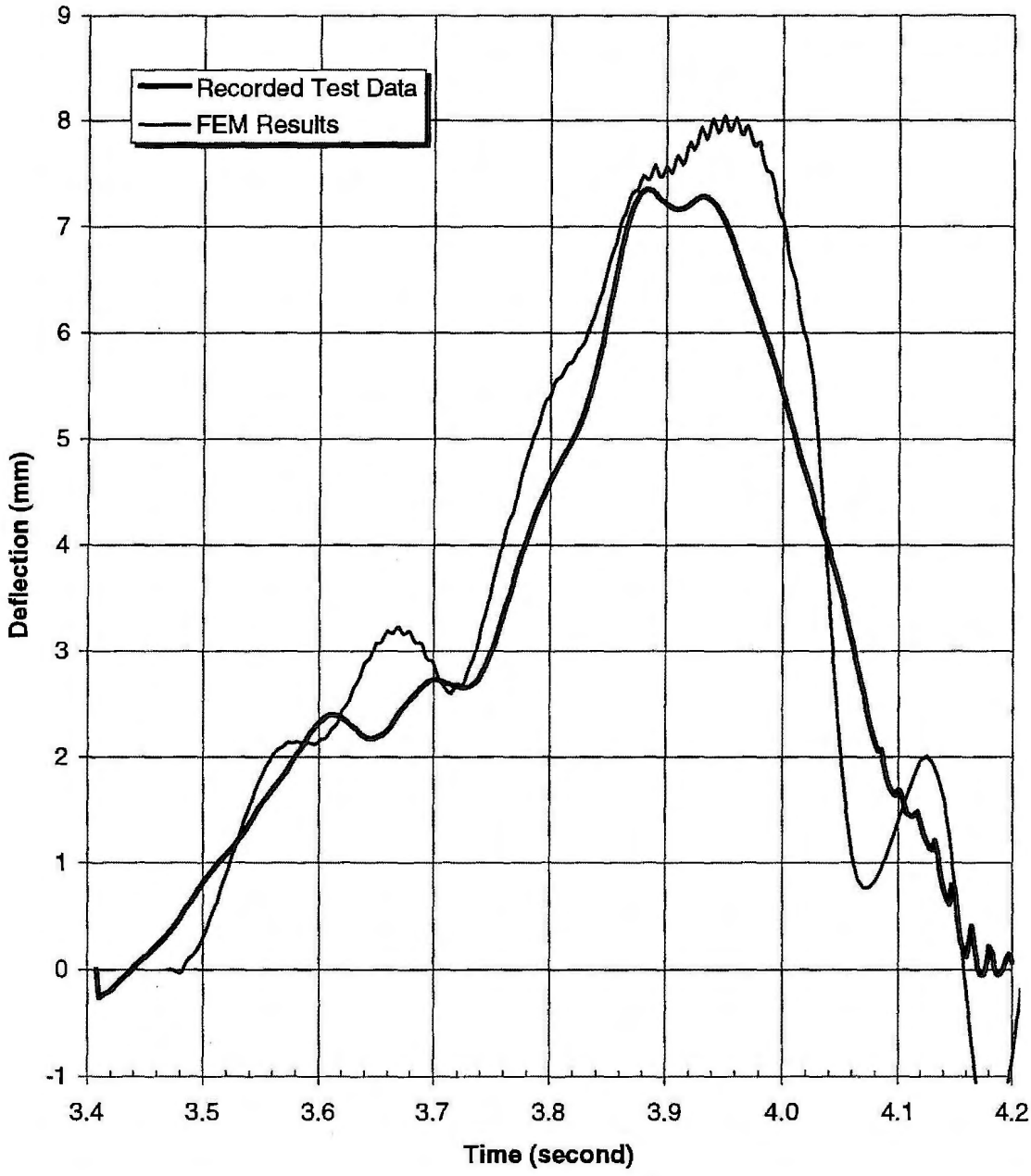

Figure 5.15. Midspan Deflection Time History for Girder B2 After Rehabilitation (Test No. 1).

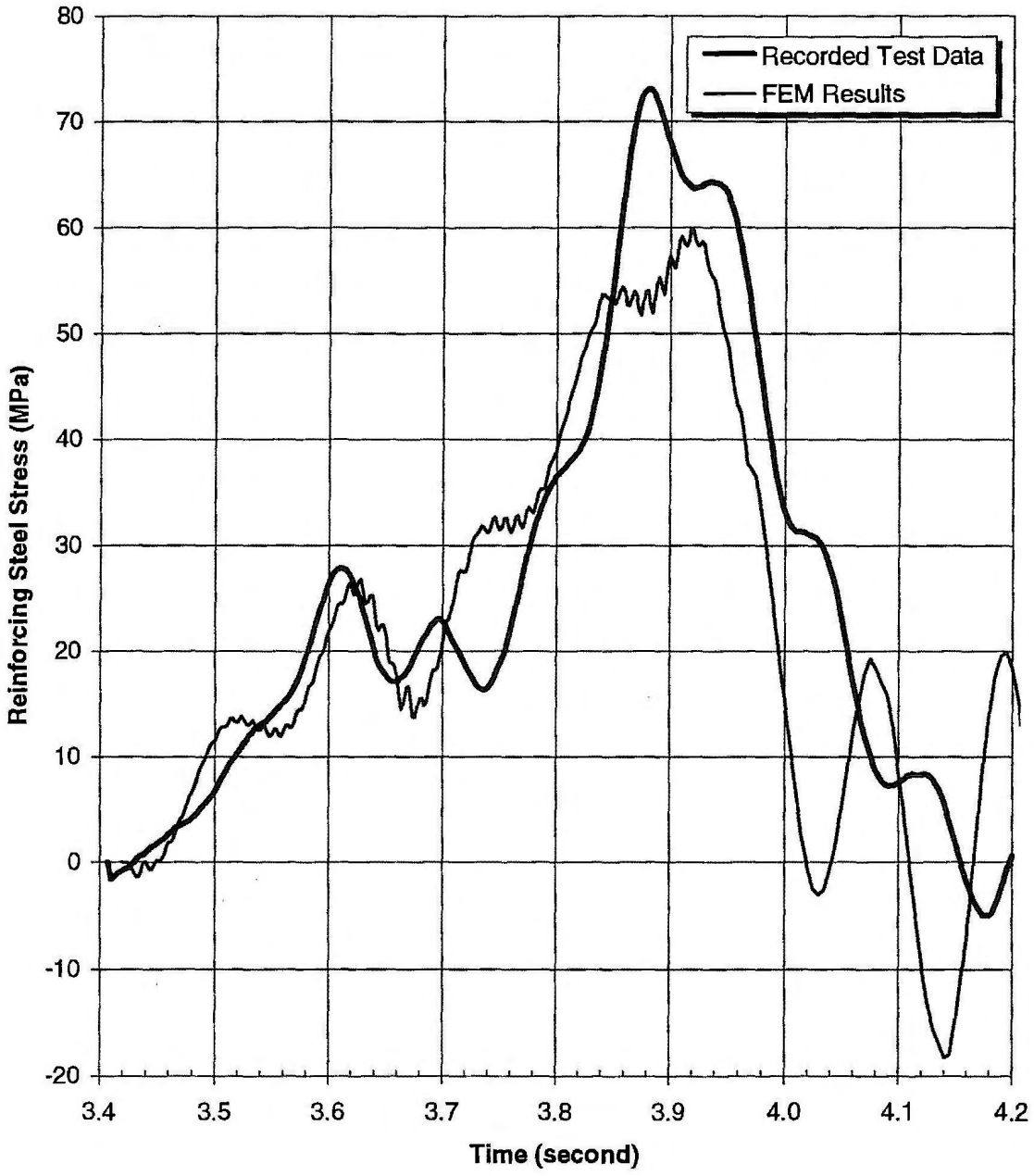

Figure 5.16. Time Histories for Midspan Reinforcing Steel Stresses for Girder B1 After Rehabilitation (Test No.1).

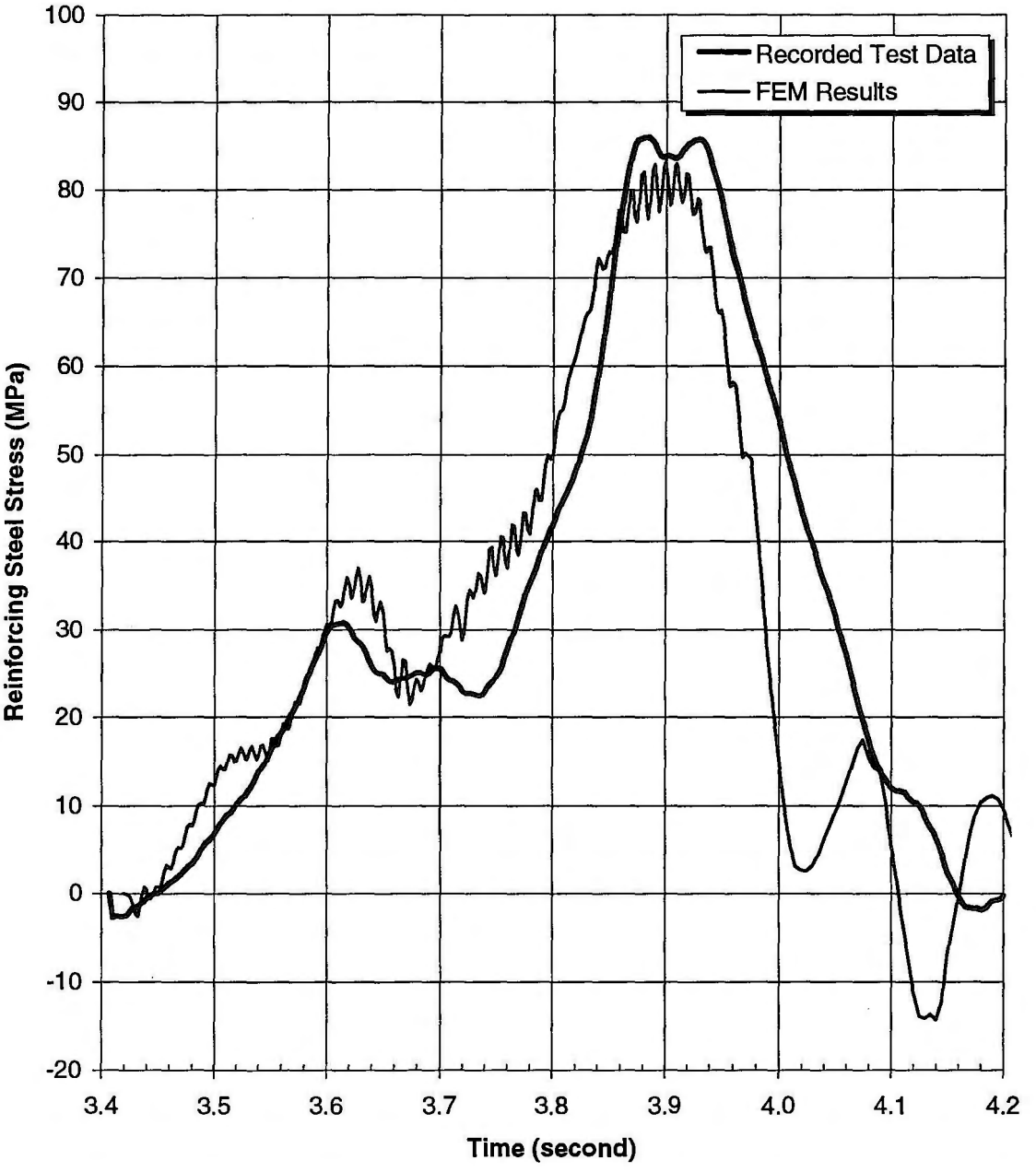

Figure 5.17. Time Histories for Midspan Reinforcing Steel Stresses for Girder B2 After Rehabilitation (Test No.1).

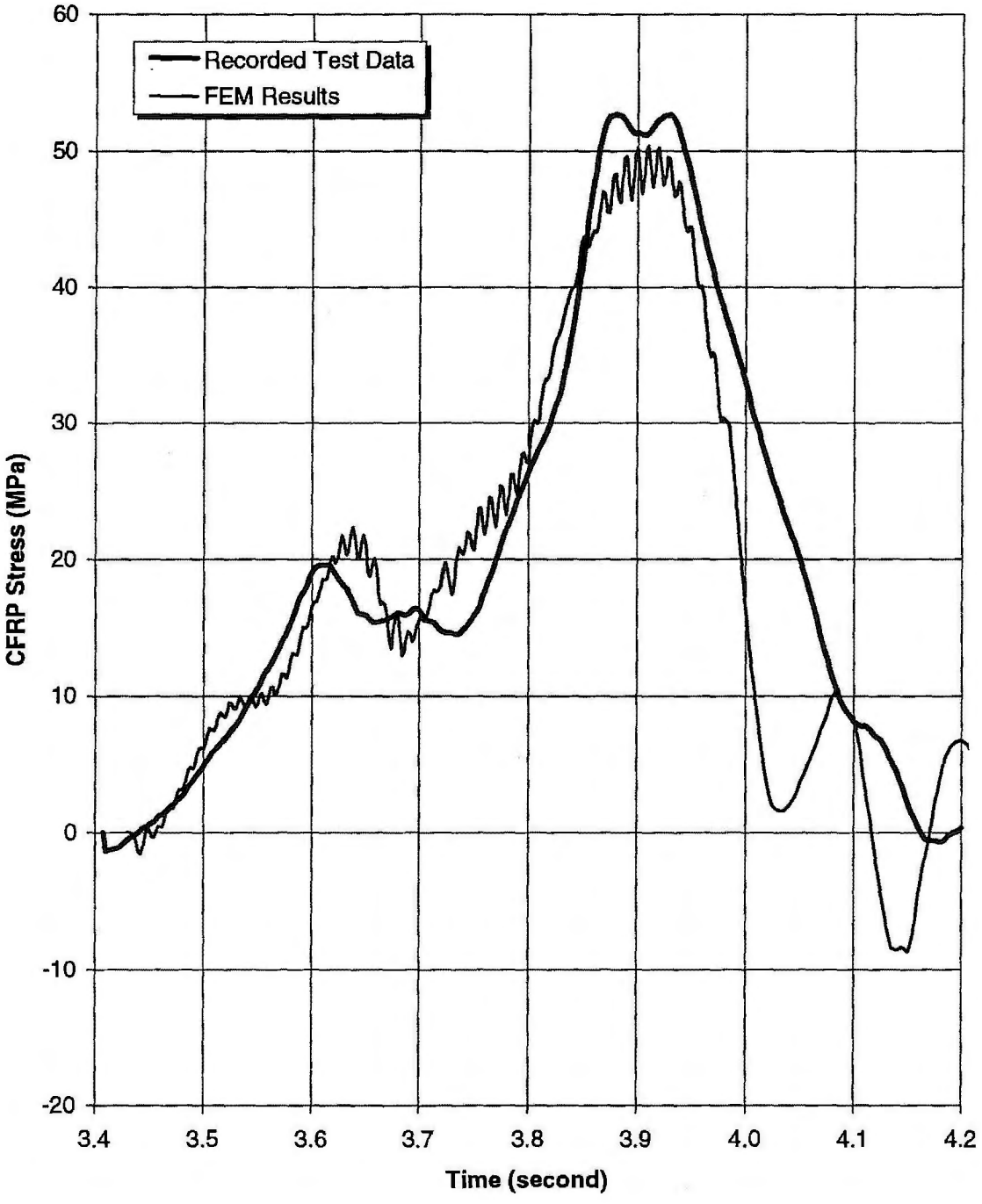

Figure 5.18. Time Histories For Midspan Stresses in CFRP Plate for Girder B2 After Rehabilitation (Test No. 1)

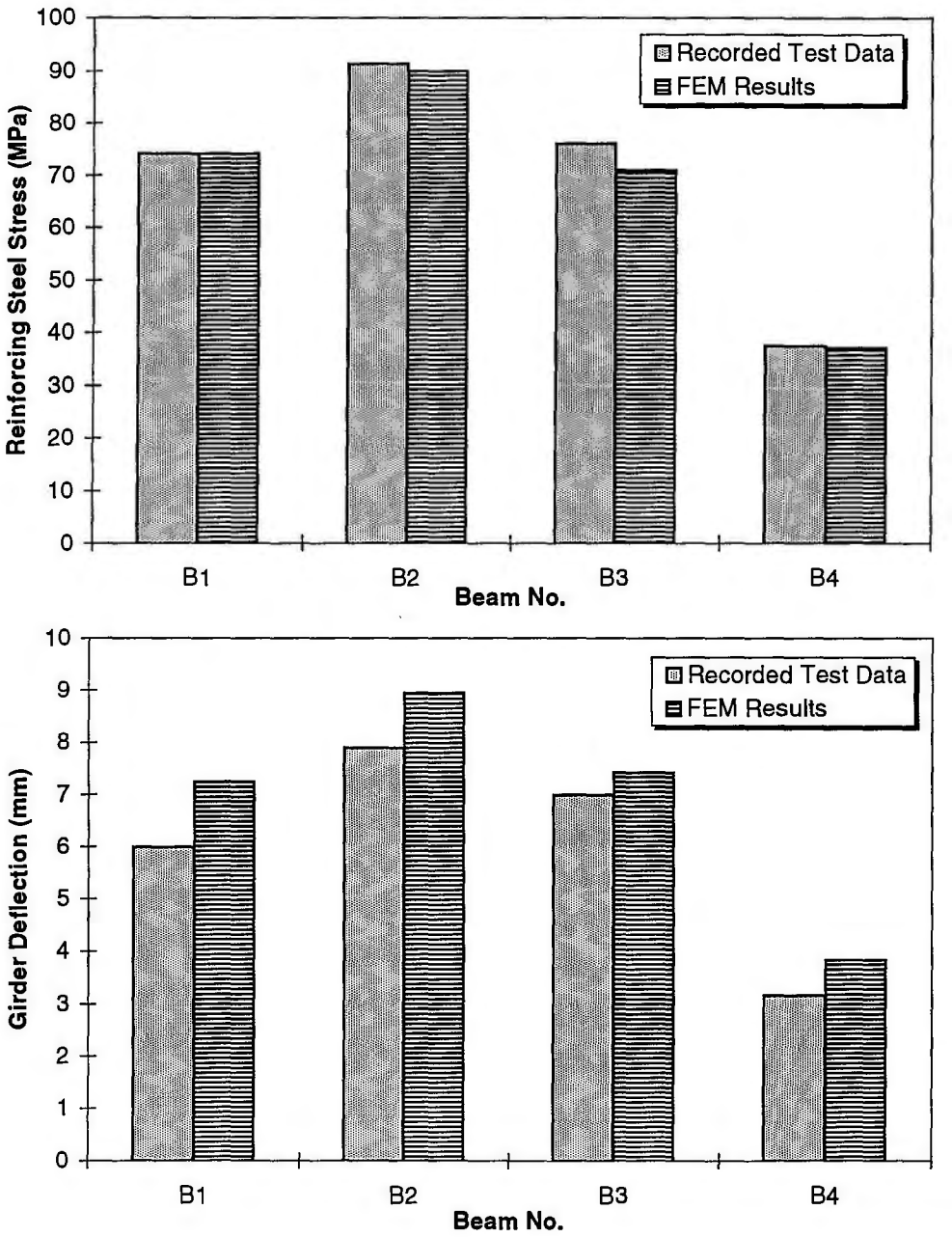

Figure 5.19. Maximum Reinforcing Steel Stresses and Girder Deflections at Midspan Before Rehabilitation (Static Load Position 1, Average, East Gage).

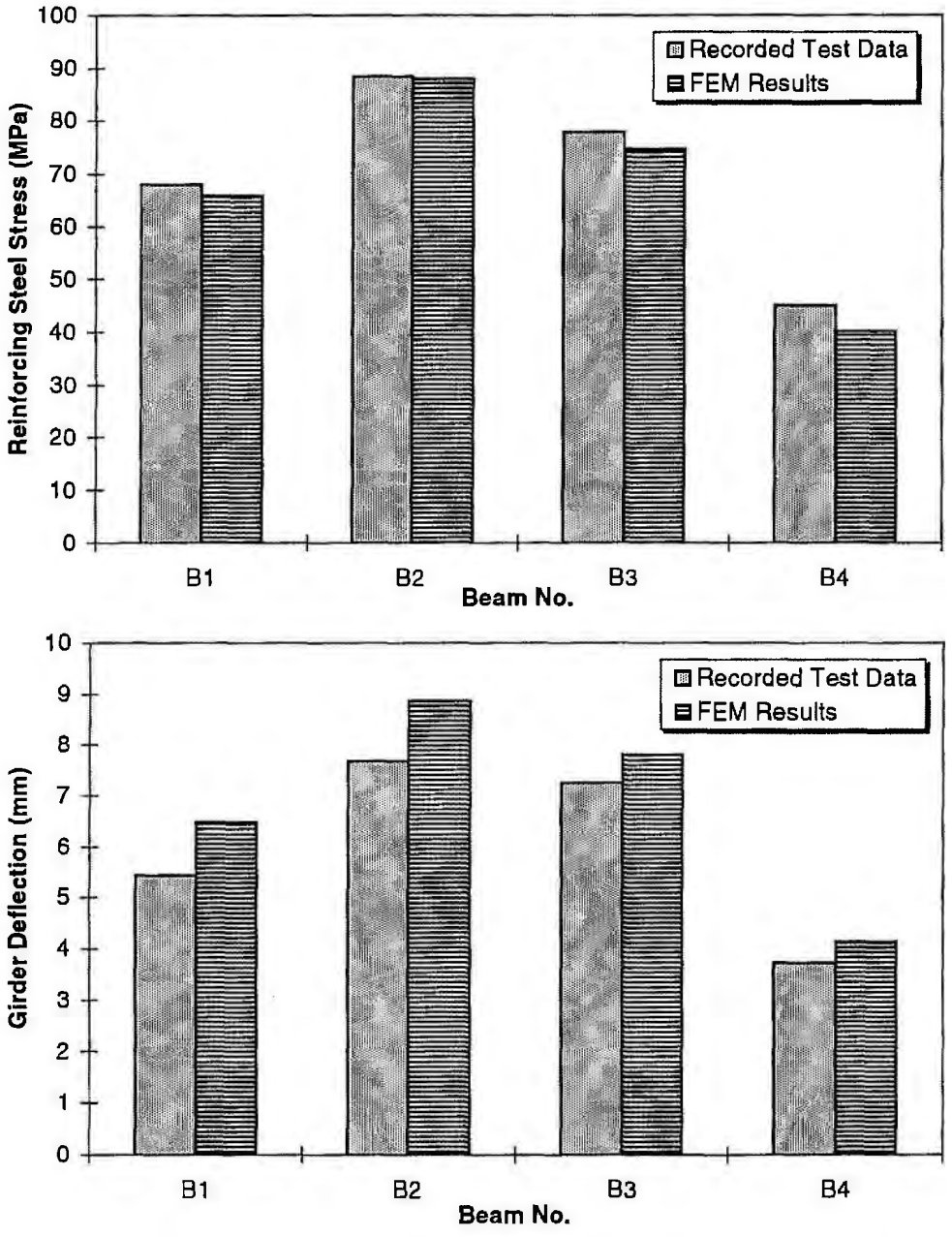

Figure 5.20. Maximum Reinforcing Steel Stresses and Girder Deflections at Midspan Before Rehabilitation (Static Load Position 2).

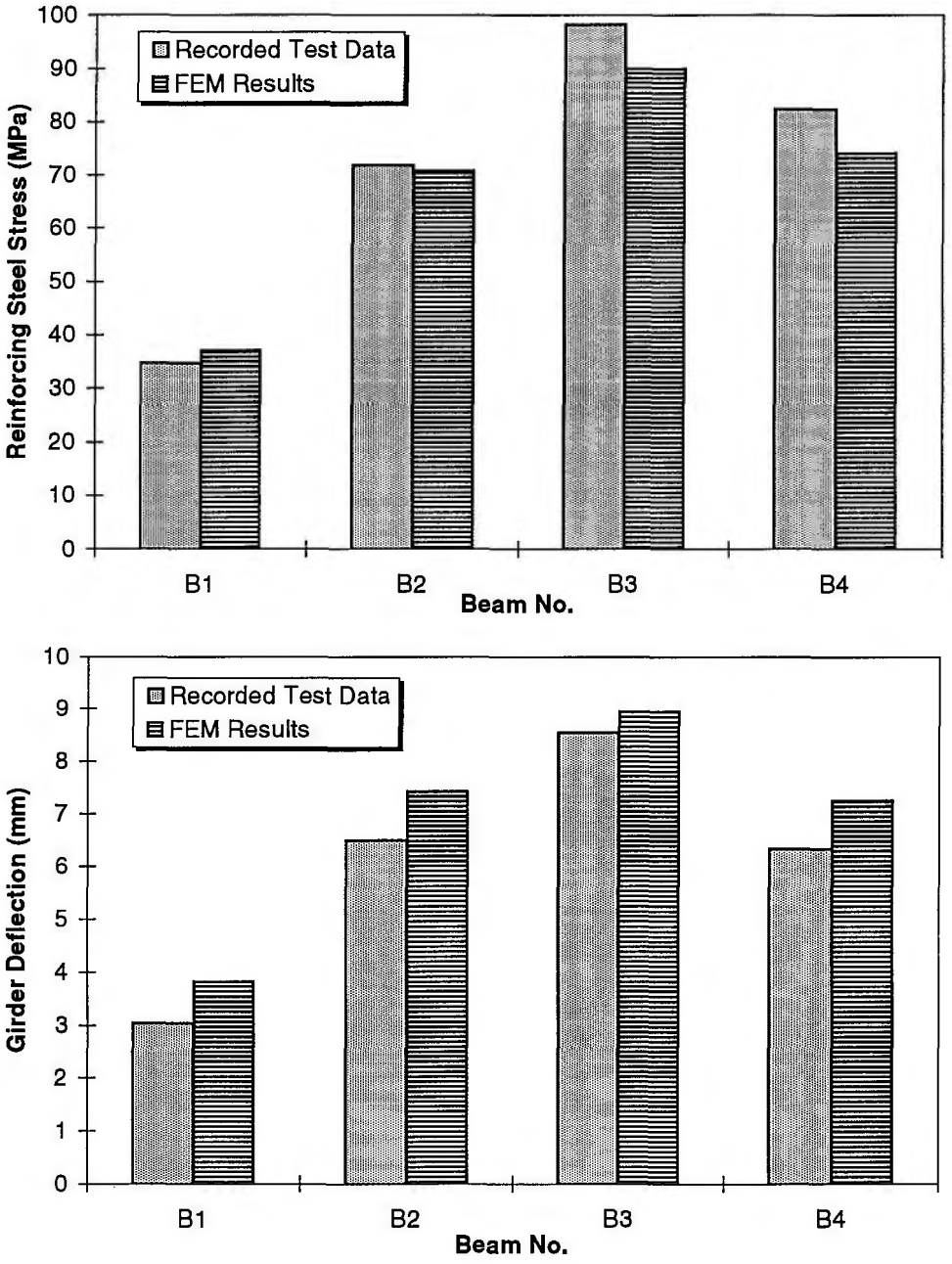

Figure 5.21. Maximum Reinforcing Steel Stresses and Girder Deflections at Midspan Before Rehabilitation (Static Load Position 3).

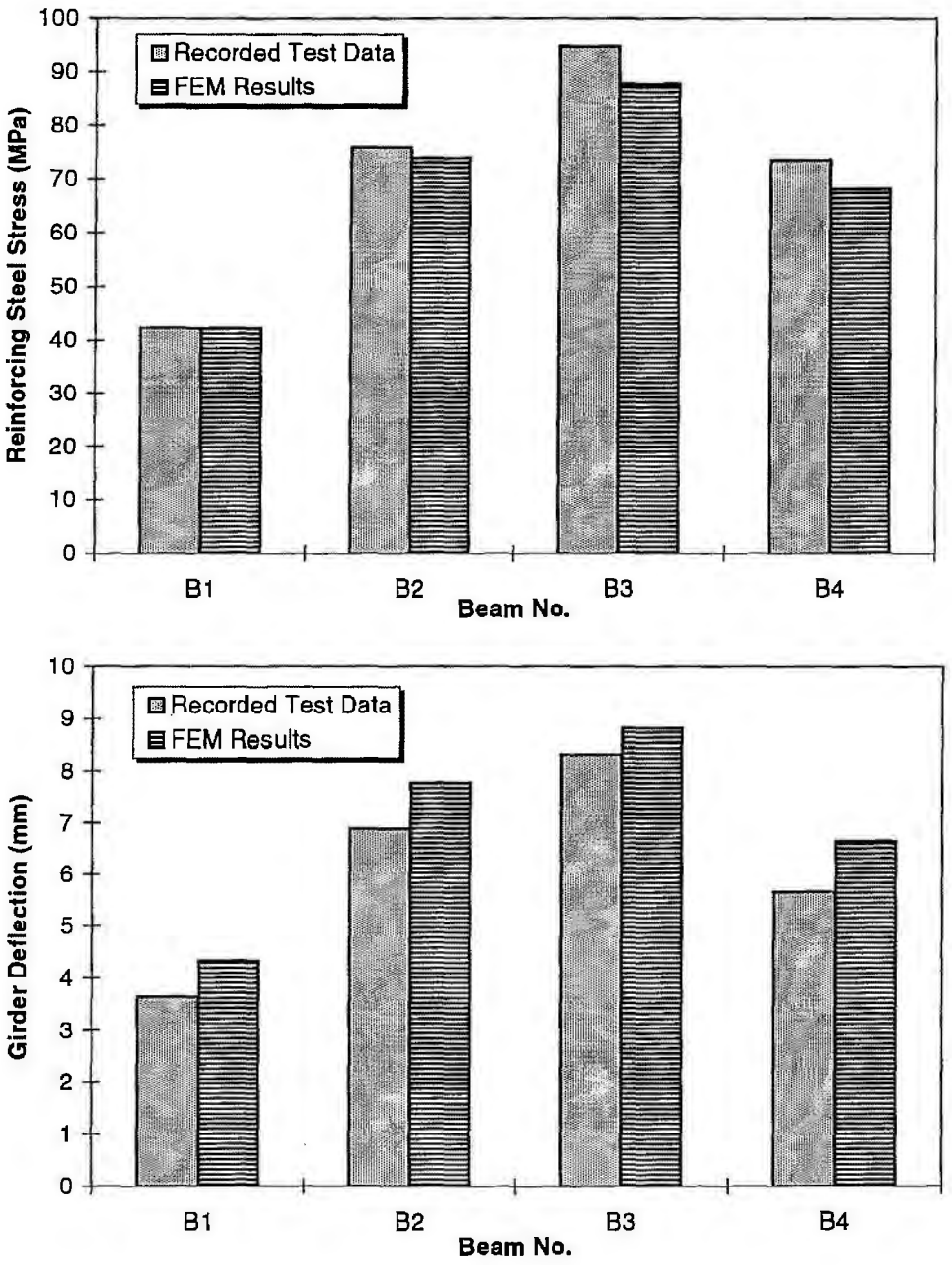

Figure 5.22. Maximum Reinforcing Steel Stresses and Girder Deflections at Midspan Before Rehabilitation (Static Load Position 4).

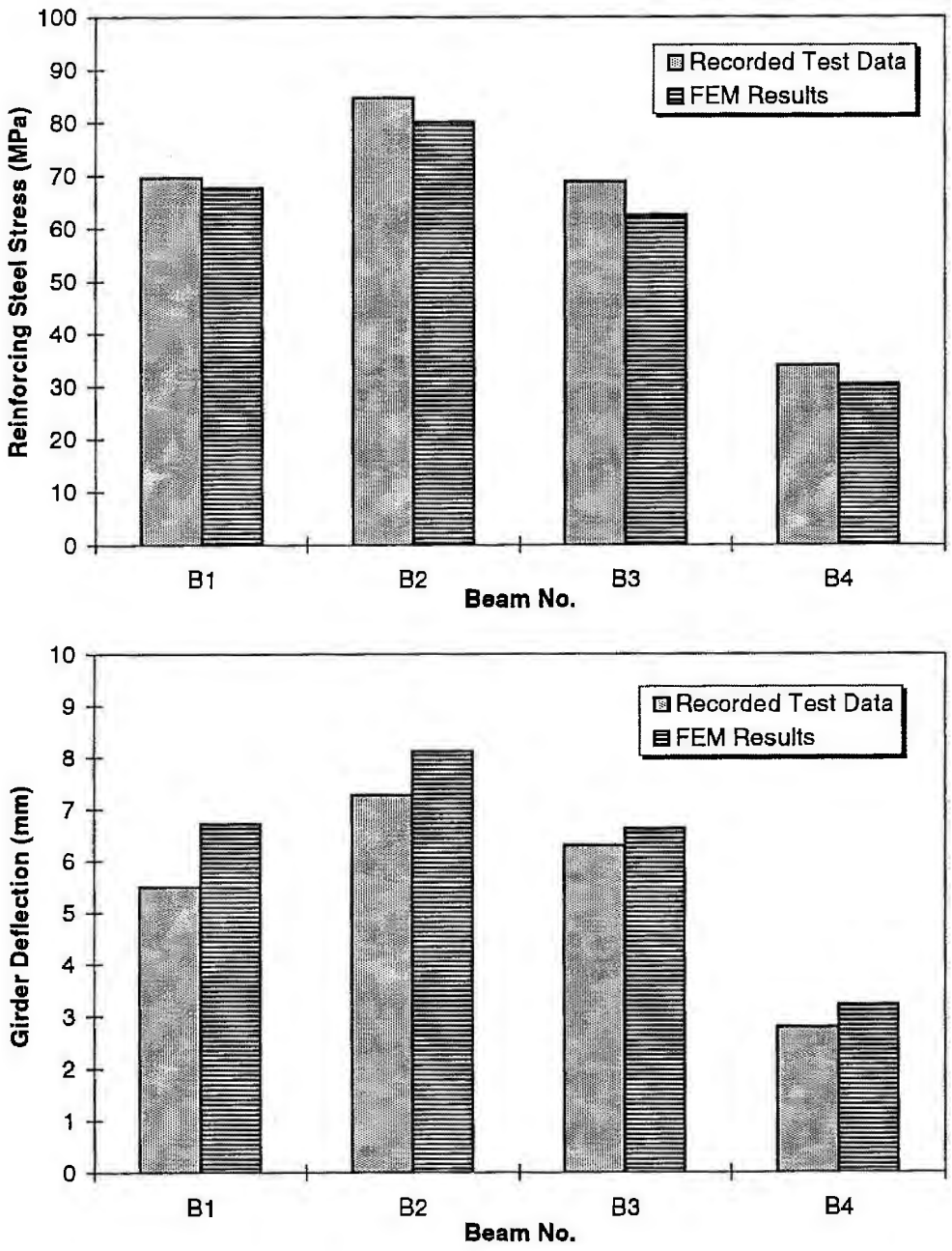

Figure 5.23. Maximum Reinforcing Steel Stresses and Girder Deflections at Midspan After Rehabilitation (Static Load Position 1) (Avg. East Gage).

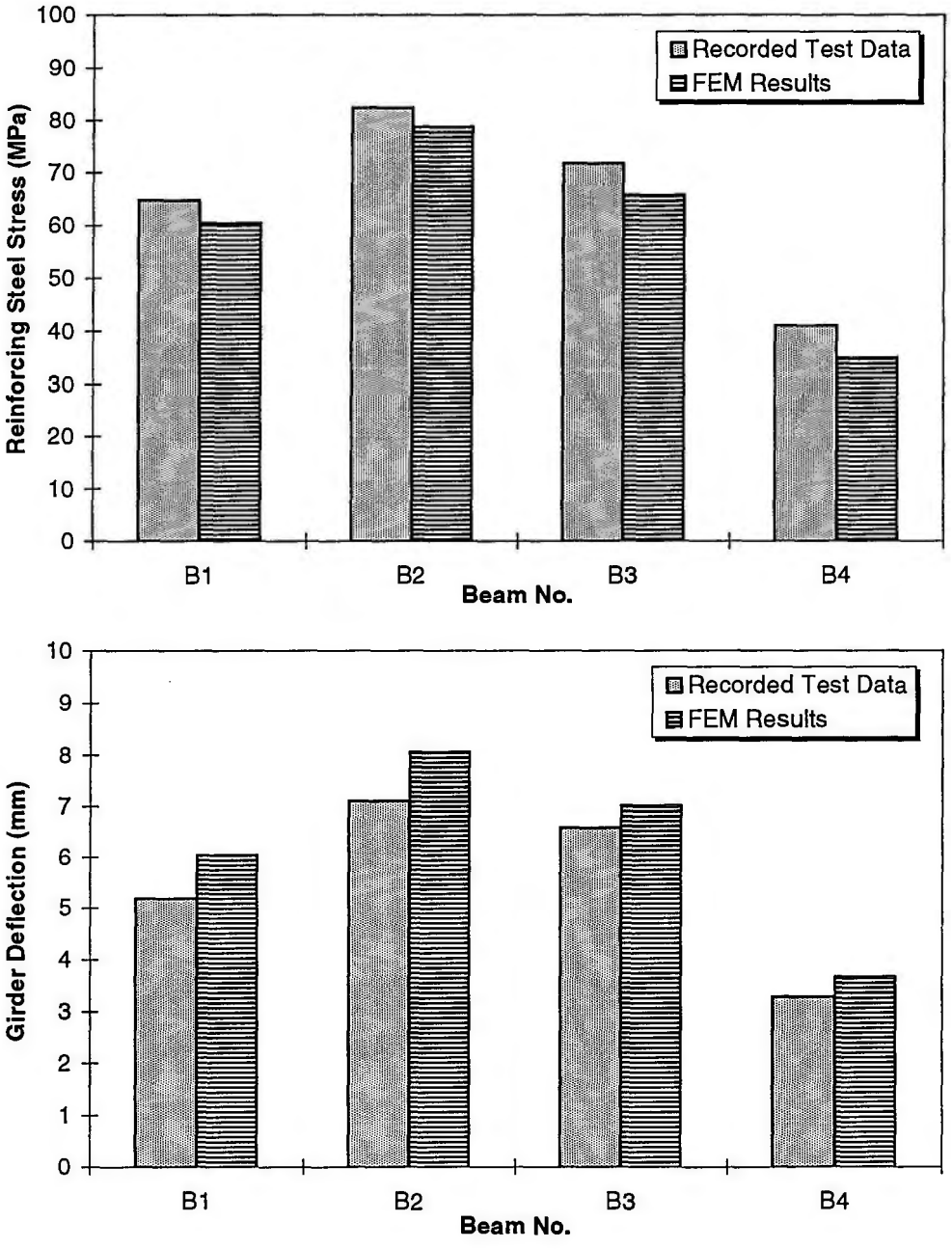

Figure 5.24. Maximum Reinforcing Steel Stresses and Girder Deflections at Midspan After Rehabilitation (Static Load Position 2).

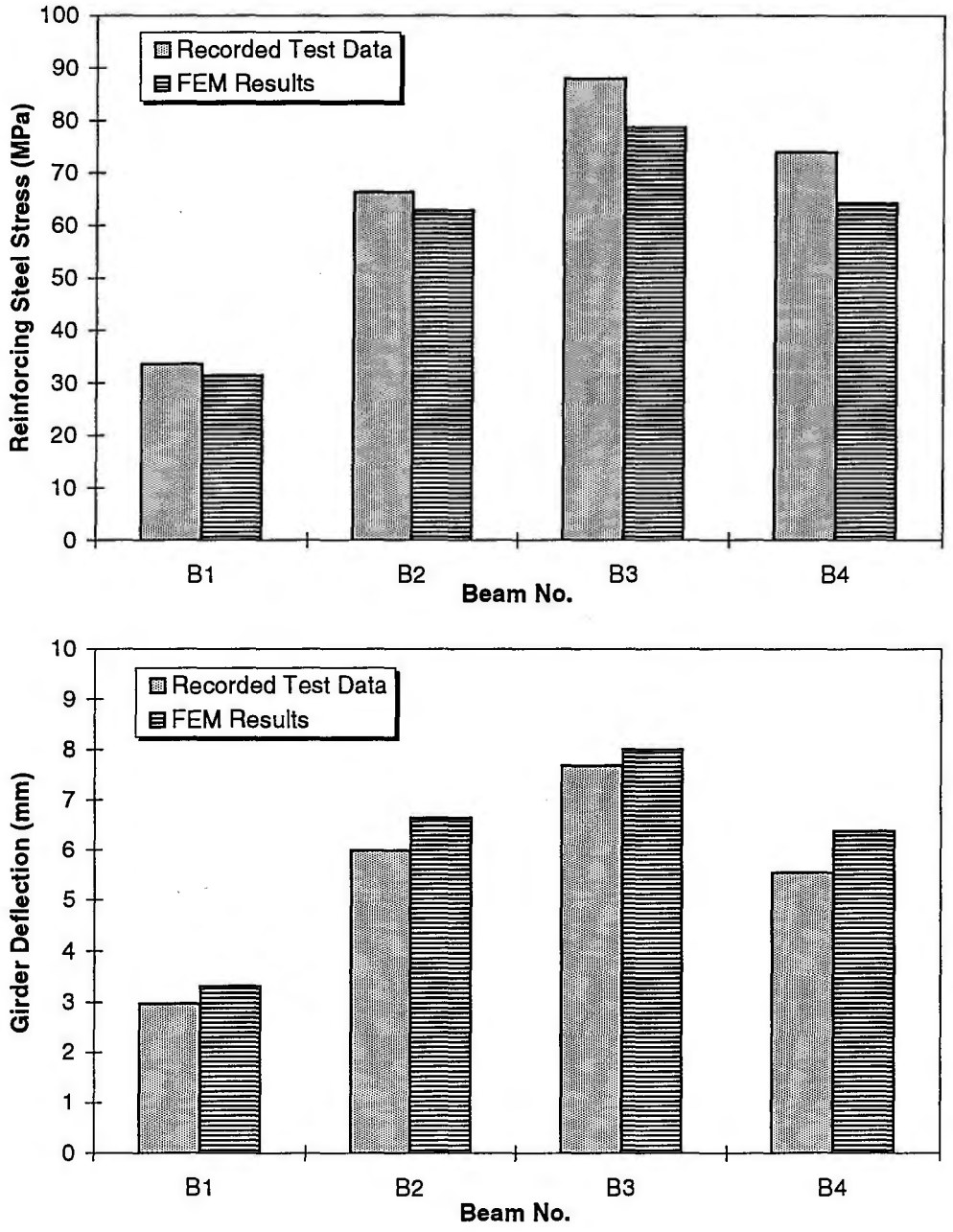

Figure 5.25. Maximum Reinforcing Steel Stresses and Girder Deflections at Midspan After Rehabilitation (Static Load Position 3).

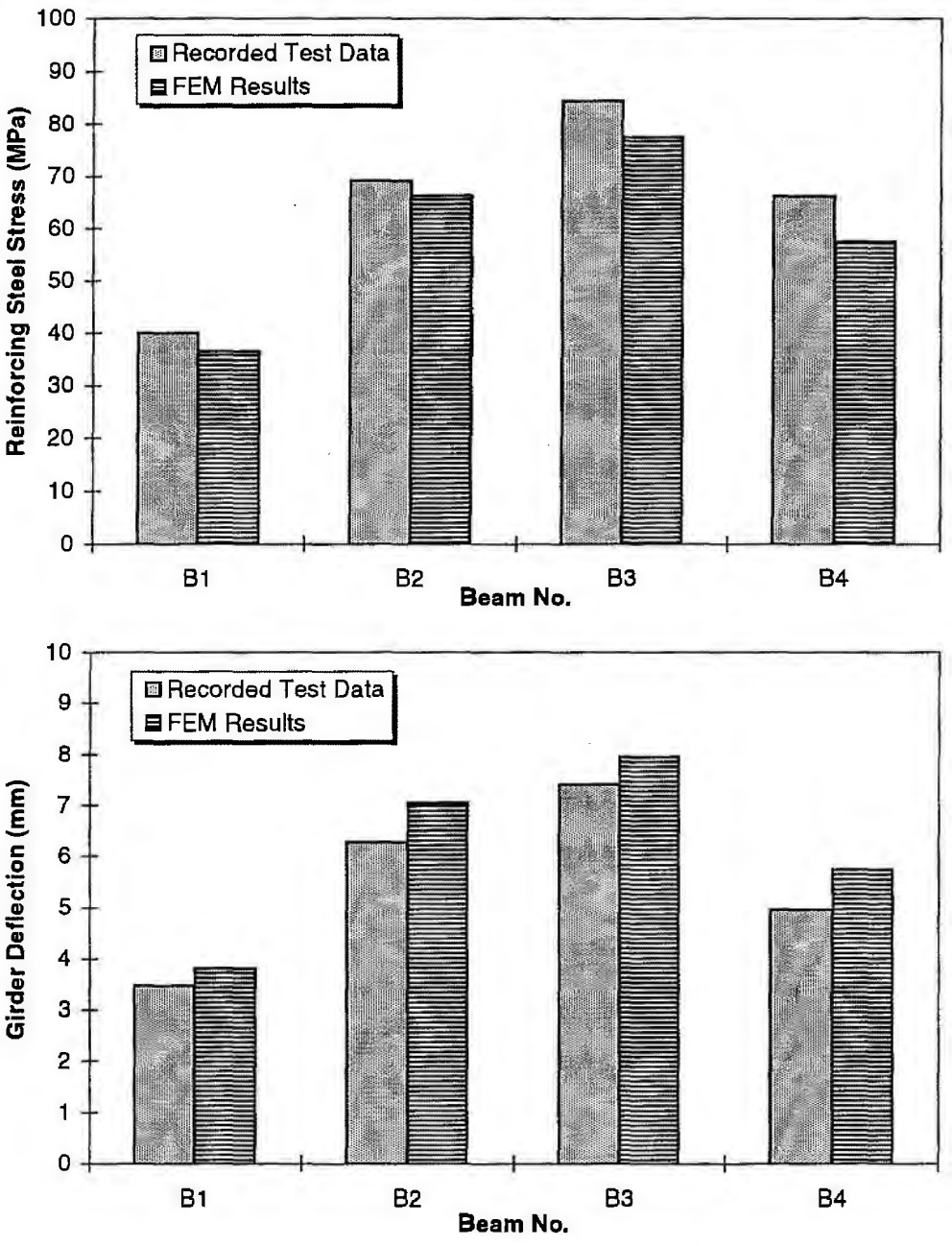

Figure 5.26. Maximum Reinforcing Steel Stresses and Girder Deflections at Midspan After Rehabilitation (Static Load Position 4)

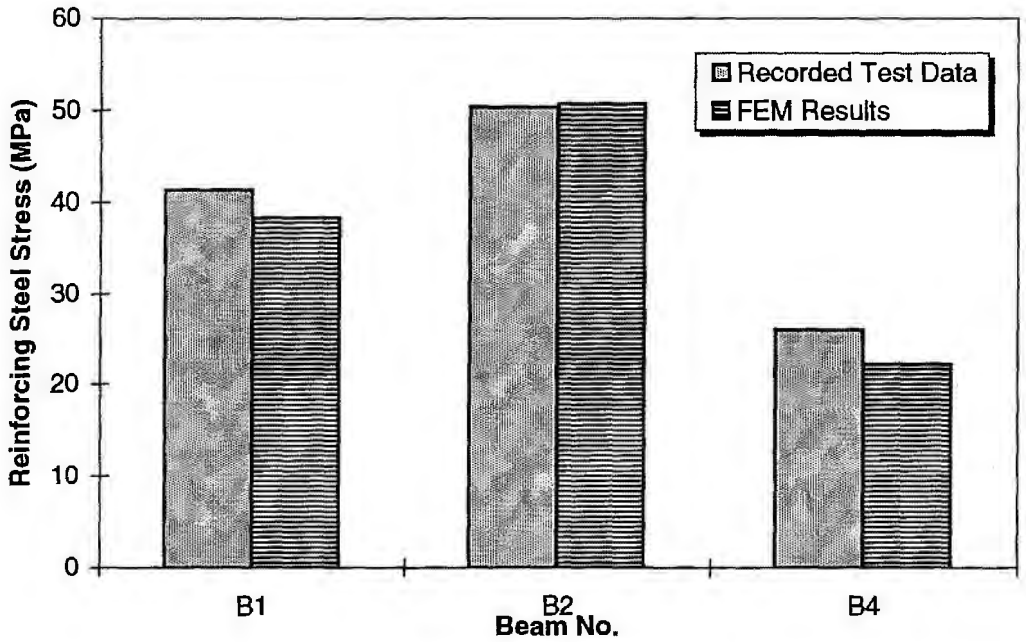

Figure 5.27. Maximum CFRP Stresses at Midspan for Each Beam. (Load Position 2).

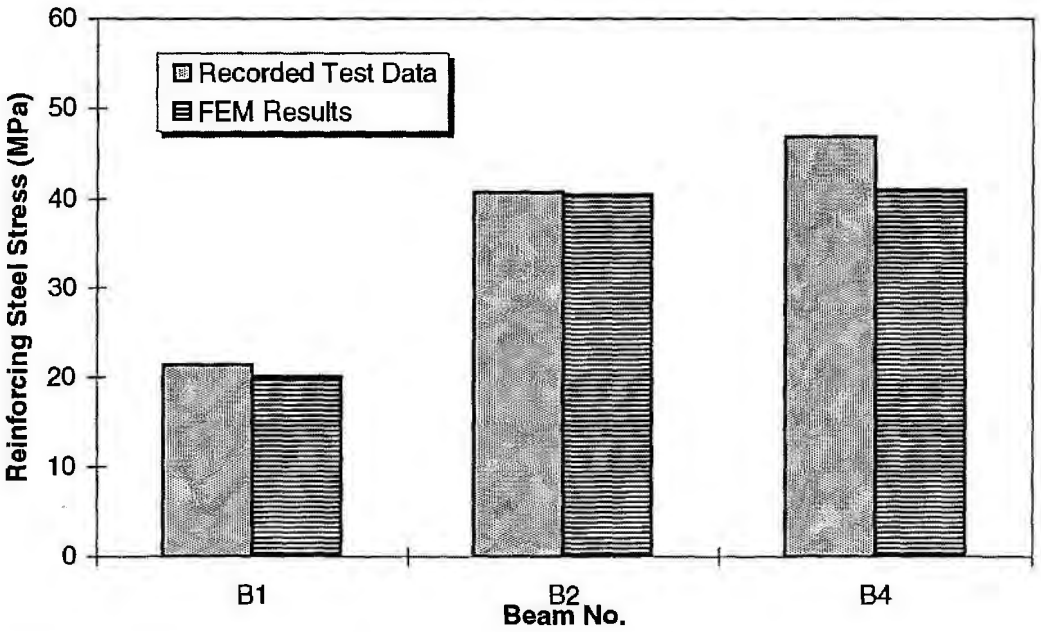

Figure 5.28. Maximum CFRP Stresses at Midspan for Each Beam (Load Position 3).

Parametric Study

The effect of changing the CFRP cross sectional area and modulus of elasticity on the maximum midspan deflection and reinforcing steel stresses of girder B3 was investigated for both the dynamic and static field loading conditions. Increasing the value of either CFRP parameter reduces both the reinforcing steel stresses and girder deflections for the dynamic load case, as illustrated in Figure 5.29 and Figure 5.30, respectively. These observations are attributed to the downward shifting of the neutral axis (for the decrease in reinforcing steel stresses) and the increase in the flexural rigidity, EI (for the decrease in girder deflections).

Table 5.2. Comparison Between Maximum Midspan Stresses (MPa) in CFRP Obtained from Recorded Test Data and the FEM Analysis.

Static load Position	B1		B2		B4		Average difference (%)
	Test	FEM	Test	FEM	Test	FEM	
1	44.5	43.4	51.9	51.5	21.5	19.4	4.5
2	41.3	38.3	50.3	50.6	26.0	22.2	6.7
3	21.4	20.1	40.7	40.4	46.9	41.0	6.5
4	25.5	23.3	42.4	42.6	41.7	36.6	6.8

Figure 5.31 summarizes the effect of increasing the CFRP cross sectional area on reducing both the maximum girder deflection and reinforcing steel stresses for the dynamic load case. Increasing the CFRP cross sectional area can reduce the maximum girder deflection by as much as 22%, and reduce the maximum reinforcing steel stress by as much as 20% , as illustrated in Figure 5.31.

The effect of varying the modulus of elasticity of the CFRP on the dynamic girder deflections and steel reinforcing bar stresses is illustrated in Figure 5.32. It can be concluded that the bonding of the CFRP plates has a significant effect on enhancing the girder performance even for plates with a relatively low modulus of elasticity. However girders repaired with a higher strength material will

exhibit a higher ultimate flexural capacity. The decrease in the maximum girder deflection could be as high as 16% for CFRP plates having a modulus of elasticity of 150,000 MPa.

The parametric study was expanded in the static loading cases to include all four bridge girders. Figure 5.33 illustrates the effect of varying the CFRP cross sectional area on the average change in maximum static girder deflections and reinforcing steel stresses at midspan. From this figure it is apparent that, increasing the CFRP cross sectional area has a significant effect on reducing both girder deflections and reinforcing stresses. It is also evident from Figure 5.33 that the relation between the CFRP cross sectional area and the percentage of change for both girder deflections and reinforcing steel stresses is nearly linear.

The effect of varying the modulus of elasticity of the CFRP bottom plate for all four girders was also studied. Figure 5.34 illustrates the effect of varying the CFRP modulus of elasticity on the average change in maximum static girder deflections and reinforcing steel stresses at mid span. This figure clearly shows that the higher the CFRP modulus of elasticity, the greater is the decrease in both girder deflections and reinforcing steel stresses. Bonding of the CFRP laminates enhances the concrete tension zone confinement as well as the girder flexural stiffness regardless of its modulus. These results also indicate that girders repaired with CFRP having a low modulus of elasticity will still exhibit a significant reduction in girder deflection and reinforcing steel stresses at the service load stage. However, at the ultimate load stage, the CFRP tensile strength is the critical parameter controlling the increase in capacity. For example, if the bridge were repaired by bonding GFRP plates (E=23.7 GPa) to the bottom of the girders instead of CFRP plates, approximately an 8% reduction in both reinforcing steel stresses and girder deflections would have been achieved at the service load level. However the ultimate capacity of the bridge would have been increased only 7% using GFRP bottom plates instead of the 20% increase realized for the CFRP bottom plates.

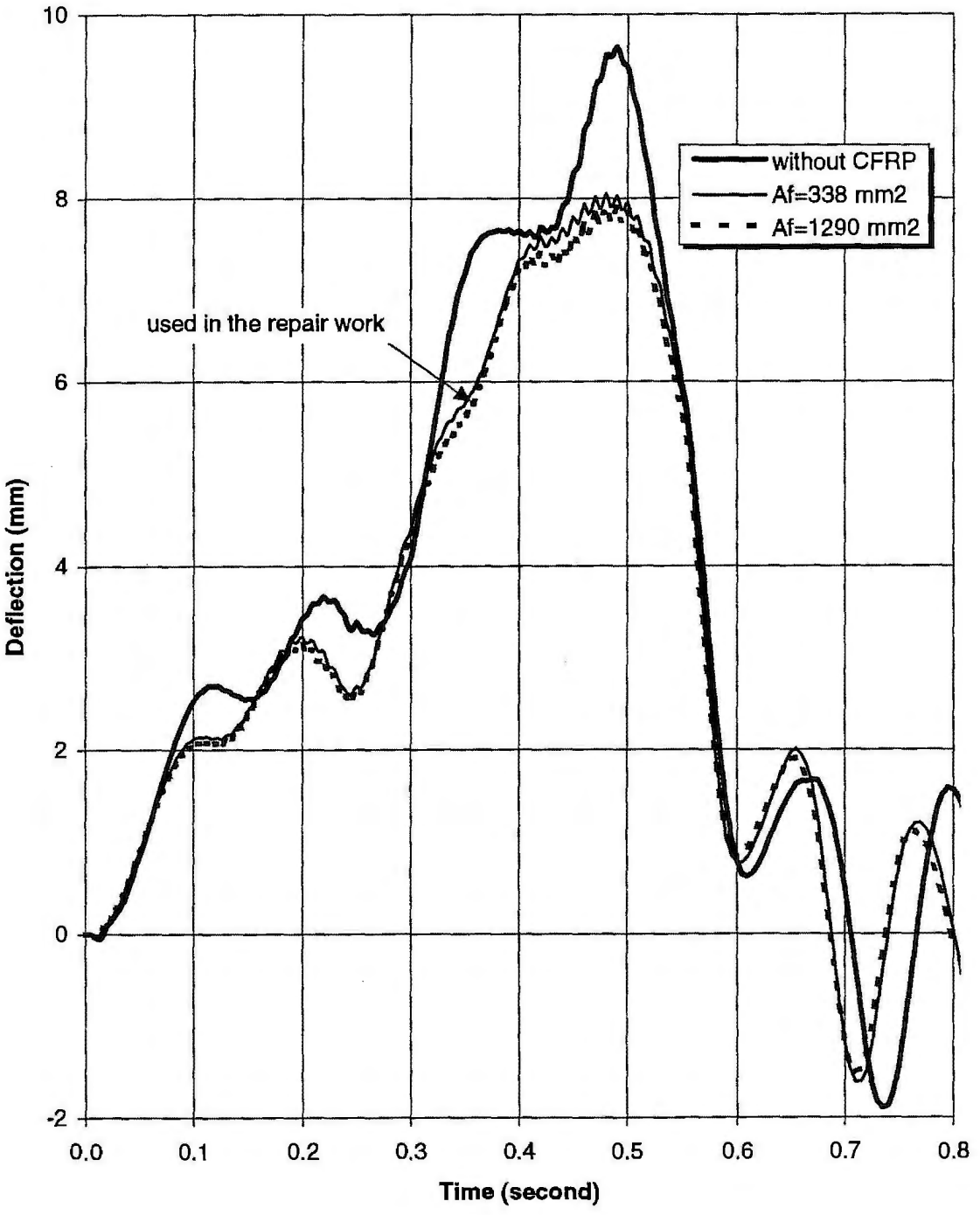

Figure 5.29. Midspan Deflection Time Histories for Girder B3 for Different CFRP Cross Sectional Areas.

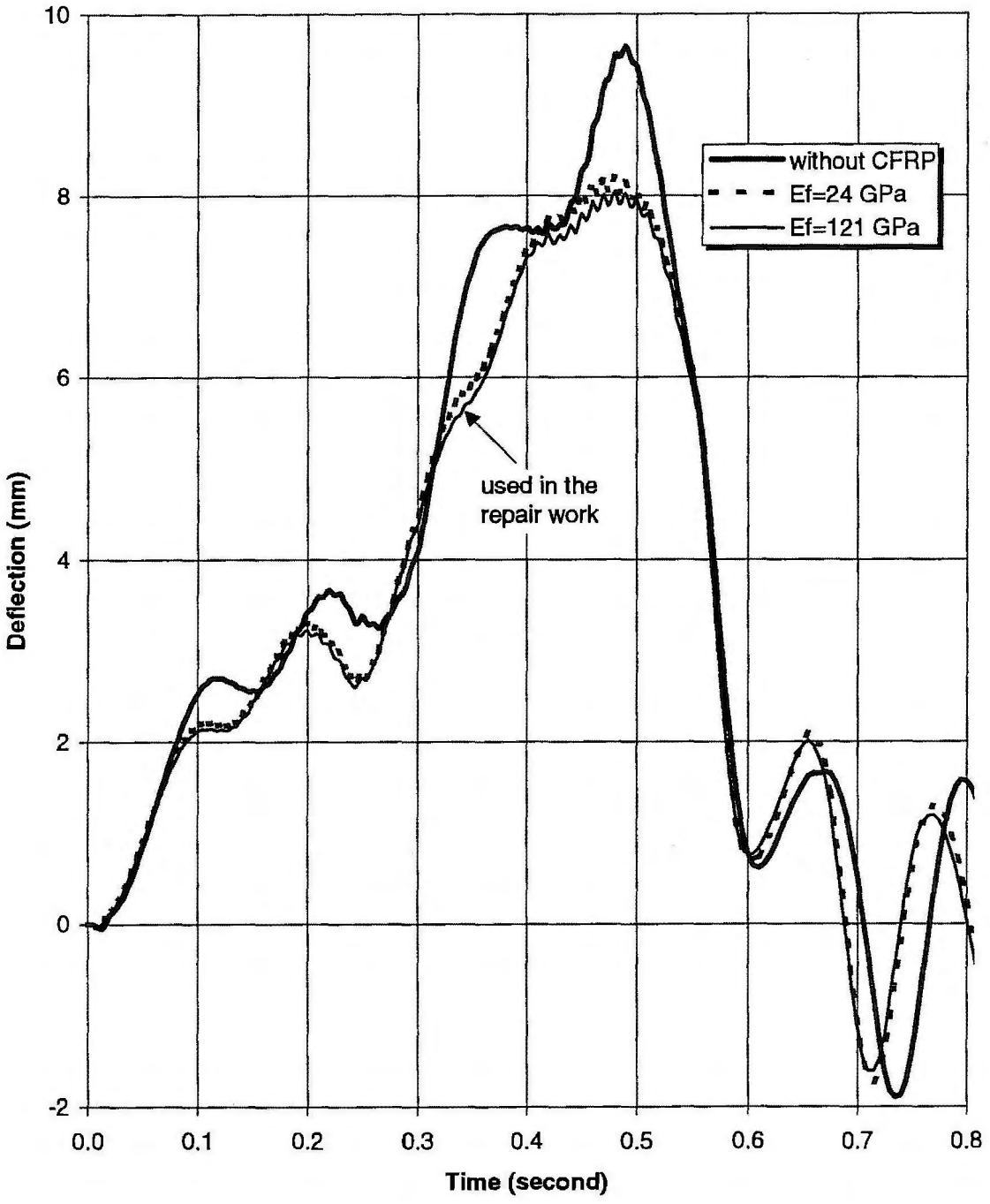

Figure 5.30. Midspan Deflection Time Histories for Girder B3 with Different CFRP Modulii of Elasticity.

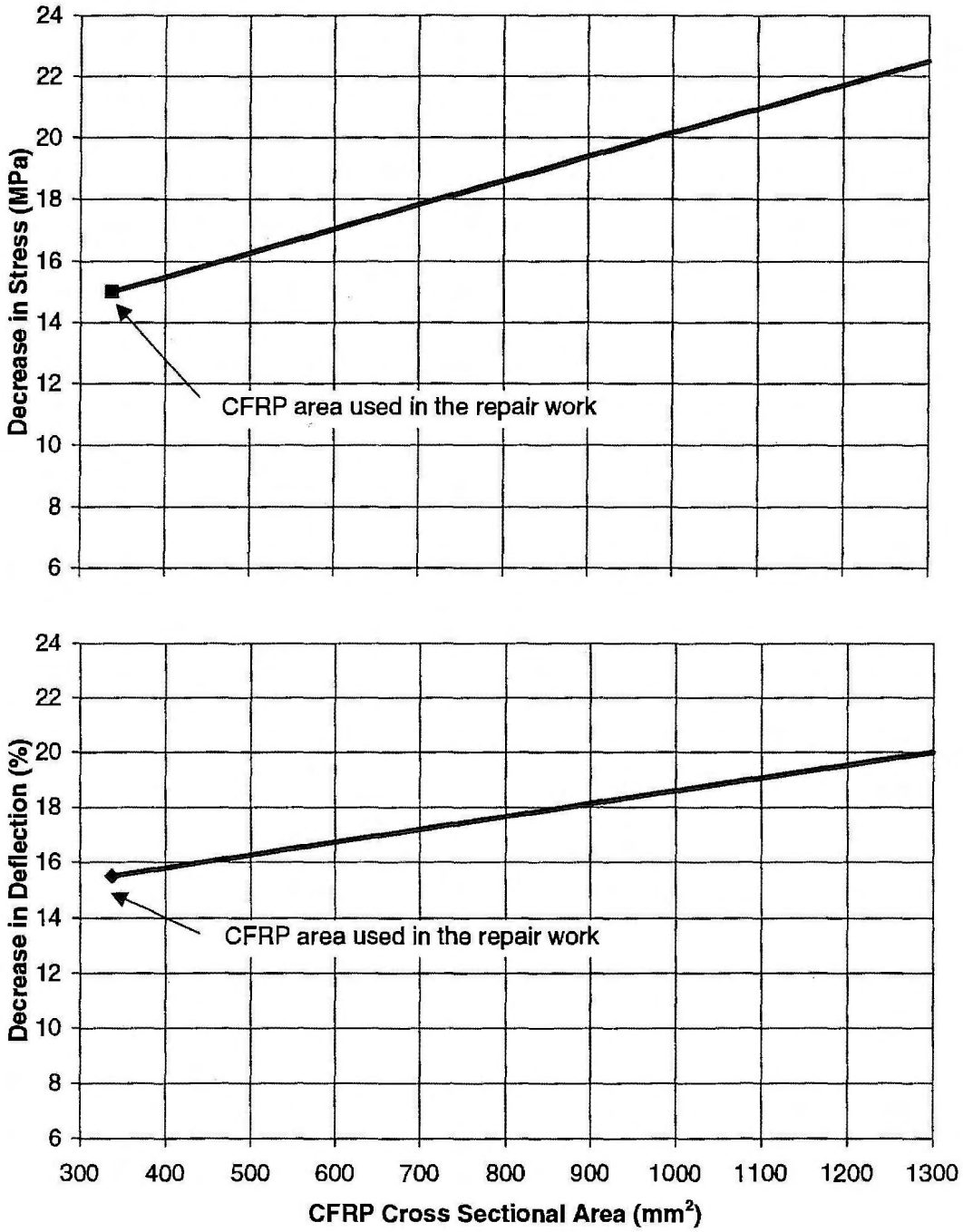

Figure 5.31. Effect of the CFRP Cross Sectional Area on Reduction of Maximum Girder Deflection and Maximum Stress in Reinforcing Steel (Girder B3).

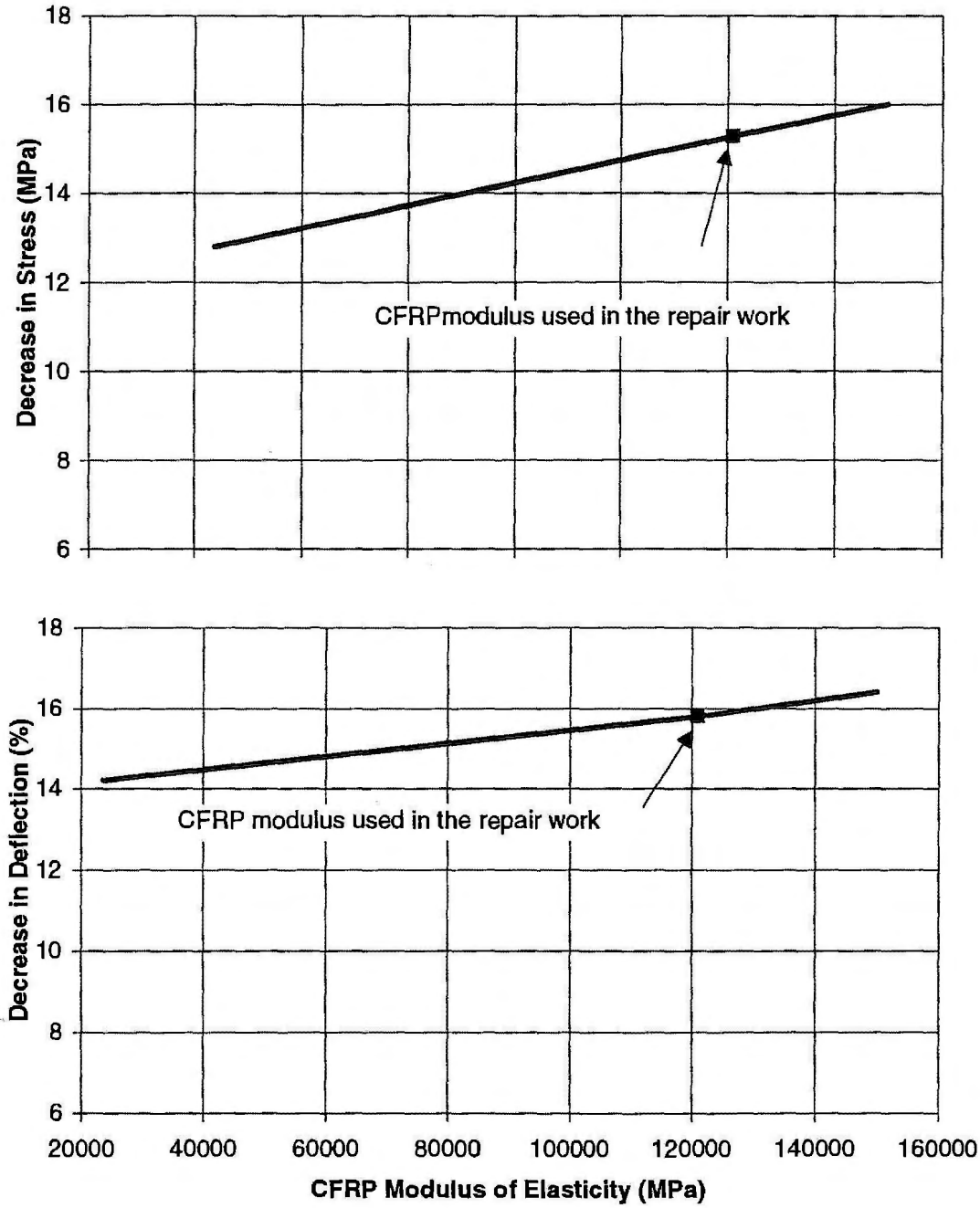

Figure 5.32. Effect of the CFRP Modulus of Elasticity on Reduction of Maximum Girder Deflection and Maximum Stress in Reinforcing Steel (Girder B3).

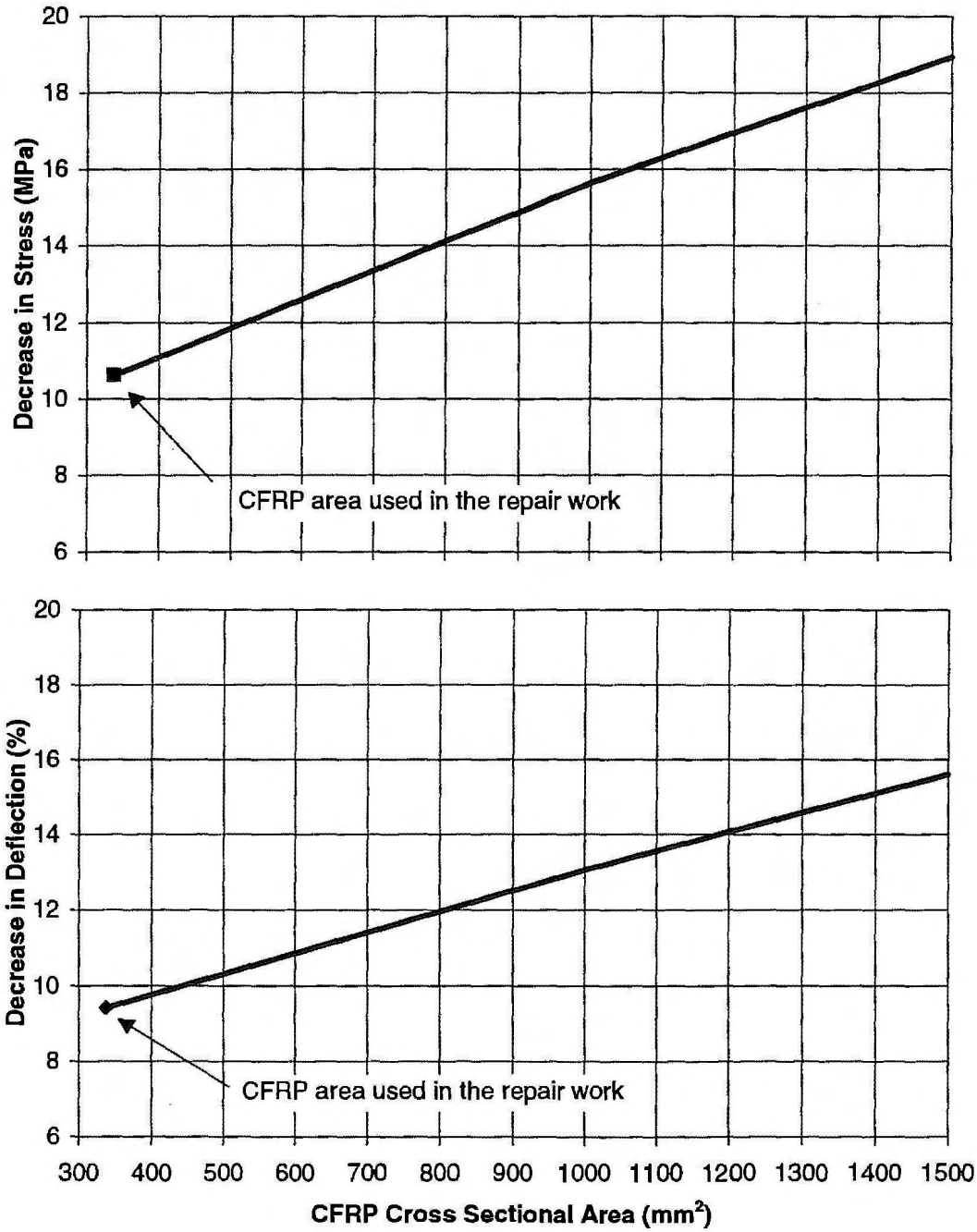

Figure 5.33. Effect of Varying the CFRP Cross Sectional Area on the Average Change in Static Girder Deflections and Reinforcing Steel Stresses at Midspan.

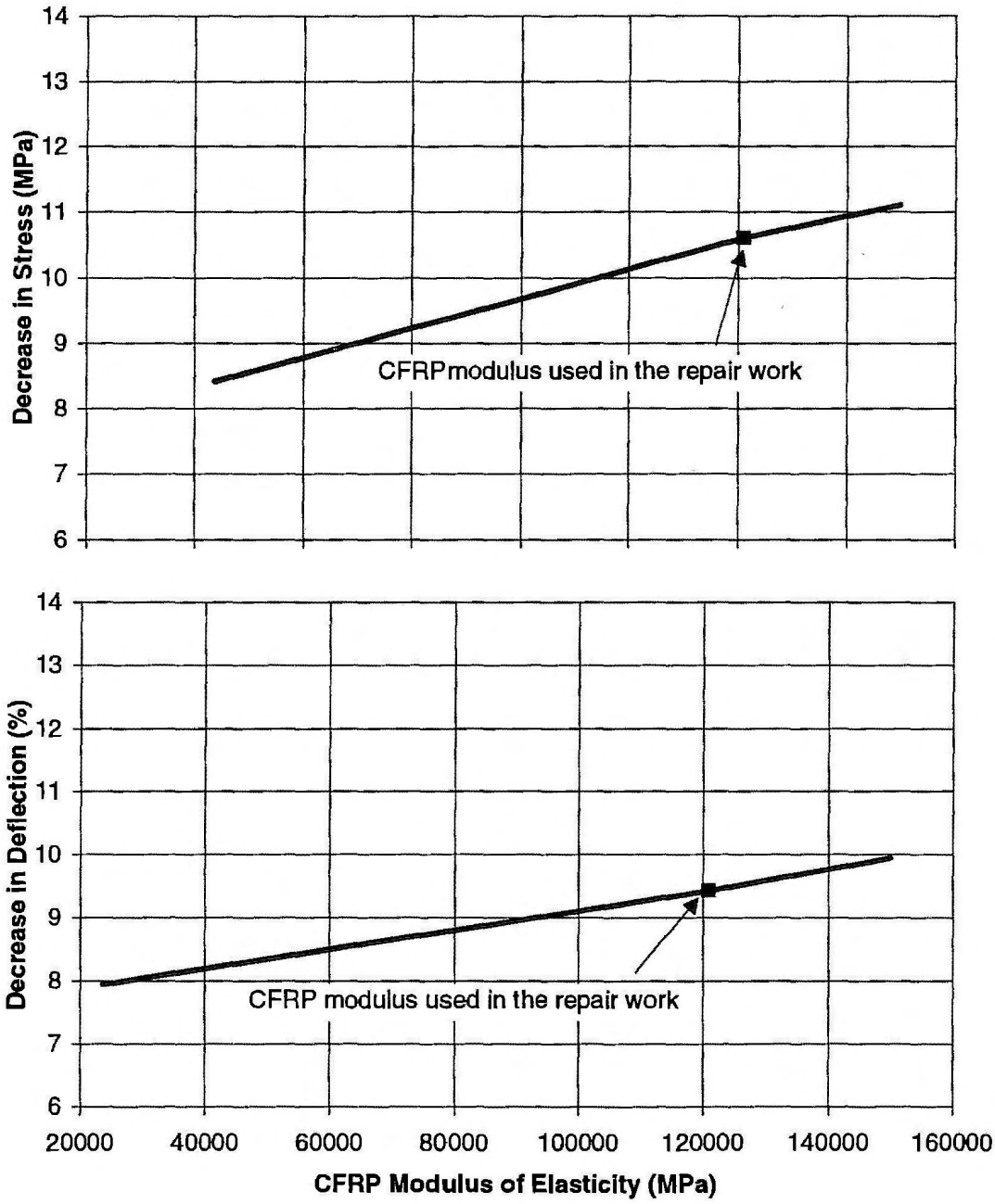

Figure 5.34. Effect of Varying the CFRP Modulus of Elasticity on the Average Change in Static Girder Deflections and Reinforcing Steel Stresses at Midspan.

SECTION ANALYSIS

A section analysis was conducted to study the effect of bonding the FRP laminates to the girders on enhancing the ultimate load capacity of the bridge. The analysis was performed using strain compatibility and equilibrium equations. The details of the section analysis procedure are presented in Appendix A. The concrete girders were analyzed as T-sections, having an effective flange width determined in accordance of ACI 318-95 (ACI 1995) criteria. The total tensile steel reinforcement for the rehabilitated girders consisted of two layers of No. 11 bars (i.e. 3 bars in each layer) and the CFRP plate bonded to the bottom of the girder. The GFRP side plates were not considered in this calculation. It was determined that the CFRP plates would attain their ultimate strain before the concrete strain in the extreme compression fiber of the girders attained its ultimate strain (0.003). This mode of failure is referred to as steel yield-FRP rupture.

In this mode of failure, when the FRP ruptures, the girder ultimate capacity will drop to its virgin strength (i.e. without the FRP laminates) corresponding to the current strain field, and continue to deform until failure is precipitated by crushing of concrete. To calculate the concrete stress at any stage below the ultimate condition, a non linear constitutive concrete model (a modified Hognestad formulation) was used as shown in Figure 5.35. A computer program was developed to calculate the ultimate load capacity for both rectangular and T-sections repaired with FRP plates.

Effect of CFRP Cross Sectional Area on Girder Ultimate Strength

The effect of varying the CFRP cross sectional area on the bridge ultimate capacity was investigated using the previously defined section analysis method. This was achieved by analyzing each individual girder with an effective flange width determined in accordance ACI 318-95 (ACI 1995), and assuming that premature failure due to CFRP laminate separation at the ends of the girder would not occur. It was determined that increasing the CFRP plate cross sectional area not only

affects the girder ultimate strength but the mode of failure as well.

Table 5.3 summaries the effect of varying the CFRP cross sectional area on the ultimate flexural strength and the mode of failure of the girder. It can be concluded that, increasing the CFRP cross sectional area increases the ultimate strength in a linear fashion as illustrated in Figure 5.36. For example, if the CFRP cross sectional area used in the repair work was increased by 400 percent, the ultimate capacity would have increased by 100 percent. Beyond the threshold where the concrete crushing-steel yield mode of failure controls, the rate of increase in the ultimate strength decreases because the CFRP stress has been maximized at its tensile strength.

The mode of failure for the subject bridge, at it was repaired, is expected to be the steel yield-FRP rupture mode as shown in Table 5.3. At the failure load, the CFRP will rupture and the bridge will abruptly return to its original virgin (unrepaired) strength. Thicker plates tend to move the neutral axis of the girder downward and decrease the CFRP strain at failure, indicating that the CFRP will not attain its tensile strength. In this case failure will occur with the steel reinforcement yielding and subsequent crushing of the concrete (tension failure). Both the FRP rupture and tension failure modes are ductile and will exhibit significant deformation before collapse. If the CFRP cross sectional area is increased further, the steel reinforcement will not yield and failure will be controlled by concrete crushing in the compression zone (compression failure). This type of failure is highly undesirable, but is unlike to occur in girder T-sections with wide flanges because the area of the CFRP required to balance the compression force would have to be extremely large. However, for rectangular sections or T-sections with narrow flanges, this type of failure may be encountered, especially in sections with high steel reinforcement ratios.

Effect of CFRP Tensile Strength on the Ultimate Strength of The Girder

The CFRP bottom plate tensile strength affects the ultimate capacity of the bridge whenever

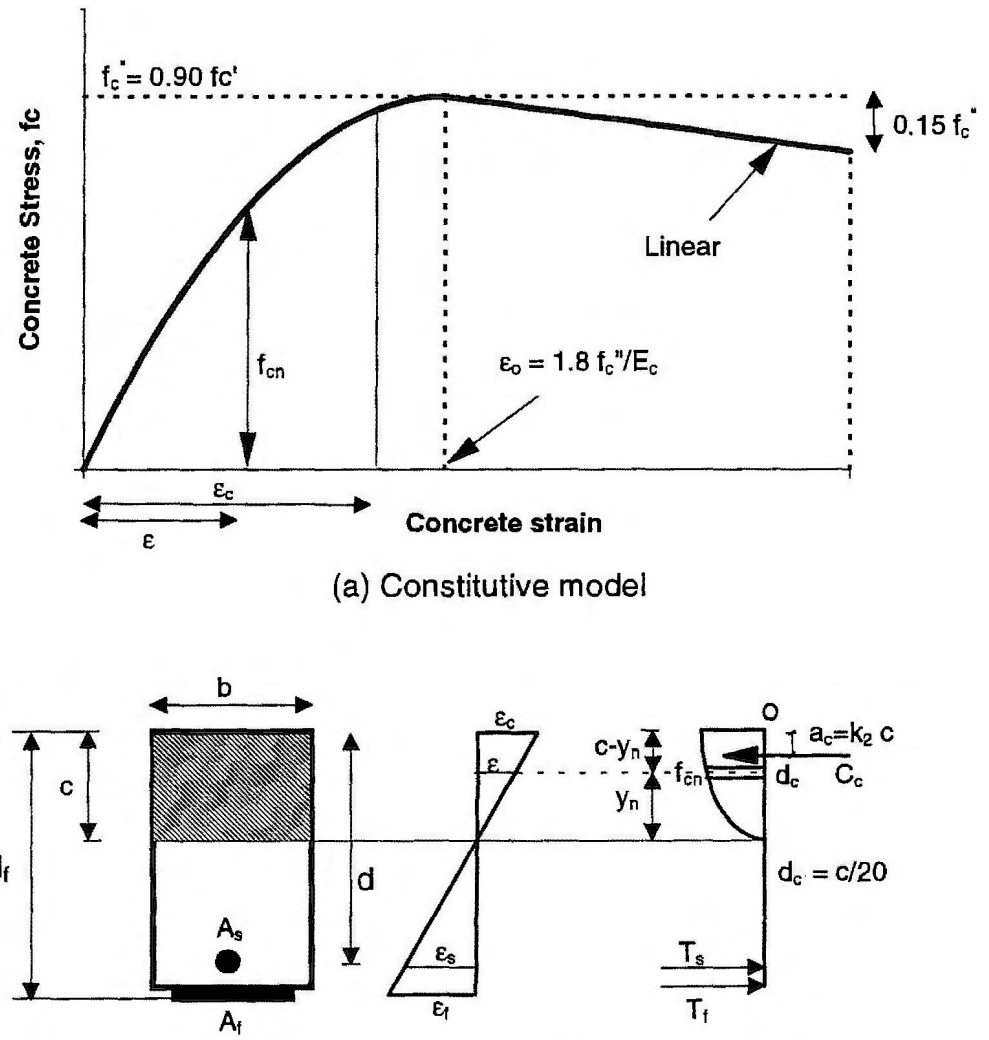

Figure 5.35. Modified Hognestad Concrete Stress-Strain Curve used in the Sectional Analysis Computer Program.

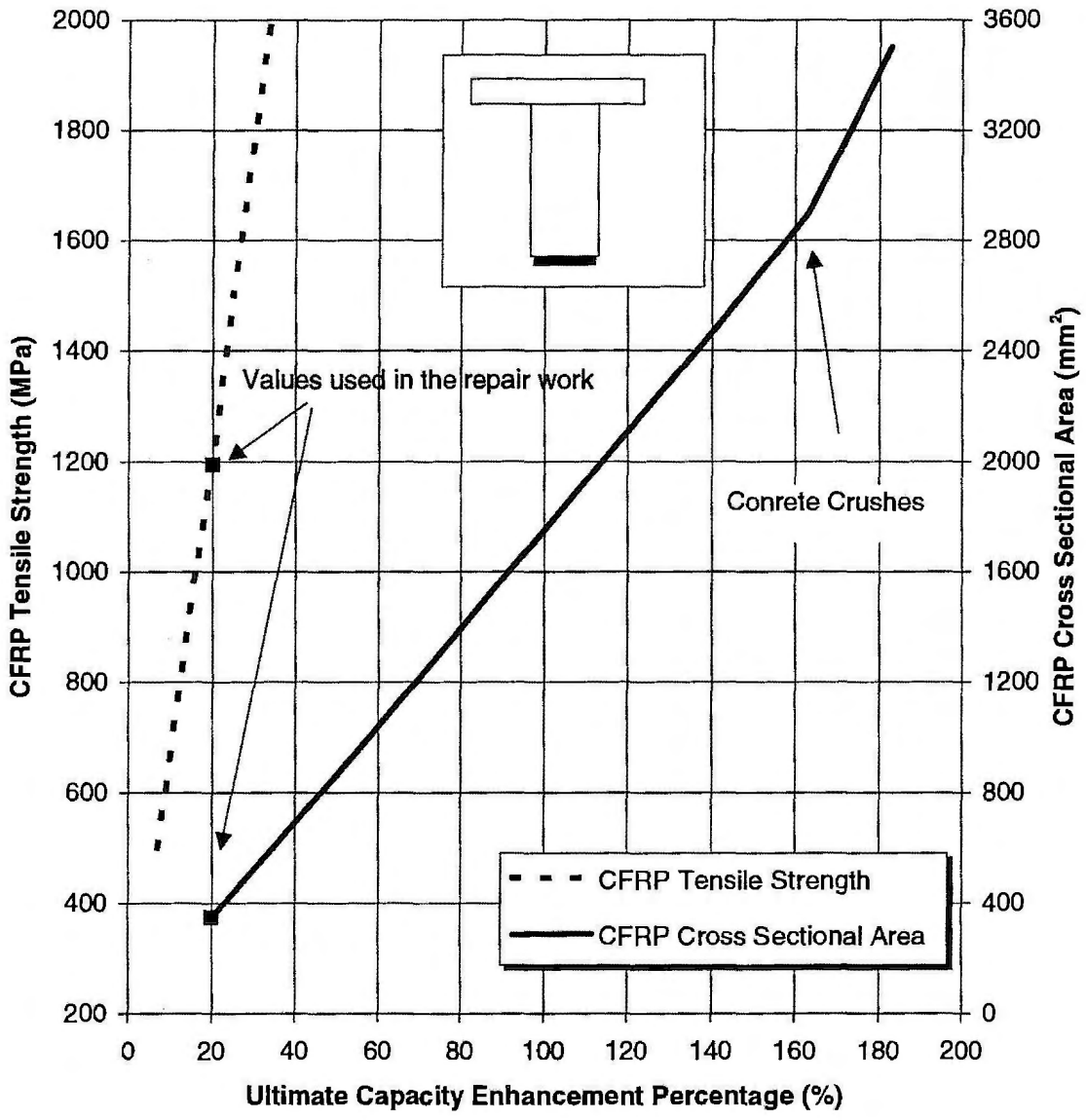

Figure 5.36. Effect of CFRP Cross Sectional Area and Elastic Modulus on Enhancement Percentage of Girder Ultimate Capacity.

the FRP rupture mode of failure controls. In this case the modulus of elasticity of the plate will have no effect on the ultimate capacity. However, it affects the girder stiffness, reinforcing steel strains and girder deflections. On the other hand, if the steel yield-concrete crush mode of failure controls, the CFRP modulus of elasticity will have an effect on the girder ultimate capacity. The tensile strength of the CFRP plate will have no effect on the girder ultimate capacity as long as the plate does not rupture. However, as previously discussed, for most standard T-sections the FRP mode of failure will dominate, therefore FRP tensile strength is an important consideration when calculating the girder ultimate strength.

Table 5.4 illustrates the effect of CFRP tensile strength on the girder ultimate flexural strength. It is obvious that increasing the CFRP tensile strength increases the girder ultimate capacity in an almost linear trend. In all cases investigated, the neutral axis lies within the slab thickness, therefore the CFRP reaches its ultimate tensile strain while the concrete strain remains well below its ultimate strain ϵ_{cu} (0.003).

Design Charts

For any future repair work, the amount of the FRP required to upgrade a structure to a certain pre-specified capacity can be difficult to calculate. This difficulty is attributed to the fact that the enhanced capacity of the repaired structure depends on many factors such as concrete strength, steel reinforcement ratio and grade, FRP cross sectional area, FRP modulus of elasticity and FRP tensile strength. Also, a trial and adjustment (iterative) procedure is required to achieve a solution. The process can be simplified by using appropriate design charts. A computer program has been developed to calculate the ultimate flexural strength and mode of failure for both rectangular and T-section girders for any given concrete strength, steel reinforcement ratio and FRP cross sectional area and material characteristics. Using this computer program, design charts similar to that shown in Figure 5.37 may be generated.

Table 5.3. Effect of CFRP Cross Sectional Area on Ultimate Flexural Strength of Girder

Area of CFRP mm^2	Concrete strain at failure	Ultimate moment Kn.m	% increase in ultimate strength	Mode of Failure
0	0.0030	1215	N/A	Steel Yield-Concrete Crushes
347*	0.0015	1454	20	Steel Yield-FRP Rupture
500	0.0016	1566	29	Steel Yield-FRP Rupture
1000	0.0019	1922	58	Steel Yield-FRP Rupture
1500	0.0021	2263	86	Steel Yield-FRP Rupture
2000	0.0023	2605	114	Steel Yield-FRP Rupture
2500	0.0026	2936	142	Steel Yield-FRP Rupture
3000	0.0030	3225	165	Steel Yield-Concrete Crushes
3500	0.0030	3446	183	Steel Yield-Concrete Crushes

** CFRP ultimate strength used in the bridge repair

Table 5.4. Effect of CFRP Tensile Strength on Ultimate Flexural Strength of Girder

CFRP ultimate strength (MPA)	Concrete strain at failure	Ultimate moment Kn.m	% increase in ultimate strength	Mode of Failure
0	0.0030	1215	N/A	Steel Yield-Concrete Crushes
500	0.0014	1300	7	Steel Yield-FRP Rupture
1000	0.0015	1415	16	Steel Yield-FRP Rupture
1194**	0.0015	1454	20	Steel Yield-FRP Rupture
1500	0.0016	1518	25	Steel Yield-FRP Rupture
2000	0.0017	1623	34	Steel Yield-FRP Rupture

** CFRP ultimate strength used in the bridge repair

In the analysis, the compression reinforcement was ignored and the ratio of the FRP depth (d_f) to the reinforcing steel depth (d) was set fixed at 1.2. Such design charts must be constructed for each type of FRP considered for use. To use the chart, simply locate the point corresponding to the given steel reinforcement ratio (ρ) and the required girder moment capacity (M_u). Read from the chart the required FRP ratio (ρ_f), from which the required cross sectional area of FRP is determined from the expression:

$$A_f = \rho_f \, b \, d \tag{5.5}$$

It should be noted that, if the point selected for the given and required M_u does not fall within the family of curves presented on the chart, it is an indication that a different type of FRP (i.e. different tensile strength and/or elastic modulus) must be selected. These charts can be used for the repair of existing girders or for the design of new beams with bonded FRP laminates.

CONCLUSIONS

The bridge was analyzed through a comprehensive series of three-dimensional FEM analyses. Both static and dynamic FEM analyses were conducted in an attempt to replicate the field load tests described in Chapters 3 and 4. The FEM analyses were then extended to evaluate the effects of a variety of parameters contributing to the structural response of FRP repaired bridges. An analytical section analysis procedure was also conducted to study the effects of bonding the FRP laminates to the bridge girders on enhancing the ultimate load capacity of the bridge.

The correlation of the FEM analysis results with the results of the field load tests was excellent. Comparisons of midspan girder deflections and rebar stresses simulated by the FEM analyses with those obtained from the field load tests were within 5% for almost all cases investigated, both static and dynamic. Comparisons of field measured stresses in the CFRP laminates at midspan with those predicted by the FEM analyses exhibited only slight differences, ranging from 4.5% to 6.8%. Moreover, the fundamental period of vibration for the bridge predicted from the FEM frequency

analysis was within 2% of that measured from the midspan girder deflection time history recorded in the dynamic field load tests.

Having established the veracity of the FEM model, a parametric study was then conducted to evaluate the effects of varying the CFRP cross sectional area, modulus of elasticity and tensile strength on the structural response of the bridge. Results of the study indicated that increasing the CFRP cross sectional area could reduce the maximum girder deflections and reinforcing steel stresses by as much as 22% and 20%, respectively. The results also indicated that increasing the modulus of elasticity of the CFRP plates could reduce the girder deflections by as much as 16%. It was also concluded that the tensile strength of the CFRP plates significantly affected the ultimate load capacity of the bridge structure, but had very little influence on the bridge response at the service load stage.

A section analysis procedure was developed using strain compatibility and equilibrium equations. This procedure provides a convenient method for determining the ultimate strength of bridge girders repaired with FRP laminates. From this procedure a specified level of strength enhancement can be decided in terms of CFRP cross sectional area, modulus of elasticity and tensile strength. The section analyses procedure has been computerized to afford the development of design aids for specific case studies.

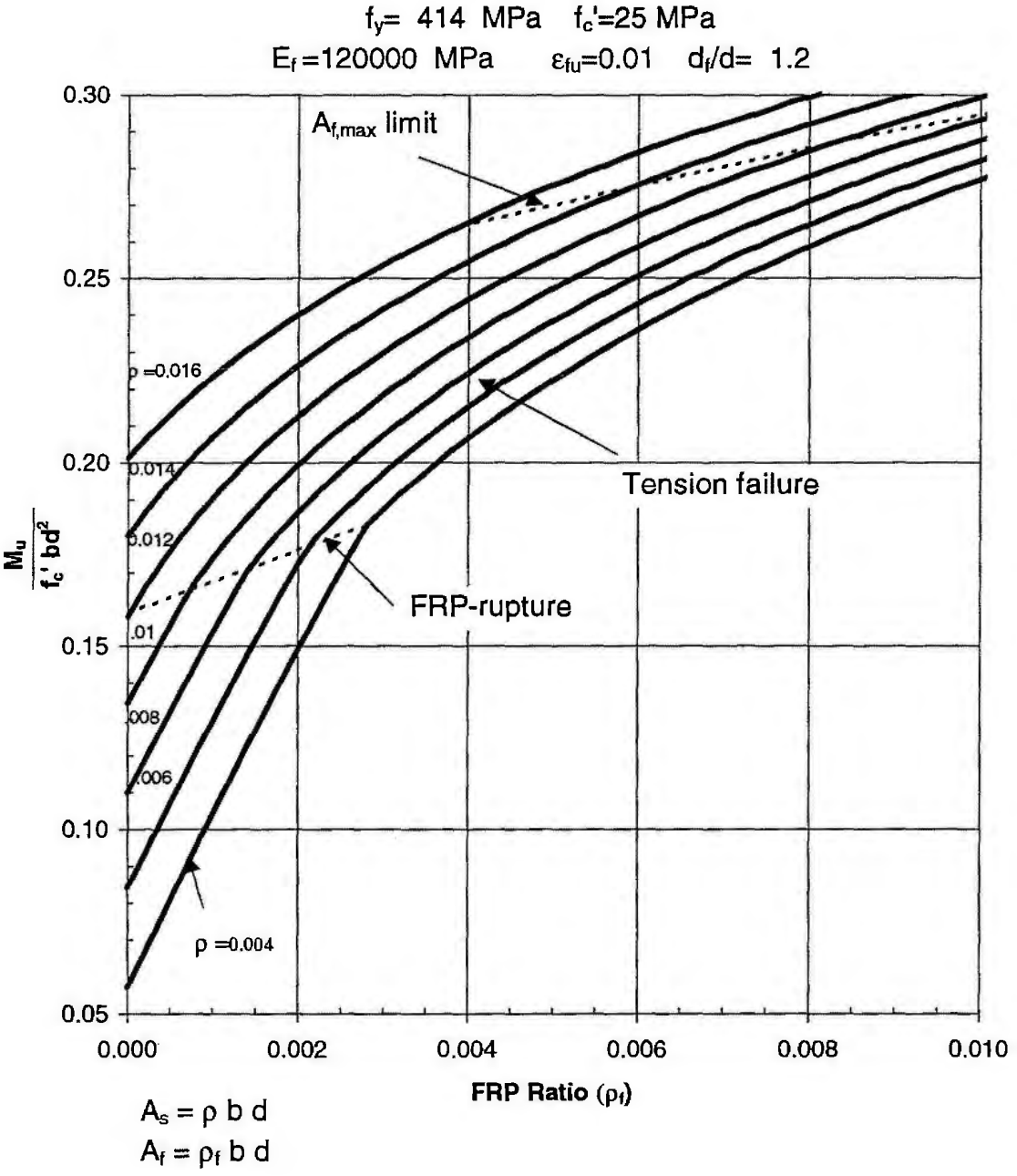

Figure 5.37. Typical Design Chart for Girders Strengthened with CFRP.

CHAPTER SIX
BRIDGE INSPECTION AND MONITORING

The bridge structure selected for rehabilitation was visually inspected for evidence of structural distress and deterioration prior to application of the FRP laminates. The girders were examined closely with hand held lights powered by an electric generator. All cracks were outlined with a black permanent marker and their locations relative to the east support were recorded. Photographs were taken of typical crack patterns in the girders.

After FRP application, the girders were inspected to detect the presence of voids in the bond between the FRP and the concrete. Each void was outlined on the FRP plates with a black permanent marker. The FRP was thereafter inspected periodically to determine if the void spaces were increasing in either size or number.

INITIAL CONDITION OF CONCRETE BRIDGE GIRDERS

Prior to FRP application, the four concrete bridge girders exhibited a similar pattern of cracking as illustrated by the sketch in Figure 6.1. The primarily vertical cracks were typically located in the central three-fourths of the span at a horizontal spacing of approximately 140 mm between cracks. There was an average of 46 cracks in each girder. The maximum number of cracks in a girder was 54, found in girder 4. The minimum number of cracks was 41, found in girder 2. Photographs of typical crack patterns are shown in Figure 6.2.

CONDITION OF GIRDERS IMMEDIATELY FOLLOWING APPLICATION OF FRP

After the FRP was applied, the girders were inspected to determine how well the FRP bonded to the concrete. This inspection was carried out by tapping the surface of the FRP plates with a hard object such as a coin. A change in pitch in the sound of the tapping indicated the presence of a void. The entire surface of each FRP plate was inspected in this manner, and the shape of each void outlined.

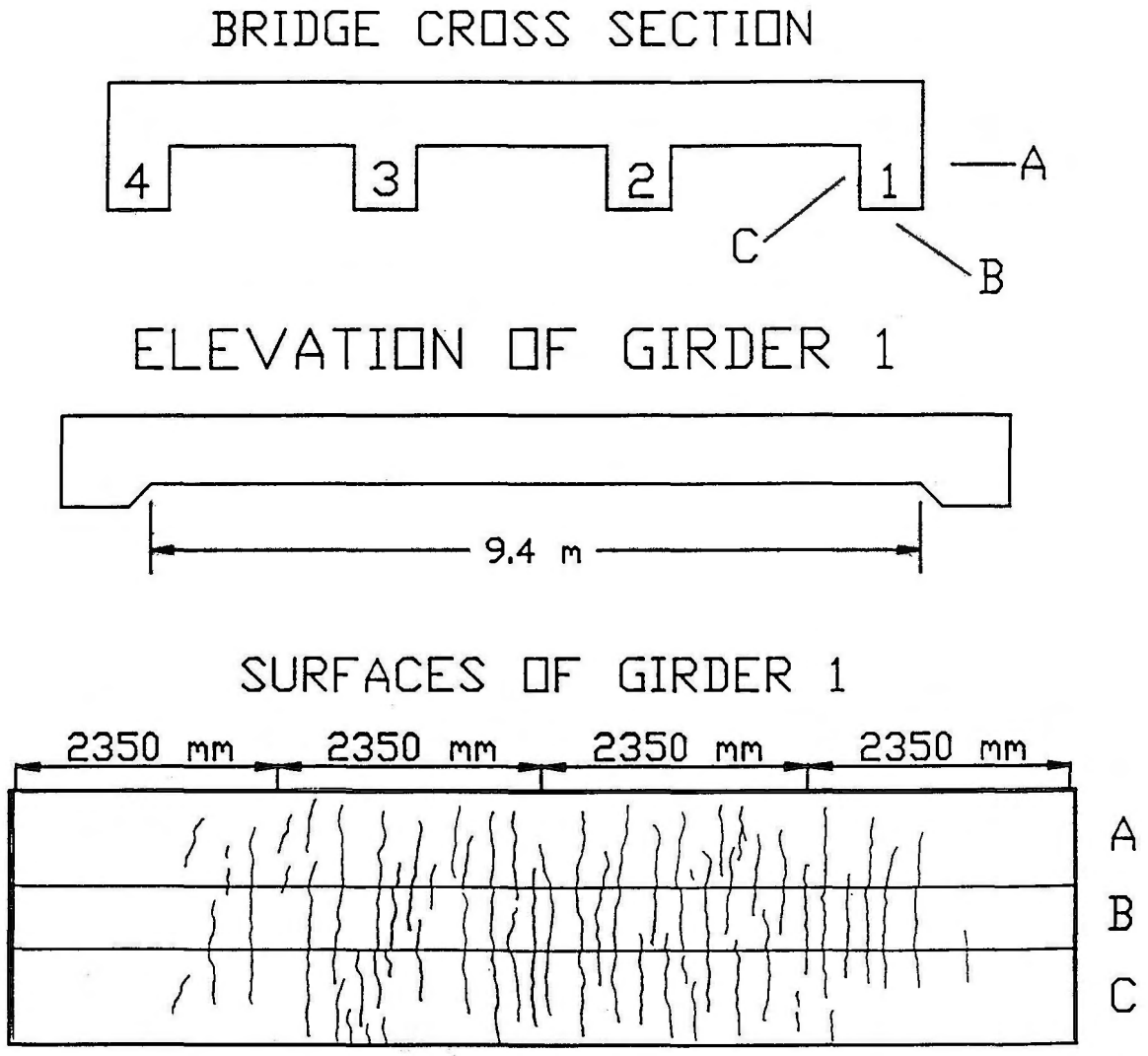

Figure 6.1. Sketch of Crack Pattern in Typical Girder Prior to FRP Application

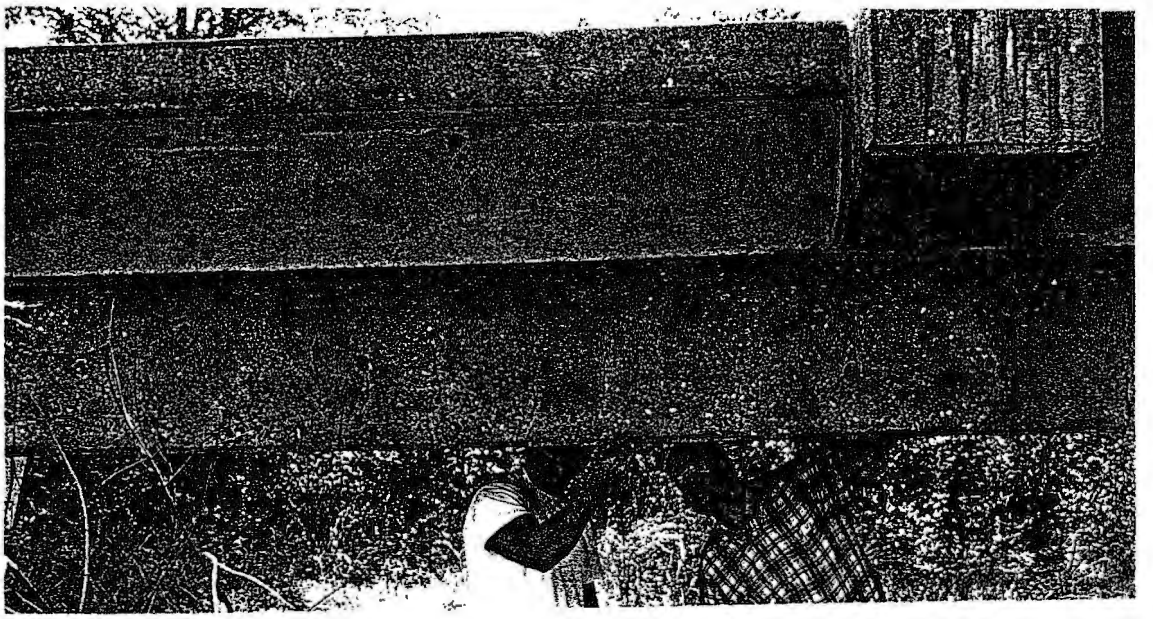

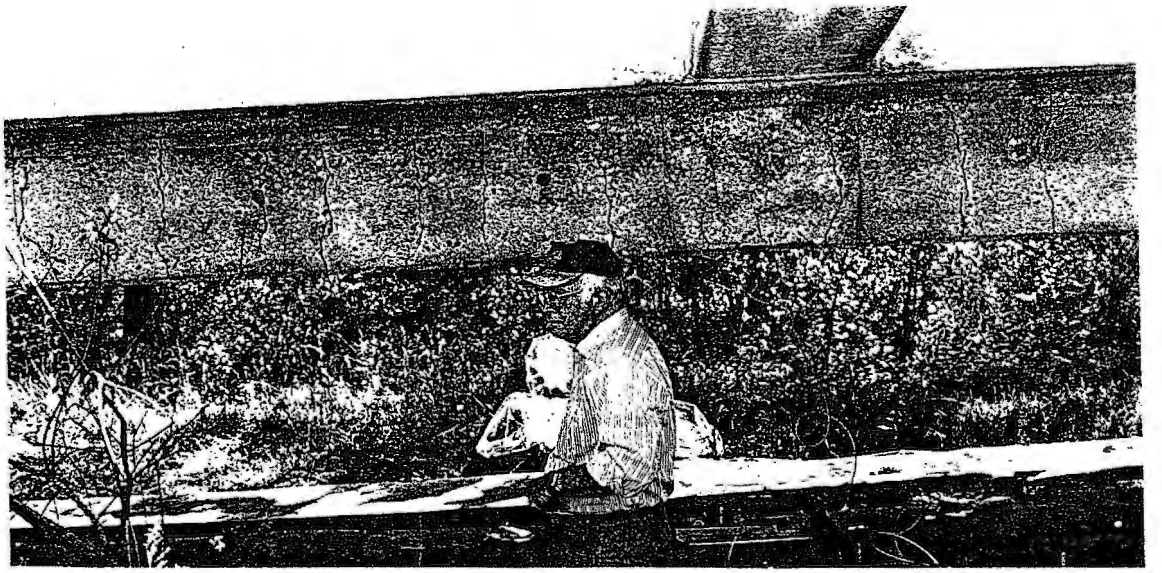

Figure 6.2. Typical Crack Patterns in Concrete Girders Prior to FRP Application

Figure 6.3 through Figure 6.6 show examples of voids found beneath the GFRP plates bonded to the sides of the girders. The instance of best adherence of the GFRP to the concrete was noted on the north face of girder 2. The voids were distributed uniformly over the span. In the eastern half of the same girder, a total area of 76,800 mm^2 of voids were measured. An area of 4% of the total northern surface of girder 2 did not bond.

The instance of worst adherence of the GFRP to the concrete was noted on the north face of girder 4. The voids were distributed uniformly over the span. A total area of 322,300 mm^2 of void space was measured in the western half of the beam. An area of 18% of the total northern surface of girder 4 did not bond. The largest single void found beneath any GFRP surface was on the northern face of girder 4. This void covered an area of 48,400 mm^2.

Figure 6.7 through Figure 6.9 show examples of the voids found beneath the CFRP plates. The CFRP plates appeared to bond to the concrete better than the GFRP plates. The largest percentage of unbonded CFRP surface area was 4%, which was found on girder 2. The largest void, shown in Figure 6.10, was found on girder 4. This void covered an area of approximately 28,800 mm^2.

RESULTS OF PERIODIC INSPECTIONS

The bridge girders were inspected at periodic intervals after the completion of the field work in an attempt to assess the durability of the bond between the FRP and the concrete girders. The bond was inspected in the manner described in the previous section to detect the presence of any new voids and to determine if the voids previously identified had grown. At a period of 16 months after the FRP was installed, no new voids had been detected and the sizes of the previously identified voids remain constant. Therefore, to the present time, it is concluded that the void spaces are due to the failure of the adhesive to bond the FRP to the concrete at the time of installation. This condition can be attributed to several factors, such as impurities on the FRP or concrete surfaces, the presences of uneven areas and ridges on the girder surfaces, and uneven application of the adhesive to the FRP plates.

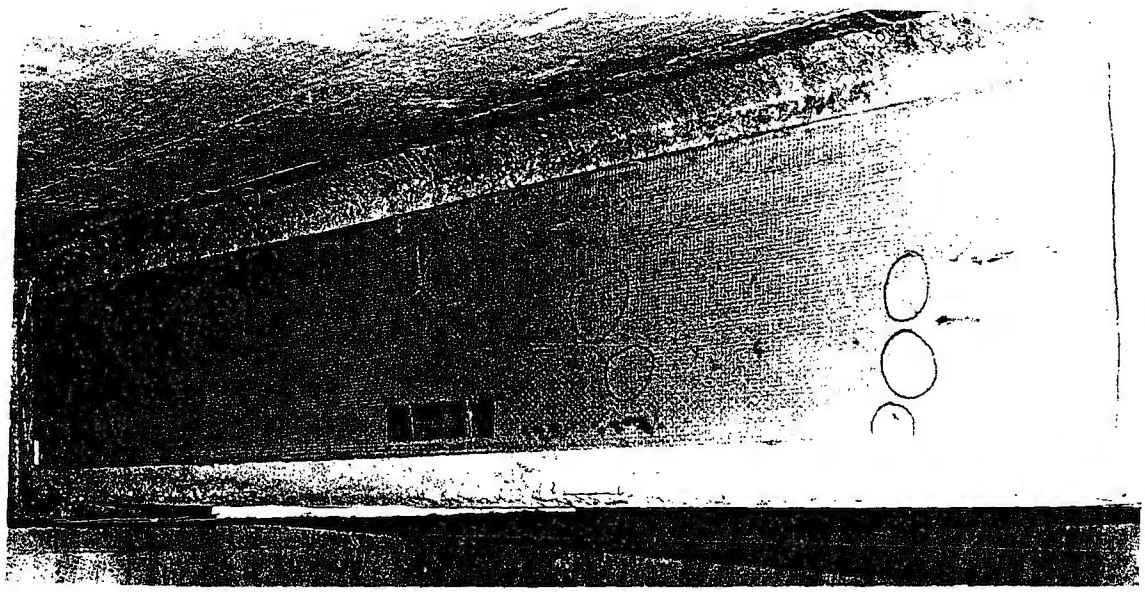

Figure 6.3. Voids Under GFRP at East End of Girder 2 - North Face

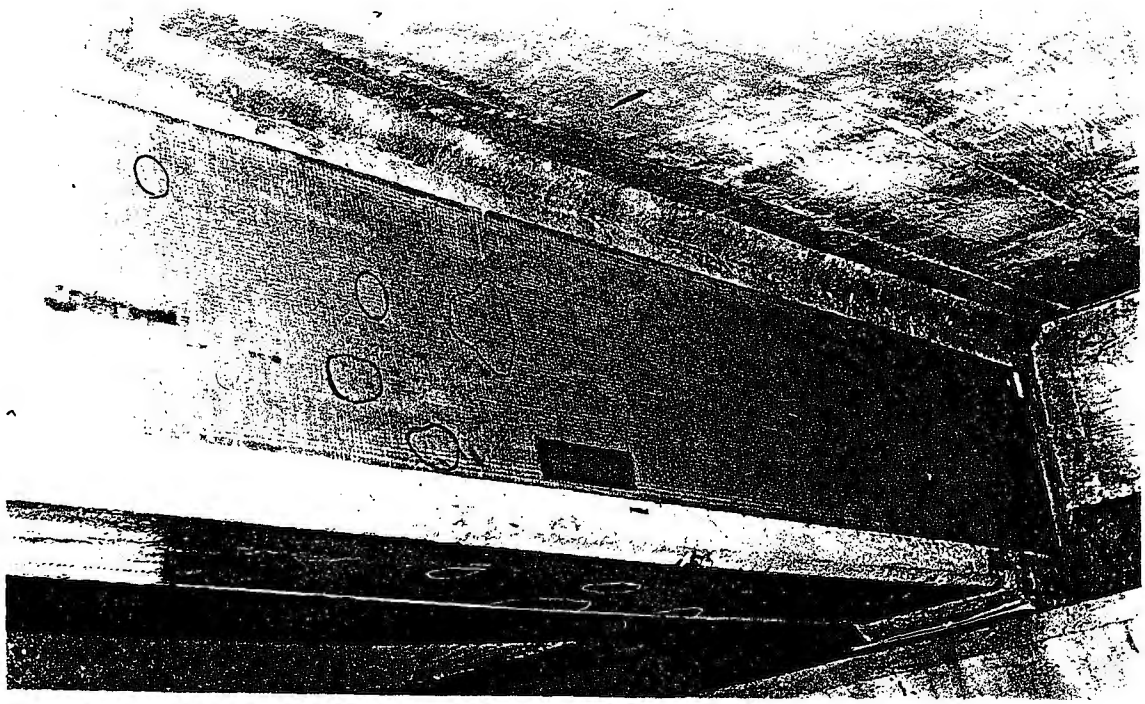

Figure 6.4. Voids Under GFRP at East End of Girder 2 - South Face

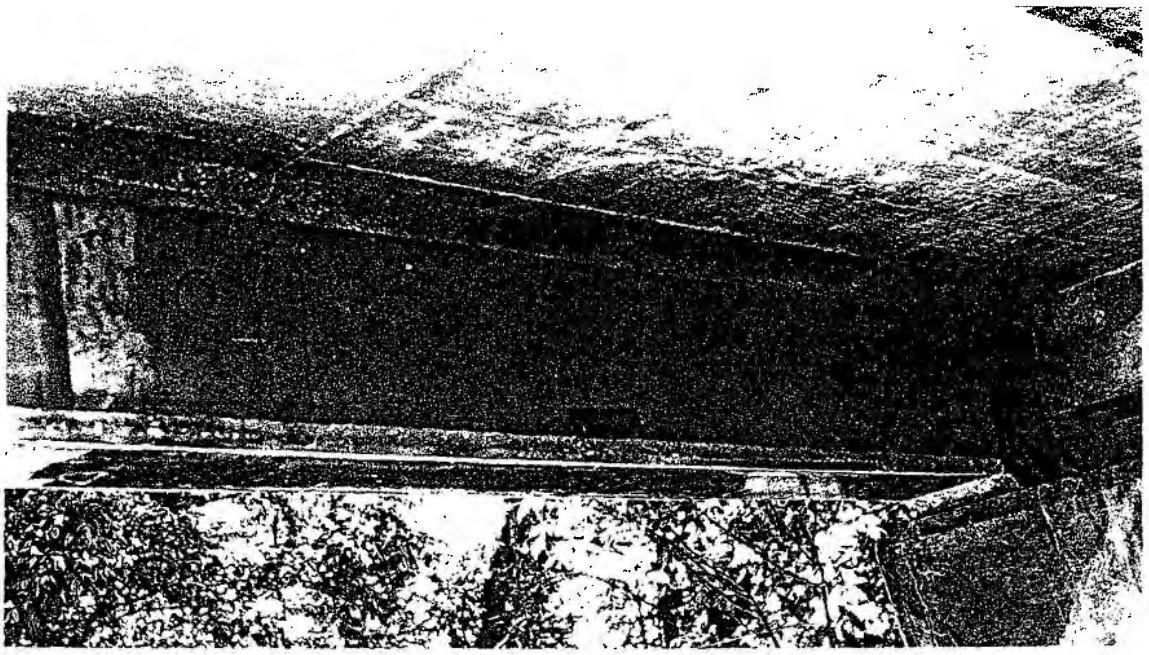

Figure 6.5. Voids Under GFRP at West End of Girder 4 - North Face

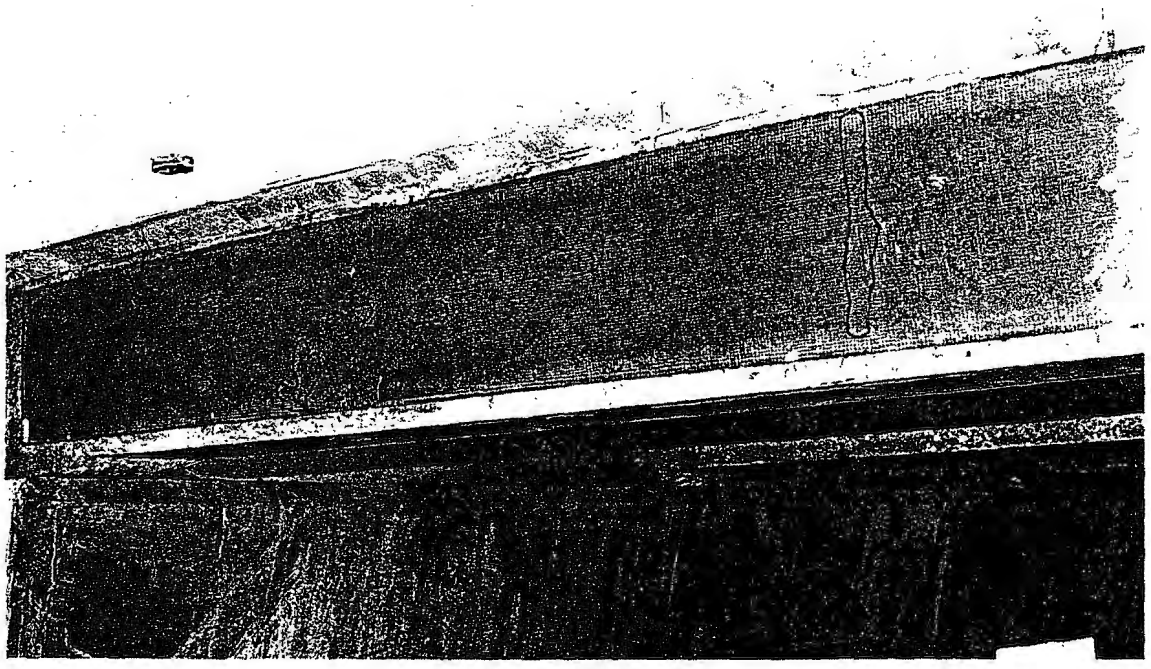

Figure 6.6. Voids Under GFRP at West End of Girder 4 - South Face

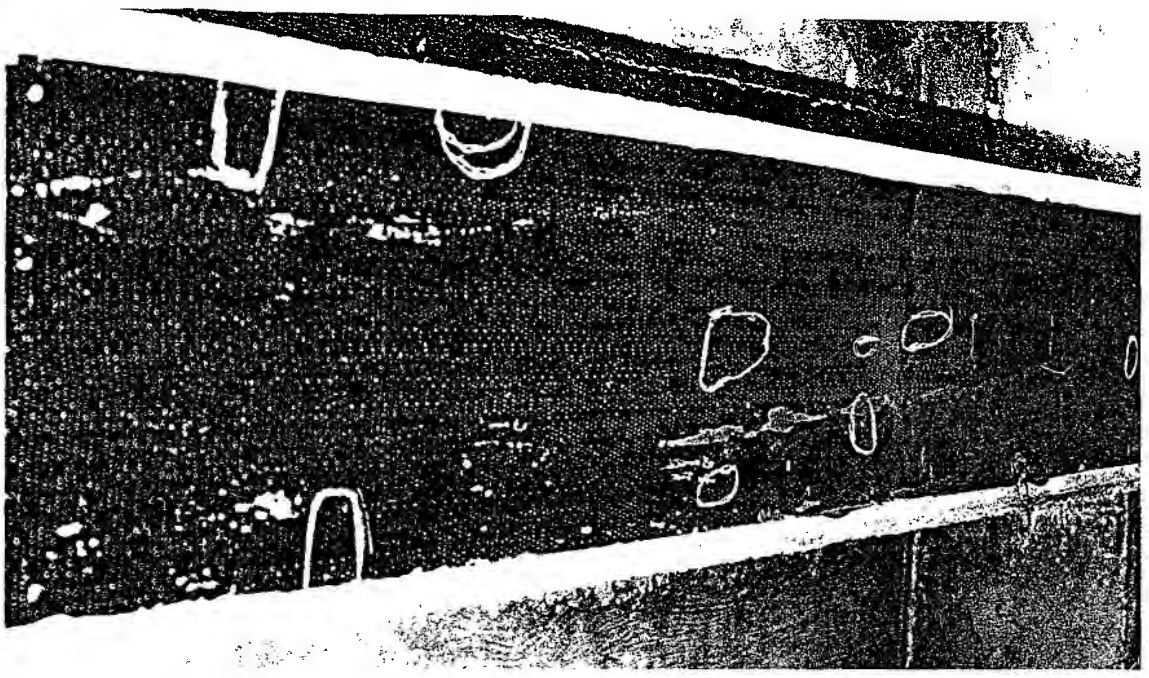

Figure 6.7. Voids Under CFRP at West End of Girder 1

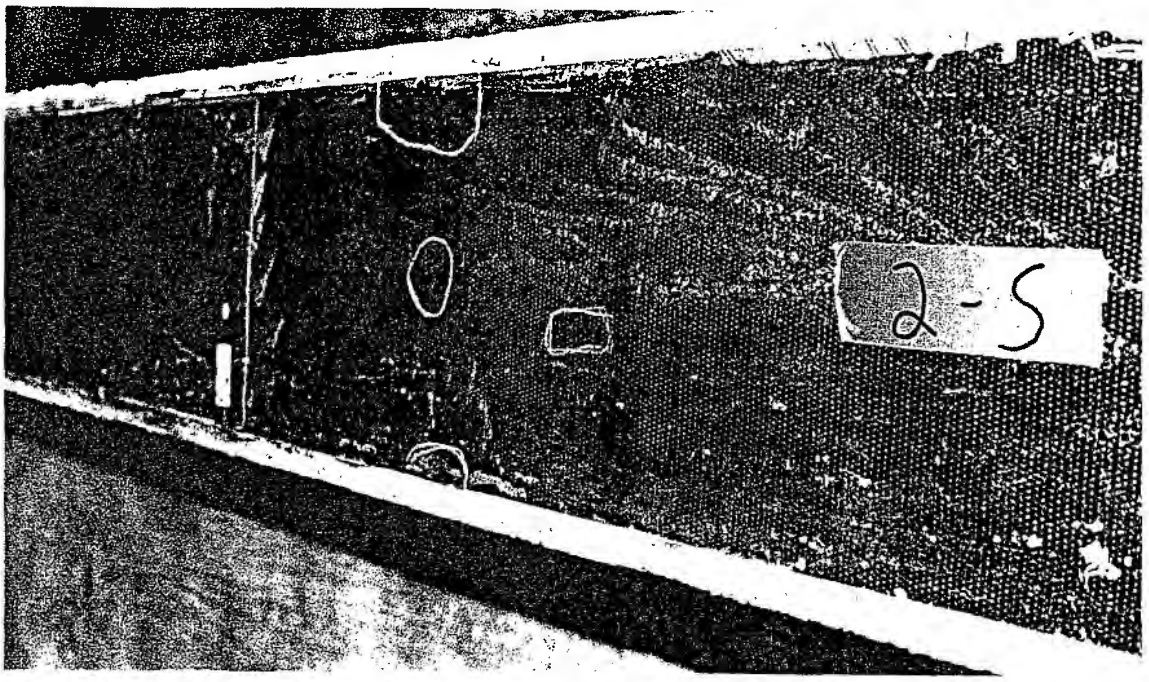

Figure 6.8. Voids Under CFRP at West End of Girder 2

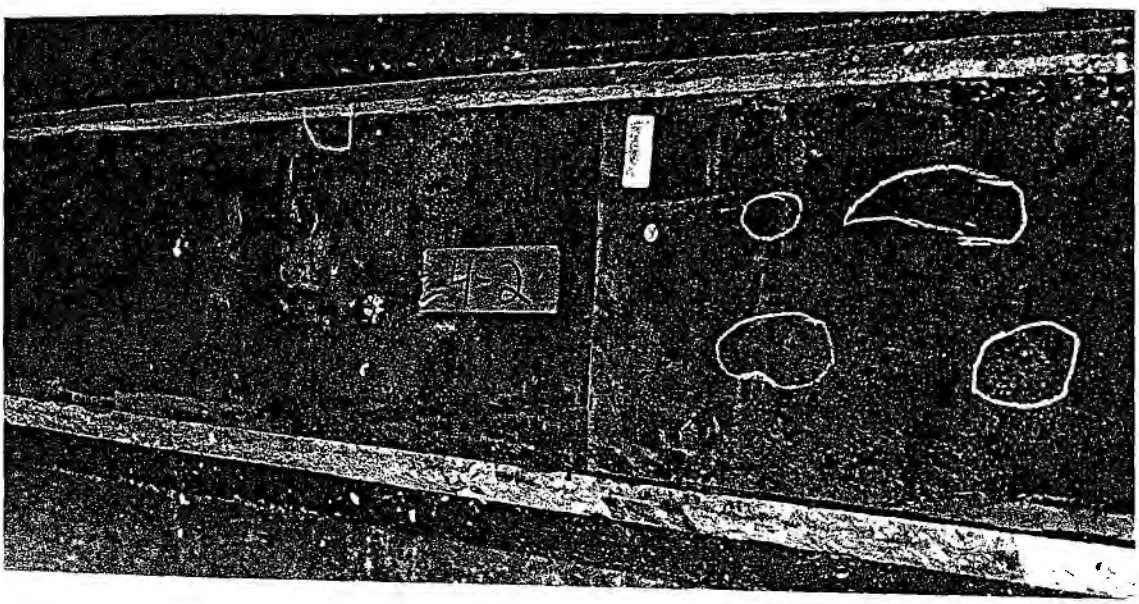

Figure 6.9. Voids Under CFRP at East End of Girder 4

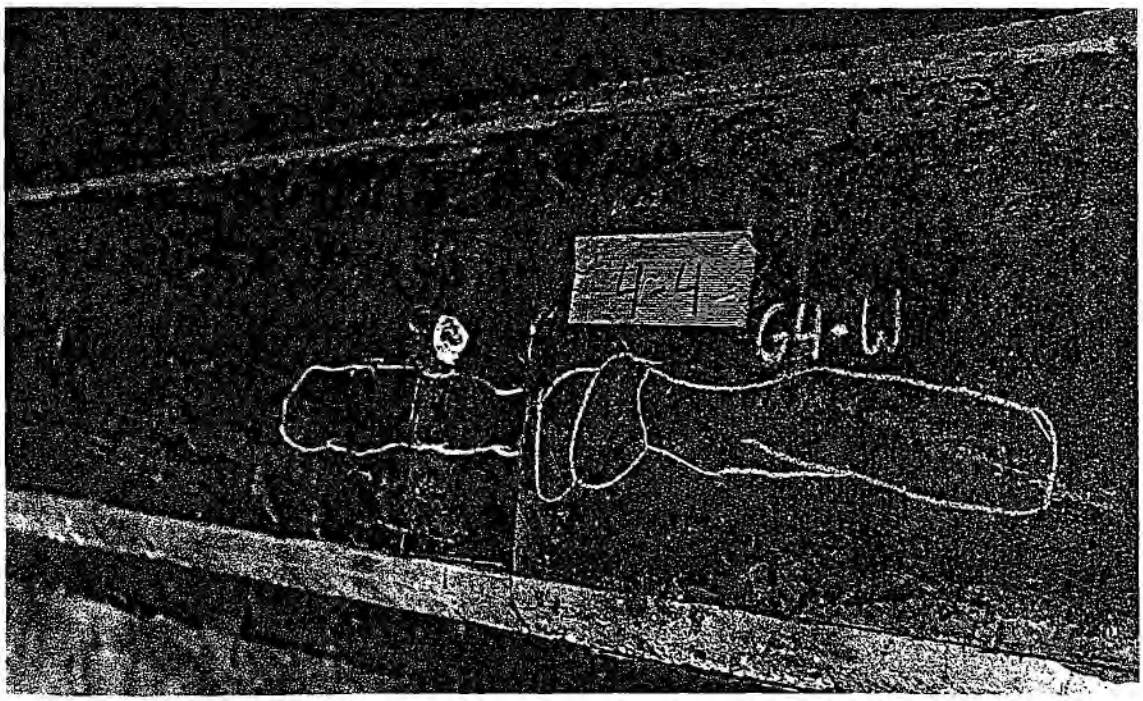

Figure 6.10. Largest Void Found Under CFRP

CHAPTER SEVEN
CONCLUSIONS AND RECOMMENDATIONS

CONCLUSIONS

The results of the field study to investigate the effects of externally bonded FRP composite plates on the structural performance of a reinforced concrete bridge were presented. Based on the experience gained from applying the FRP plates and from analysis of the static and dynamic load tests data, the following conclusions are presented:

1. Application of FRP plates to concrete bridge girders was successfully performed using a simple and straightforward process. The only specialized equipment required, beyond normal bridge maintenance equipment and tools, was a vacuum pump for maintaining constant pressure to the plates during the curing period of the adhesive.
2. Application of the FRP plates produced significant reductions in the reinforcing bar stresses and vertical midspan deflections of the girders. Reductions of reinforcing bar stresses ranged from 4% to 12% for the static tests and from 4% to 9% for the dynamic tests. Girder deflection reductions ranged from 2% to 12 % for the static tests, and from 7% to 12% for the dynamic tests. These reductions indicate that the FRP plates were behaving as an effective component of the girder cross sections.
3. A classical calculation of the cracked-section moment of inertia of the girder cross sections indicated that application of the FRP plates increased the girder moment of inertia by approximately 5%. Since the reductions in stresses and deflections resulting from the FRP repair were generally greater than 5% more advanced cross sectional analysis procedures are necessary to accurately account for the beneficial effects of FRP repairs.
4. The reductions in reinforcing bar stresses and girder deflections were noticeably greater for the three girders repaired with GFRP side plates as compared to the one girder without the side

plates. This suggests that lower cost GFRP side plates might be used to add stiffness to the girder cross sections, while more expensive CFRP plates be attached to girder bottom surfaces to increase the load capacity.

5. The strain recorded on the splice plate between primary FRP plates indicates that the composite splice design is an effective mean to transfer stress between plates of primary reinforcing.

The results of a comprehensive, three-dimensional FEM analysis of the bridge were also presented. Comparisons of the FEM results with the field load tests data have verified the accuracy of the analyses. The FEM analyses were therefore extended to include a parametric study for the purpose of evaluating the effects of varying the CFRP cross sectional area, modulus of elasticity and tensile strength on the structural response of the bridge. Based on the results of the parametric study, the following additional conclusions are presented:

6. There is a linear relationship between increasing the cross sectional area of the CFRP plates and the corresponding decrease in both maximum girder deflections and maximum stresses in the reinforcing steel. Decreases of 22% and 20% respectively, for the maximum girder deflections and maximum reinforcing steel stresses are possible.
7. The modulus of elasticity of the CFRP plates also has an effect on the bridge structural response similar to that observed for the cross sectional area, but to a lesser degree.
8. At the service load stage, bridge structural response is relatively insensitive to CFRP tensile strength. However, at the ultimate load stage, the CFRP tensile strength is the critical parameter affecting increased load capacity.
9. Finally, an analytical section analysis procedure was developed based upon equilibrium and strain compatibility. The details of the procedure, presented in Appendix A, were subsequently incorporated into a computer program capable of calculating the ultimate load capacity for both rectangular and T-sections repaired with FRP plates. The computer program has the feature of

generating design aids for user specified bridge cases requiring strength enhancement.

RECOMMENDATIONS

A procedure for repairing deteriorated or distressed reinforced concrete bridges has been developed. A methodology based on fundamental engineering principles to evaluate the strength enhancement provided by the repair procedure has also been developed. Based upon these developments, a strategy for rehabilitating deteriorated and/or structurally deficient reinforced concrete highway bridges is recommended as follows:

1. From the ALDOT inventory of state and county bridges, identify all reinforced concrete bridges that would be suitable candidates for the developed repair procedure.
2. Conduct an on-site inspection of the candidate bridges to confirm their suitability for the repair procedure.
3. Select a small number of these bridges for repair (approximately 5).
4. Design a repair methodology for each bridge from the procedures developed in this report.
5. Train ALDOT maintenance personnel in implementation of the repair procedure.
6. Implement the repairs to the candidate bridges.
7. Monitor the performance of the repaired bridges by monthly inspections for a two-year probationary period.

REFERENCES

Automatic Dynamic Incremental Nonlinear Analysis (ADINA). (1990). Report ARD 90-1. ADINA R & D, Inc. Watertown, MA.

American Concrete Institute (ACI). (1995). Building Code Requirements for Reinforced Concrete. Detroit, MI.

An, W., Saadatmanesh, H. and Ehsani, M.R. (1991). "RC Beams Strengthened with FRP Plates. II: Analysis and Parametric Study." Journal of Structural Engineering, ASCE, 117 (11), pp. 3434-3455

Bathe, K.J. (1996). Finite Element Procedures. Prentice Hall, Inc. Englewood Cliffs, NJ.

Chajes, M.J., Thomson, Januszka, T.F. and Finch, W.W. (1994). "Flexural Strengthening of Concrete Beams Using Externally Bonded Composite." Construction and Building Materials, 8(3), pp. 191-201.

Chajes, M.J., Januszka, T.F., Mertz, D.R., Thomson, T.A. and Finch, W.W. (1995). "Shear Strengthening of Reinforced Concrete Beams Using Externally Applied Composite Fabrics." ACI Structural Journal, 92 (3), pp. 295-302.

Ghaleb, B.M. (1992). Strengthening of Damaged Reinforced Concrete Beams by External Fiber Glass Plates, Thesis, King Fahd University of Petroleum and Minerals, Saudi Arabia.

Hefferman, P.J. (1994). Behavior of Reinforced Concrete Beams Strengthened with CFRP Sheets, Thesis, Royal Military College of Canada, Canada.

Kobayashi, A., Endoh, M., Kuroda, H. and Kliger, H. (1995). "Use of Carbon Fiber Tow Sheet Reinforcement for Improved Bridge Capacity Rating in Japan." International SAMPE Symposium, May 8-11, pp. 513-521.

Meir, U. and Kaiser, H. (1991). "Strengthening Structures with CFRP Laminates." Proceedings of Advanced Composite Materials in Civil Engineering Structures, ASCE, Las /Vegas, Nevada, pp. 224-232.

Meir, U. and Deuring, M. (1992). "Strengthening of Structures with CFRP Laminates." Advanced Composite Materials in Bridges and Structures. Canadian Society for Civil Engineering, pp. 243-251.

Meir, U. (1992). "Carbon Fiber Reinforced Polymers: Modern Materials in Bridge Engineering." Stryctyrak /engineering International, International Association for Bridge and Structural Engineering, Switzerland, pp. 7-11.

Nanni, A. (1995). "Concrete Repair with Externally Bonded FRP Reinforcement." Concrete International, June, pp. 22-26.

Plevris, N. and Triantafillou, T.C. (1994). "Time Dependent Behavior of RC Members Strengthened with FRP Laminates." Journal of Structural Engineering, ASCE, 120(3), pp. 1016-1039.

Qu, R. (1994). "Theoretical Analysis of Reinforced and Prestressed Concrete Bridge Members Strengthened with FRP Laminates." Thesis, Florida Atlantic University, Florida.

Raghavachary, S. (1995). Experimental Studies on Flexural Behavior of CFRP Retro fired Concrete Members, Thesis, Florida Atlantic University, Florida.

Ritchie, P.A. (1988). External Reinforcement of Concrete Beams Using Fiber Reinforced Plastic, Thesis, Leigh University.

Ross, C.A., Jerome, D.M. and Hughes, M.L. (1994). Hardening and Rehabilitation of Concrete Structures Using Carbon Fiber Reinforced Plastics (CFRP), Final Report, Wright Laboratory Armament Directorate, Eglin Air Force Base, Florida.

Rostasy, F., Hankers, C. and Ranisch, E. (1992). "Strengthening of RC and PC Structures With Bonded FRP Plates," Proceedings of the First International Conference on Advanced Composite Materials in Bridges and Structures, Sherbrooke, pp. 253-263.

Saadatmanesh, H. and Ehsani, M.R. (1990). "Fiber Composite Plates Can Strengthen Beams," Concrete International, March, pp. 65-71.

Saadatmanesh, H. and Ehsani, M.R. (1991). "RC Beams Strengthened with GFRP Plates, I: Experimental Study," Journal of Structural Engineering, ASCE, 117 (11), pp. 3417-3433.

Triantafillou, T.C. and Plevris, N. (1992). "Strengthening of RC Beams with Epoxy Bonded Fibre Composite Materials," Materials and Structures, 25(1), pp. 201-211.

Ziraba, Y.N. (1993). Non-Linear Finite Element Analysis of Reinforced Concrete Beams Repaired by Plate Bonding, Dissertation, King Fahd University of Petroleum and Minerals, Saudi Arabia.

APPENDICES

APPENDIX A

Flanged sections are often encountered in reinforced concrete bridge structures. Generally, the neutral axis at the ultimate state falls within the slab (flanges), and therefore the T-section may be analyzed as a rectangular section having a compression face width equal to the flange width b, as illustrated in Figure A.1. However, for sections reinforced with FRP plates, at the ultimate stage, the FRP strain in a T-section usually approaches its ultimate strain ε_{fu} before the concrete in compression zone attains its ultimate strain (0.003). Therefore, the usual rectangular stress block cannot be used and the calculation of the concrete compression force is performed by integrating nonlinear the concrete stress distribution over the compressed area. Such calculations are tedious and complicated, therefore a methodology for calculating the ultimate section capacity was developed using the concrete model shown in Figure 5.34.

By dividing the compression zone into twenty equal segments and evaluating the concrete compressive stress (f_{cn}) at the mid point of each segment in accordance with the corresponding concrete strain ε, the total resultant concrete compressive force C_c and its location (k_2 c) are determined by the

following equations

$$C_c = \sum_{n=1}^{n=20} f_{cn}\, b\, dc = \alpha_c\, f_c' \qquad \text{..... A.1}$$

where

$$\alpha_c = \frac{\sum_{n=1}^{n=20} f_{cn}\, dc}{f_c'\ c} = \frac{\sum_{n=1}^{n=20} f_{cn} / 2}{f_c'} \qquad \text{..... A.2}$$

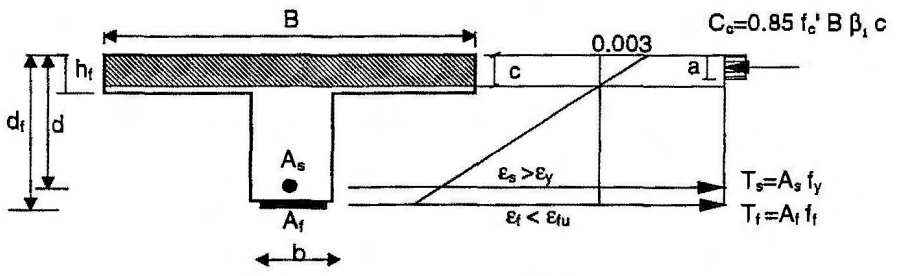

a)neutral axis within the flange (tension failure)

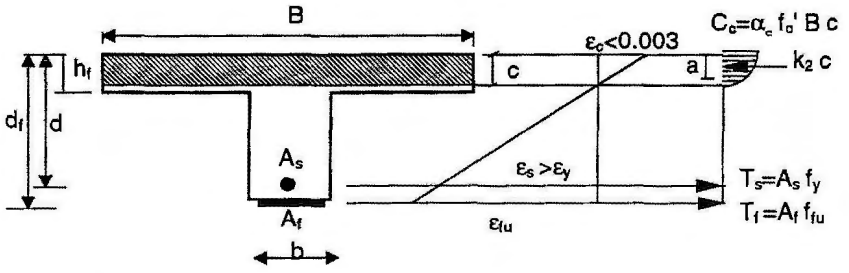

b)neutral axis within the flange (FRP rupture)

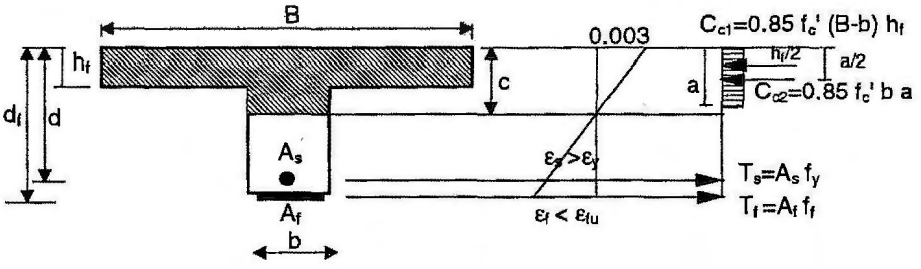

c)neutral axis outside the flange (tension failure)

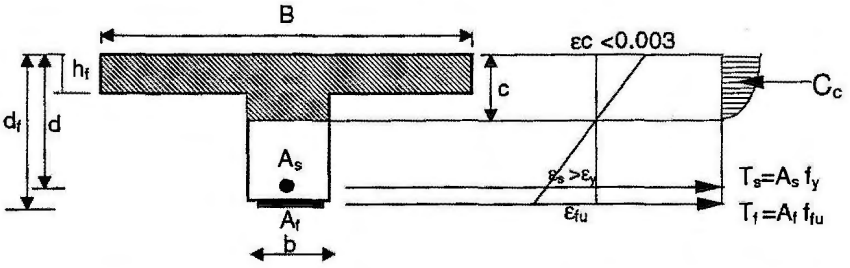

d)neutral axis outside the flange (FRP rupture)

Figure A.1. Neutral Axis Position for T-Sections.

Noting that

$$if\ \epsilon \le \epsilon_o\ then....f_{cn} = f_c''[\ \frac{2\ \epsilon}{\epsilon_o} - \frac{(\epsilon)^2}{\epsilon_o}\ ] \quad \text{..... A.3a}$$

$$if\ \epsilon \succ \epsilon_o\ then.....f_{cn} = f_c''\ [\ 1 - \frac{0.15}{0.0038 - \epsilon}\ (\ \epsilon \quad \epsilon_o\ )\ ] \quad \text{... A.3b}$$

where

$$\epsilon_o = \frac{1.8\ f_c''}{E_c}\ ,\ dc = \frac{c}{20}\ ,\ f_c'' = 0.9 f_c'\ ,\ y_n = (n - 0.5)\ dc = (n - 0.5)\ \frac{c}{20} \quad \text{...A.4}$$

$$\epsilon = \epsilon_c\ \frac{y_n}{c} = \epsilon_c\ \frac{(\ n\ -\ 0.5\ )}{20} \quad \text{.....A.5}$$

Summing moments about point O (refer to Figure A.1) we have

$$\sum_{n=1}^{n=20} f_{cn} b\, dc\, (c - y_n) = C_c k_2 c \quad \text{..... A.6}$$

$$k_2 = \frac{\sum_{n=1}^{n=20} f_{cn} b\, dc\, (c - y_n)}{C_c c} = \frac{\sum_{n=1}^{n=20} f_{cn} b \frac{c}{20} (c - y_n)}{(\alpha_c\ f_c' b c)\, c} = \frac{\sum_{n=1}^{n=20} \frac{f_{cn}}{20} (1 - \frac{y_n}{c})}{\alpha_c f_c'} \quad \text{..... A.7}$$

and where

$C_c = \alpha_c\ f_c'\ b\ c$ A.8

Table A.1 Lists the values of α_c, k_2 at any given concrete strain for a compressive strength of 27 MPa. The resultant compressive force C_c is given by Equation A.6 and its center of pressure is located a distance (k_2 c) from the top compression fiber.

An iterative procedure is employed to determine the neutral axis position and the nominal moment capacity. The concrete strain is assumed to be less than 0.003 and α_c is determined from Table A.1. The neutral axis position is determined from the compatibility of strains as illustrated in Figure A.1 and

calculated as

$$c = d_f \frac{\epsilon_c}{\epsilon_c + \epsilon_{fu}} \quad \text{..... A.9}$$

Table A.1. Values of α, k_2 for Concrete Compressive Strength of 27 Mpa.

Top Concrete Strain	α_c	K_2	Top Concrete Strain	α_c	k_2
0.0005	0.229	0.343	0.0018	0.616	0.374
0.0006	0.269	0.345	0.0019	0.633	0.377
0.0007	0.308	0.347	0.002	0.649	0.381
0.0008	0.345	0.349	0.0021	0.662	0.385
0.0009	0.38	0.351	0.0022	0.674	0.388
0.0010	0.413	0.353	0.0023	0.684	0.392
0.0011	0.445	0.355	0.0024	0.694	0.396
0.0012	0.475	0.357	0.0025	0.702	0.4
0.0013	0.503	0.36	0.0026	0.71	0.403
0.0014	0.529	0.362	0.0027	0.716	0.407
0.0015	0.553	0.365	0.0028	0.722	0.41
0.0016	0.576	0.368	0.0029	0.728	0.414
0.0017	0.597	0.371	0.003	0.732	0.417

All forces acting on the cross section are given by:

$C_c = \alpha_c f_c' b c$ A.10a

$T_s = A_s f_y$ A.10b

$T_f = A_f f_{fu}$ A.10c

From the equilibrium condition of $C_c = T_s + T_f$ we have:

$\alpha_c f_c' b c = A_s f_y + A_f f_{fu}$ A.11

$$\alpha_{c,new} = \frac{A_s f_y + A_f f_{fu}}{c f_c' b} \quad \text{..... A.12}$$

A trial and adjustment procedure is performed by the assuming concrete strain ϵ_c, locating the corresponding value of α_c from Table A.1 and calculating the neutral axis distance (c) from Equation A.9 until the product $\alpha_c c$ approximately equals to the value obtained from Equation A.12. The moment of the cross section forces taken about the concrete compression force is given in Equation A.13 as

$M_n = A_s f_y (d - a_c) + A_f f_{fu} (d_f - a_c)$ A.13

in which

$a_c = k_2 c$ A.14

Bridge Girder Enhancement Percentage Using Section Analysis

Given Data:

A_s = 5748 mm^2

f_c' = 27 MPa

f_y = 414 MPa

E_f = 121000 MPa

f_{fu} = 1194 MPa

A_f = 347 mm

d_f = 657 mm

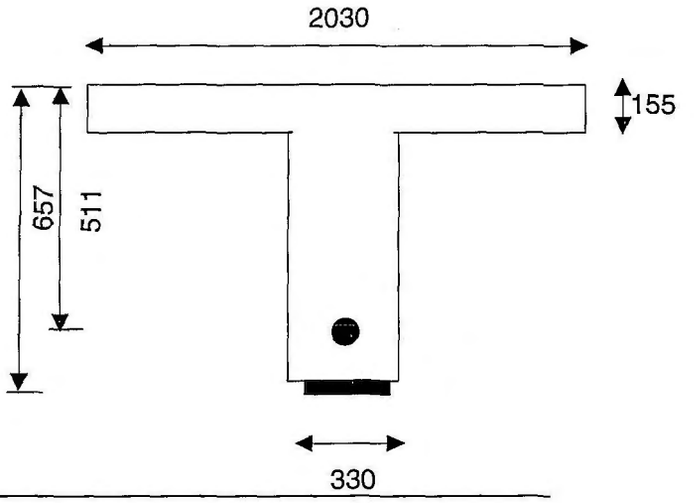

Girder Ultimate Flexural Capacity Before Rehabilitation

β_1 = 1.09 - 0.008 (27) = 0.87 > 0.85

β_1 = 0.85

Assume that the neutral axis is within the flange, thus

$$a = \frac{5748\ 414}{0.85\ (27)\ 2030} = 51.07\ mm \qquad (\ within\ the\ flange \tag{1}$$

$\phi M_{nb} = 0.9\ A_s\ f_y\ (d-a/2)$ (2)

$\phi M_{nb} = 0.9 \times 5748 \times 414\ (\ 511 - 51.07 / 2\ ) = 1039$ KN.m (3)

Girder Ultimate Flexural Capacity After Rehabilitation

Assume the FRP mode of failure will control (i.e. concrete strain is less than 0.003), therefore the strain in the FRP is calculated as

$\epsilon_{fu} = f_{fu} / E_f = 1194 / 121000 = 0.0098$ (4)

Calculate effective flange width (b is the least of the following):

1. $b = 16\ h_f + b_w = 16\ (152) + 330 = 2762$ mm

2. $b = 10.36 \times 1000 / 4 = 2590$ mm

3. $b = 2030$ mm (half the clear distance on each side plus beam width b_w)

$b = 2030$ mm controls

Assume that the neutral axis is within the flange, and apply equilibrium Equation A.11 as

$$\alpha_c f_c' b c = A_s f_y + A_f f_{fu} \quad (5)$$

in which

$$\alpha_c (27) (2030) c = 5748 (414) + 347 (1194) \quad (6)$$

or

$$\alpha_c c = 50.97 \quad (7)$$

and

$$c = d_f \frac{\epsilon_c}{\epsilon_c + \epsilon_{fu}} = 657 \frac{\epsilon_c}{\epsilon_c + 0.0098} \quad (8)$$

The iteration procedure on Equation (8) is performed by assuming a concrete strain ε_c, and determining the corresponding value of α_c from Table A.1 until the term (α_c c) approximately equals the value 50.97 obtained from Equation 7. The calculations are summarized in Table A.2

Table A.2. Calculation of $\alpha_c c$ for Example Problem

Assumed Concrete strain ϵ_c	α_c (from Table A.1)	c (from Equation A.12)	α_c c
0.0017	0.597	97.12	57.98
0.0016	0.576	92.21	53.11
0.0015	0.553	87.21	48.23
0.00155	0.565	89.72	50.69

From Table A.1 with a concrete strain equal 0.00155, k_2=0.366 and we have

k_2 c = 0.366 (89.72) = 32.83 mm

and the nominal moment capacity calculated from Equation A.13 as

M_{na} = 5748 x 414 (511-32.83) + 347 x 1194 (657- 32.83) = 1396 KN-m.

ϕM_{na} = 0.9 x 1398 = 1256 KN-m.

The enhancement percentage can thus be computed as

$(M_{na}/\phi - M_{nb}/\phi)/ M_{nb}/\phi$ x 100

or

(1256 - 1039) / 1039 x 100 = 20.8 %

Thus the FRP increases the ultimate flexural capacity by approximately 21%

Example Using Design Charts

Alternatively, design charts may be used to calculate the upgraded girder ultimate flexural capacity as follows:

$$\rho = \frac{5748}{2030\ 511} = 0.0056 \quad , \quad \rho_f = \frac{347}{2030\ 511} = 0.00033$$

β_1 = 1.09 - 0.008 (27) = 0.87 > 0.85

β_1 = 0.85

d_f/d = 657/511 = 1.28

Using the design chart in Figure A.2 (β_1=0.85, f_y=414 MPa, ϵfu=0.0098, df/d ≈1.2, E_f =120,000 MPa)

$$\frac{M_u}{f_c' b d^2} = 0.088 = \frac{\phi M_n}{27\ 2030\ 511^2}$$

M_n = 1399 kN.m, which is approximately equal the calculated ultimate flexural (1396 kN.m) capacity using the analytical section analysis procedure.

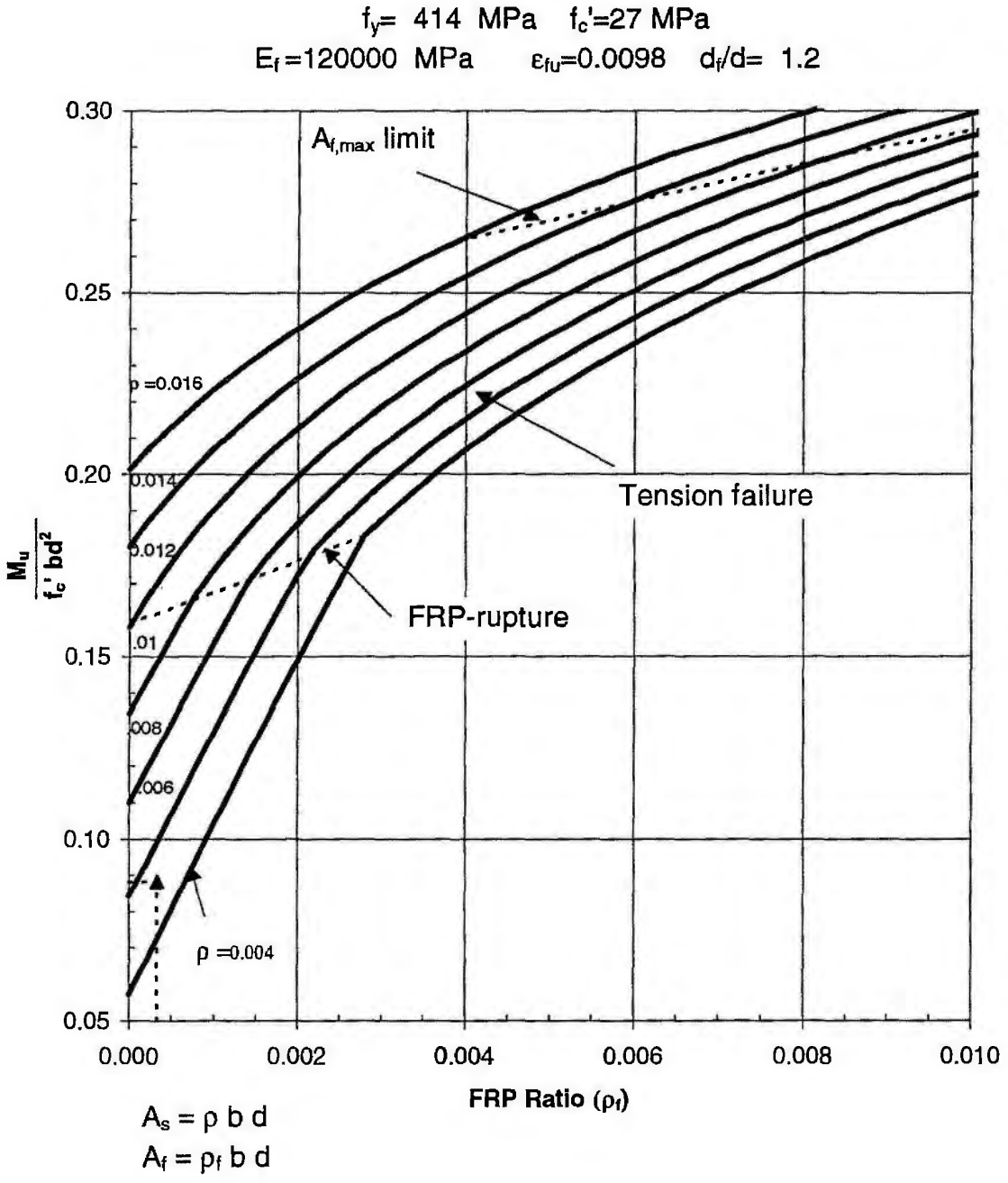

Figure A.2. Design Chart for RC Sections with FRP.